Novel routes to polymer-based self-healing systems for cementitious materials

Lu, Leyang

DOI
10.4233/uuid:a65910c1-d291-455b-841b-01820bd58d21

Publication date
2018

Document Version
Final published version

Citation (APA)
Lu, L. (2018). *Novel routes to polymer-based self-healing systems for cementitious materials*. [Dissertation (TU Delft), Delft University of Technology]. https://doi.org/10.4233/uuid:a65910c1-d291-455b-841b-01820bd58d21

Novel routes to polymer-based self-healing systems for cementitious materials

Novel routes to polymer-based self-healing systems for cementitious materials

Proefschrift

ter verkrijging van de graad van doctor
aan de Technische Universiteit Delft,
op gezag van de Rector Magnificus prof. dr. ir. T.H.J.J. van der Hagen,
voorzitter van het College voor Promoties,
in het openbaar te verdedigen op dinsdag 25 september 2018 om 10.00 uur.

door

Leyang LU

Master of Science in Material Science, Shenzhen Univerisity, China
geboren te Shandong, China

Dit proefschrift is goedgekeurd door de promotoren.

Samenstelling promotiecommissie bestaat uit:

Rector Magnificus,	voorzitter
Prof. dr. ir. E. Schlangen	Technische Universiteit Delft, promotor
Prof. dr. N. Han	Shenzhen University, China, promotor
Onafhankelijke leden:	
Prof. dr. ir. K. van Tittelboom	Universiteit Gent, België
Prof. dr. ir. S.M.J.G. Erkens	Technische Universiteit Delft
Prof. dr. J. Su	Tianjin Polytechnic University, China
Dr. B. Savija	Technische Universiteit Delft
Dr. H.M. Jonkers	Technische Universiteit Delft

Printed by: Drukkerij Haveka B.V.

ISBN 978-94-6366-078-5

Doing
out of thinking
better than saying

Contents

List of abbreviations

ESEM	Environmental scanning electron microscope
SEM	Scanning electron microscope
EDS	Energy dispersive spectrometer
OM	Optical Microscope
TGA	Thermogravimetric analysis
PF	Phenol formaldehyde
UF	Urea formaldehyde
MF	Melamine formaldehyde
DCPD	Dicyclopentadiene
O/W	Oil in water emulsion
XCT	X-ray computated tomography
WSRPs	Water swelling rubber particles
SAP	Super absorbent polymer
SIC	Shell-interlayer-cement paste
ROMP	Ring opening metathesis polymerization
NaOH	Sodium hydroxide
HCl	hydrochloric acid
PAA-Na	Poly (acrylic acid sodium salt)
LVDT	Linear variable differential transformer
ROI	Region of interest
CSM	Continuous stiffness method
RT	Room temperature
ITZ	Interfacial transition zone
C-S-H	Calcium silicate hydrates
C_3S	Tricalcium silicate
$Ca(OH)_2$	Calcium hydroxide
$CaCO_3$	Calcium carbonate

1

Introduction

A craftsman who wishes to do his work well
must first sharpen his tools.

Confucius

In this chapter, the research background is briefly introduced. The objectives, scope and outline of this research are described. A summary of all the chapters is given.

1

1.1. Research background

Cementitious materials are the most widely used construction materials in the world, due to their relatively low price, high reliability, and good compatibility with other materials such as reinforcing steel. However, they are susceptible to damage during their service life. Excessive cracking may form a serious threat to the safety, integrity and durability of concrete structures. In cementitious materials, microcracks develop as a result of mechanical loading, environmental loading (e.g. freezing and thawing), and volumetric instability (e.g. shrinkage in fresh or hardened concrete, thermal contraction). The existence of cracks provides access for harmful elements, such as moisture, chlorides and sulfates, that may cause deterioration of concrete structures due to corrosion, sulfate attack and alkali-silica reaction. Maintenance of buildings and infrastructures has long been an important issue. Although manual repair can prolong the service life of reinforced concrete structures, it gives rise to large amounts of rehabilitation work, associated costs and a waste of resources every year. A recent estimate shows that, in EU, around 50 % of annual construction budget is spent on refurbishment and repair of existing structures [1]. Even so, according to the data provided by ConRepNet research [2], 20 % of these repairs fail within 5 years. In fact, this number rose to 55 % within 10 years and 90 % within 25 years of service. In view of this, a more efficient way to reduce the maintenance/repair frequency and improve the service life of concrete structures is needed.

In recent years, inspired by biological self-recovery phenomena, a new concept named ”self-healing” showed great potential in cementitious materials. In general, two self-healing mechanisms in cementitious materials can be distinguished: autogenous healing and autonomous healing. Autogenous healing is an intrinsic self-healing property of cementitious material which comes from the further hydration of unhydrated cement particles, precipitation of carbonates and crystal growth. The biggest advantage of autogenous healing is that no additional ingredients are required to mix with concrete. Therefore, the chemical and mechanical properties of concrete will not be influenced. On the other hand, there are also numerous limitations to autogenous healing. First, autogenous healing can only happen in narrow cracks, typically with a crack width less than 0.3 mm [3]. Second, to achieve effective crack healing, some requirements on the healing conditions such as unhydrate cement, moisture and the existence of certain ions in the water are required. These conditions are not always practically available. Therefore, autonomous healing, as another self-healing mechanism often applied to compensate for drawbacks of autogenous healing in cementitious materials, is attracting more and more attention. For autonomous healing, healing agents are usually first sealed in a protective shell and then placed in the cementitious materials during the process of concrete mixing. Once a crack occurs in the structure, the healing agent located along the path of the crack will be triggered. The self-healing function of cementitious composites can be achieved through the release and reaction of healing agent in the crack region. Although the environment in the cementitious materials is quite harsh (i.e very alkaline), the reliability over time and triggering sensitivity of shell and healing agent have not attracted sufficient attention. The application potential of microcapsules

in cementitious materials has stimulated many investigations. Nevertheless, further study on developing carriers for healing agent, such as microcapsules, which are practically applicable for providing long-term self-healing capacity of cementitious materials, is still necessary.

Furthermore, as an essential step in the self-healing process, triggering of the healing function plays a decisive role in realizing the self-healing function. For cementitious materials containing microcapsules requiring a mechanical trigger, it is generally believed that the bonding strength with the cement matrix, the size and the mechanical properties (e.g. elastic modulus, strength) of microcapsules are factors that greatly influence the self-healing performance as well as the mechanical properties of cementitious composites [3, 4]. Thus, a proper selection and design of the microcapsules could offer a higher healing efficiency with lower degradation of mechanical properties of cementitious systems. In general, there are two available routes to design/prepare the microcapsules with desired properties. The first route is through experiments. Some experiments including morphology observation, crack surface inspection and mechanical recovery rate, have been performed on microcapsule-embedded cementitious materials with embedded microcapsules. However, experiments provide mostly a "post-mortem" analysis with limited information. The second route is predicting the relevant parameters of the microcapsules by computer simulations. Although most models use a continuum approach to predict the elastic properties of three-component composites [5, 6], such approaches experience difficulties when dealing with fracture processes in this type of materials. Moreover, bonding between shell materials and cement paste is often ignored in simulations resulting in an overestimation of the simulated values. Therefore, a reliable method for simulation and evaluation the fracture and triggering behaviour of capsule-based self-healing cementitious materials is needed.

In addition, relatively wide cracks (mm level) also need to be repaired in order to retain functionality of concrete structures. Unfortunately, most of the efforts in self-healing concrete focused on micro-scale cracks (< 500 μm). A limited number of researchers attempted to develop healing strategies for meso-scale cracks (> 500 μm). Thus, studies on developing a solution for these wide cracks is very attractive.

1.2. Objectives of this research

This thesis aims at developing novel polymer-based healing additives for cementitious materials and evaluating their effectiveness in tackling cracking-related problems. In order to achieve this goal, the main task can be divided into following subtasks:

- To synthesize a new type of microcapsule which is able to provide long-term self-healing capacity for small cracks (< 500 μm) in cementitious materials.
- To adapt and apply a numerical model for simulating the fracture behaviour and healing efficiency of microcapsule-based self-healing systems.
- To quantify the properties and function of the synthesised microcapsule self-healing system using appropriate experimental methods.

- To explore a new healing additive for sealing of wide (> 500 μm) cracks in concrete structures.

1.3. Scope of this research

Due to the diverse application purposes and implementation conditions, it is impossible to find a universal self-healing solution for all problems in cementitious materials. Actually, no repair or self-healing mechanism could perform "perfect" under all circumstances. Therefore, the scope of this research is limited to the following:

- This research only focuses on self-healing cementitious materials utilizing polymer materials as healing agent. The term "self-healing" in this thesis is particularly confined to "autonomous healing" by employing "polymer materials" as functional additives.
- The cementitious materials investigated in this research are limited to cement paste or standard mortar prepared according to the EU standard EN196-1 [7].
- In the part of numerical simulation of the capsule-based self-healing system, the properties of the interface are defined simply as material properties. Other factors, for example substrate surface roughness, that may also influence the interface properties were not taken into account in this study.
- Due to the unreliable triggering efficiency of microcapsules, the functionality of micocapsule-based self-healing systems is only quantified under ideal conditions. This means that an artificial crack was used instead of a real crack to guarantee that 1) all microcapsules can be ruptured by the crack; 2) the flowed out healing agent can completely contact with the catalyst. Meanwhile, due to the technical limitation of controlling the volume ratio of healing agent to crack (less than 100 μm wide), only artificial cracks wider than 200 μm are investigated experimentally.
- The water swelling rubber used in this research is a commercial product. The difference in swelling effect and kinetics between products from different companies and batches has not been taken into consideration in this study.

1.4. Outline of this research

This research can be divided into four parts. Figure 1.1 shows the outline of this thesis.

In the first part, chapter 1, a brief introduction of the research background, objectives and corresponding scopes is given. In chapter 2, a review of literature dealing with self-healing cementitious materials is presented in order to show the progress of the field and identify the research gaps to be bridged. The progress in the development of self-healing materials with different healing strategies and healing agents is introduced. The strengths and weaknesses of each self-healing method are briefly described.

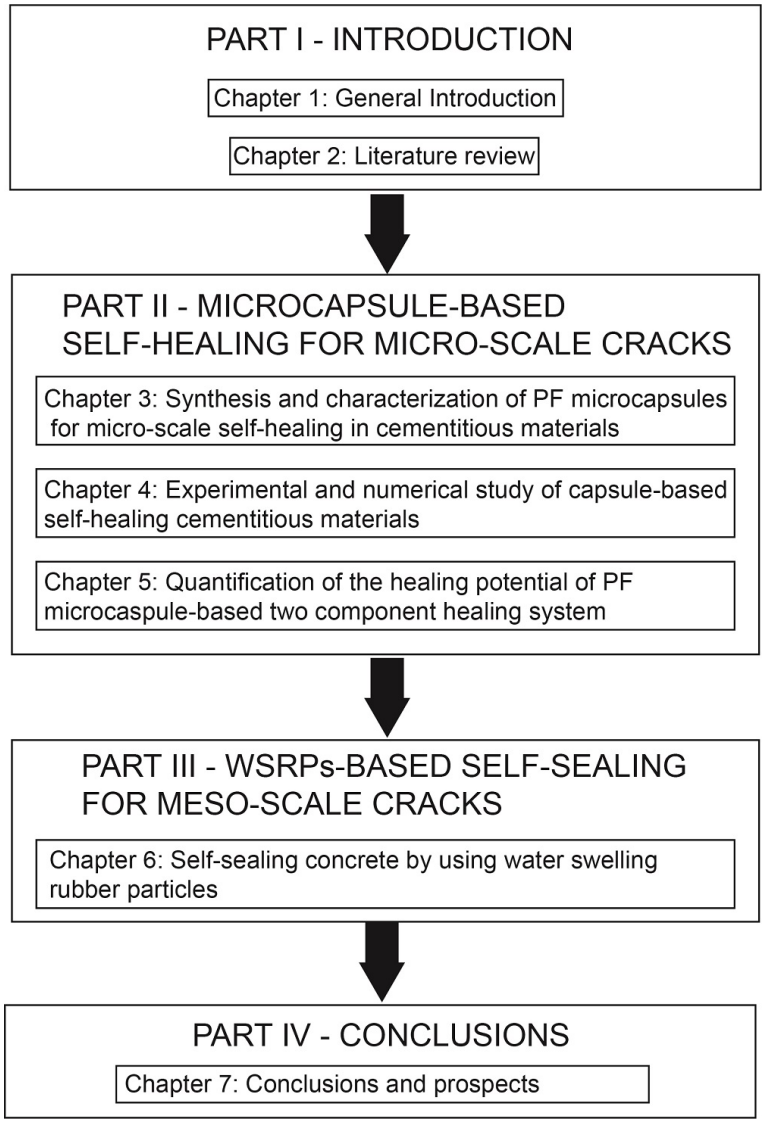

Figure 1.1: Outline of this thesis

In the second part, a series of studies towards realizing capsule-based self-healing cementitious materials for micro-level (< 500 μm) cracks are presented. Chapter 3 illustrates the synthesis and characterization of a novel polymeric microcapsule with PF resin as shell and DCPD as healing agent for self-healing cementitious materials on the micro-scale. In chapter 4, a numerical model is used to investigate the fracture behaviour and predict the healing effect of the microcapsule based self-healing cementitious materials. Chapter 5 shows the crack closing and sealing function of the microcapsule self-healing system. A simplified testing method is used to quantify the healing effects.

The third part deals with meso-scale (> 500 μm) crack in cementitious materials. Chapter 6 presents a study in which water swelling rubber particles (WSRPs) are used to deal with leakage problems in cracked cementitious materials. The feasibility of applying WSRPs is proven by using X-ray computed tomography (XCT). The self-sealing function of WSRPs embedded cementitious materials is evaluated. In addition, the crack bridging effect of WSRPs is illustrated at the end of this chapter.

The conclusions and recommendations for further research are given in the fourth part.

References

[1] G. Tilly and J. Jacobs, *Concrete repairs: Performance in service and current practice* (IHS BRE Press, 2007).

[2] G. Tilly and J. Jacobs, *Concrete repairs: Performance in service and current practice,* ConRepNet Project Report, IHS BRE Press , Watford, UK, Tech.Rep. (2010).

[3] K. Van Tittelboom and N. De Belie, *Self-healing in cementitious materials-a review,* Materials **6**, 2182 (2013).

[4] B. A. Young, A. M. K. Fujii, A. M. Thiele, A. Kumar, G. Sant, E. Taciroglu, and L. Pilon, *Effective elastic moduli of core-shell-matrix composites,* Mechanics of Materials **92**, 94 (2016).

[5] H. H. Zhu, S. Zhou, Z. G. Yan, J. W. Ju, and Q. Chen, *A two-dimensional micromechanical damage-healing model on microcrack-induced damage for microcapsule-enabled self-healing cementitious composites under tensile loading,* International Journal of Damage Mechanics **24**, 95 (2015).

[6] H. H. Zhu, S. Zhou, Z. G. Yan, W. Ju, and Q. Chen, *A 3d analytical model for the probabilistic characteristics of self-healing model for concrete using spherical microcapsule,* Computers and Concrete **15**, 37 (2015).

[7] T. EN, *196-1. methods of testing cement–part 1: Determination of strength,* European Committee for standardization **26** (2005).

2

Literature review

If you know the enemy and know yourself,
you need not fear the result of a hundred battles.

Sun Zi

This chapter gives a review of self-healing technologies applied in cementitious materials with diverse triggering mechanisms, healing agents and delivery methods. The strengths and weaknesses of different healing strategies are analyzed and discussed.

2

2.1. Introduction

Since the concept of self-healing was introduced in the field of cementitious materials decades ago, the significant potential in extending the service life and reducing maintenance costs through self-healing has attracted the attention of researchers worldwide. Development of self-healing cementitious materials requires an inter-disciplinary approach. Figure 2.1 shows the evolution of scientific publications in the field of self-healing cementitious materials. As can be seen from the figure, the number of publications related to the term "self-healing cementitious materials" increased rapidly in the past decades. These works deal with various self-healing strategies, healing agents, testing methods and numerical models etc., and provide researchers with a solid knowledge foundation to approach practical application of self-healing cementitious materials.

The aim of this chapter is to give a brief overview of the state-of-the art in self-healing cementitious materials by classifying them based on three criteria:

1. Self-healing mechanisms;
2. Healing agent delivery methods;
3. Triggering mechanisms of the self-healing system.

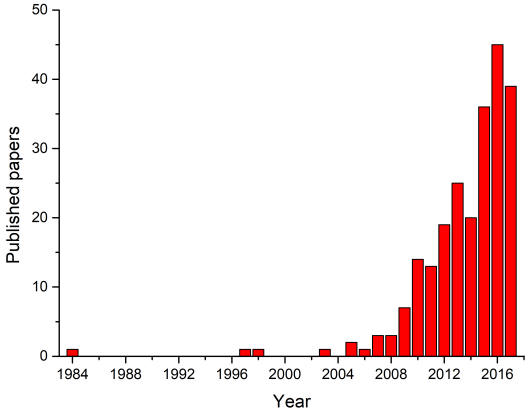

Figure 2.1: Evolution of the amount of scientific journal publications in the field of self-healing cementitious materials. Results obtained from Scopus database by searching terms: self-healing cementitious materials.

2.2. Self-healing mechanisms

As introduced in Chapter 1, the self-healing mechanisms in cementitious materials can be divided in two broad categories: autogenous healing (also known as intrinsic

healing) and autonomous healing. For autogenous healing, the self-healing effect is realized by the cementitious material itself. No additional ingredients need to be added to the mix. However, in order for autogenous healing to occur, certain environmental and curing conditions are necessary. Autonomous healing is normally realized by adding an additional ingredient (healing agent), e.g. bacteria beads, adhesive agent or swelling agent, to the material mix. Depending on the type of healing agent, self-healing in terms of mechanical properties (i.e. strength regain) or transport properties (i.e. impermeability) can be achieved. To accomplish significant self-healing of cracks in cementitious materials, approaches with different mechanisms need to be understood and used in accordance with their purpose.

2.2.1. Autogenous healing

Autogenous healing refers to the intrinsic healing ability of the material itself. The first literature report about this can be traced back to the end of nineteenth century [1]. Following that, more systematic studies were conducted to investigate the effect of autogenous healing on various aspects of cementitious materials.

The influence of autogenous healing on water permeability of cementitious materials has been studied by many researchers [2–5]. The mechanism and the chemical/physical process of autogenous self-healing was investigated theoretically and experimentally. It was generally believed that the formation of calcite in the crack is the cause for the autogenous healing. An obvious self-sealing effect can be found in the cracked cementitious material when it is exposed to water. Furthermore, a recovery of mechanical properties of cementitious materials due to the autogenous healing has also been shown. Lauer and Slate first demonstrated that the tensile strength of cementitious materials can be recovered by the autogenous healing of cracks [6]. Recently, Yang [7] demonstrated the autogenous healing effect on Engineered Cementitious Composites (ECC). The result showed that a distinct recovery in stiffness can be found on Crack-damaged ECC. Up to 100 % of the tensile strain capacity can be recovered for specimens pre-loaded up to 3 % tensile strain. Besides, the reduction of chloride ingress and reinforcement corrosion due to the autogenous healing was also investigated [8, 9].

According to the literature, the autogenous healing of cementitious materials is triggered by two mechanisms: 1) further hydration of unhydrated cement clinker remaining in the matrix [10] and 2) precipitation of calcium carbonate ($CaCO_3$) nearby the crack mouth [3, 11]. Further hydration is considered as the main healing mechanism in early age concrete. When the concrete is in contact with water, unhydrated cement particles will continue to hydrate, promoting autogenous healing. In mature concrete, the amount of unhydrated cement is much lower than at early age. In this condition, the calcium carbonate precipitation becomes the main trigger of autogenous healing. It is generally believed that the $CaCO_3$ precipitation is formed from the chemical reaction between calcium ions in the cement paste and carbonates. The carbonates come from the carbonic acid (CO_3^{2-}) as a result of carbon dioxide (CO_2) from the air dissolved in water. Since the concentration of CO_3^{2-} around the crack mouth is higher than inside the crack, the $CaCO_3$ precipitates at the site of the crack mouth [12]. With the progress of self-healing, more

CO_3^{2-} ions could reach inside the cracks, leading to calcite formation on the crack surface. Nevertheless, there are limitations to the autogenous healing ability. First, prolonged immersion of concrete in water is needed for autogenous healing to occur. In addition, the autogenous healing process can only be effective for healing narrow cracks (up to 200 μm), depending on the curing conditions [3, 13–15].

2.2.2. Mineral admixture-based self-healing

As mentioned, although autogenous healing processes in cement-based materials have been investigated for many years, the healing effect is only limited to narrow cracks with crack widths less than 200 μm. This is because the autogenous healing mechanism largely depends on further hydration of unhydrated cement particles. Therefore, for typical hardened concrete, autogenous healing is not very promising as the amount of undydrated cement is insufficient for complete healing to occur. To overcome this, adding mineral admixtures in the mix to promote self-healing is an option. The effect of various mineral additives i.e., silica-based materials [16], calcium sulfoaluminate based expansive agents [17, 18] and crystalline components [12] on promoting autogenous healing of cementitious materials has been investigated. It was found that the addition of mineral admixtures can promote autogenous healing in cementitious materials. In addition, it was found that the healing efficiency of cementitious materials could be further improved by utilizing a combination of minerals rather than a single mineral [16].

Nevertheless, there are some drawbacks when applying mineral admixtures as self-healing agent to promote the healing process. Directly adding a mineral admixture to concrete without protection may result in an immediate reaction when the mineral admixture is in contact water. Moreover, the addition of expansive agents in the concrete matrix could cause damage of the concrete structure due to its expansion [19]. And water should always be available in cracks in order to realize an effective self-healing. Additional healing, autonomous healing, is required.

2.2.3. Polymeric adhesive agent based self-healing

Adhesive agent-based self-healing is one of the earliest autonomous healing concepts in the field of cementitious materials. The objective of applying an healing agent in cementitious materials is to maintain material and structural durability by regaining water tightness and mechanical properties in concrete structures. Generally, there are two types of adhesive agents: one-component agents or two-component (or multi-component) agents. One-component adhesive agents are an ideal option for self-healing because their function can be triggered immediately, while the durability of it can be a big concern. Two-component adhesive agents have much longer shelf life than one-component agents, however the trigger and mixing of these two parts is more demanding in terms of design and delivery of adhesive. In the following, adhesive agents which have been applied in the field of self-healing cementitious materials are discussed.

$Cyanoacrylate(CA)$, also known as superglue, is a type of one-component adhesive. Its characteristics, such as low viscosity, short harding time when exposed to open air and super strong binding make the CA a very promising adhesive agent.

Li et al. [20] first introduced the application of CA into the field of self-healing cementitious materials. After that, many researchers have explored the feasibility of using CA as adhesive agent for self-healing [21–23]. These studies found that CA (superglue) is a suitable healing agent since the single-agent adhesive is able to flow into, and heal, finer cracks. However, its short shelf life and weak resistance to both water and heat might be a negative factor in practical applications.

$Epoxy$ is another type of adhesive agent that has already been used in concrete repair for a long time. In recent years, the application of epoxy in crack sealing and mechanical repair of concrete has extended to self-healing concrete [24, 25]. Two-component epoxy repair systems are the most popular adhesive agent systems in the literature. Low molecular pre-polymer epoxy and its hardener were first encapsulated separately in two different carriers and then embedded in cementitious materials. When the crack intersects the encapsulated epoxy and its hardener, the epoxy will flow out and be cured by the hardener. In practice, simultaneous triggering and mixing of epoxy and its hardener is a practical barrier to its practical application. Moreover, the relative high viscosity of epoxy makes it difficult to penetrate into the crack due to the capillary effect. Therefore, one component epoxy was applied to increase the efficiency of self-healing [26, 27]. Recently, Li et al. [28] demonstrated the use of one-component epoxy filled microcapsules to achieve strength regain in cementitious materials. To decrease the viscosity of epoxy, they proposed using benzylalcohol (BA) as a diluter.

$Methylmethacrylate(MMA)$ was first used in self-healing cementitious materials by Dry et al [29, 30]. Compared to CA, MMA has longer shelf life, better resistance to extreme temperatures and lower viscosity, which makes it more suitable for self-healing cementitious materials. However, the low viscosity MMA may be either soaked up by the pores in the cementitious material or leaked out from the crack, leading to a decrease of the healing effect. To solve this problem, Van Tittelboom et al. employed poly(methyl methacrylate) (PMMA) as thickening agent to increase the viscosity of MMA [31]. Yang et al. [32] used oil core/silica gel shell capsules to deliver the two-component adhesive agent, MMA and triethylborane (TEB), to the crack.

$Dicyclopentadiene(DCPD)$ is a new type of healing agent. It was first applied in self-healing polymers [33], asphalt [34] and then the application was extended to concrete [35]. When DCPD encounters the Grubbs' catalyst ($C_{43}H_{72}Cl_2P_2Ru$), a transition metal catalyst, the process of ring opening metathesis polymerization (ROMP) occurs. Owing to its unique properties, such as low initial viscosity, high toughness after curing and all-weather applicability, DCPD can pass through and seal the cracks, thereby reducing the ingress of water and aggressive species into cementitious materials.

Apart from abovementioned adhesive agents, feasibility of using other adhesives such as acrylate-endcapped, urethane-based precursor [36] and commercially available healing agent such as MEYCO MP355 1K has also been explored [37].

2.2.4. Bacteria based self-healing

Inspired by Gollapudi et al. [38] who suggested using bacteria to promote precipitation of calcium carbonate ($CaCO_3$) for crack healing, a bacteria based self-healing system using porous expanded clay particles with immobilized bacteria as biotic healing agent has been described by Jonkers et al. [39–41]. In this series of studies, a two-component bio-chemical self-healing agent was used to replace part of concrete aggregates. Once the crack forms in the matrix of the cementitious material, bacterial spores and calcium lactate will be released and activated by the ingress of water. Cracks up to 0.46 mm wide can be healed in bacterial concrete after 100 days of submersion in water. This is more than double compared to control specimens without bacteria (0.18 mm). Compared to other studies [42–45], the work of Jonkers et al. seems to be more promising. Since the bacteria and bio-mineral precursor were both embedded and therefore protected by the expanded clay, the activity of bacteria and the effectiveness of the bio-chemical self-healing agent became more reliable. Meanwhile, their method excludes the need of urea during the calcite precipitation process, and is therefore more environmental friendly.

Wang et al. [46, 47] demonstrated the feasibility of using microencapsulated bacterial spores to heal cracks in cementitious materials. It was found that the spores were still viable after being immobilized into a melamine-formaldehyde resin shell. Despite the influence of the mechanical properties of mortar due to the addition of microencapsulated bacterial spores, a 970 µm wide crack can be healed in the specimens with bacteria. Therefore, cracks 4 times wider compared to the control series (i.e. without bacteria) can be healed.

The main drawback for practical application of bacteria-based self-healing concrete is that certain environmental conditions are needed for healing to occur. In fact, cracks need to be exposed to water for bacteria to be active.

2.2.5. Swelling agent-based self-healing

Water swelling materials such as superabsorbent polymer (SAP) [48–51] and polyurethane (PU) [31, 37] can be used as healing agents targeting the regain of mechanical strength and the reduction of water permeability. The application of PU-based healing agent in self-healing cementitious materials was reported by Van Tittelboom [31]. The healing agent used, MEYCO MP 355 1K (BASF The Chemical Company), is a commercial PU product. This type PU starts foaming in contact with water. The foaming reaction may lead to an increase of its volume of up to 25 - 30 times. Because of this, cracks may be filled up by the swelled PU. In addition, it was found that autonomous crack healing by means of encapsulated polyurethane also has a beneficial effect on the resistance of cementitious materials with crack widths between 100 µm and 300 µm against chloride diffusion [52].

Superabsorbent polymer (SAP) particles were first used in cementitious materials for prevention of self-desiccation in hardening cement-based materials [53–55]. The pre-embedded SAP particles will lead to the formation of water-filled macropore inclusions in the fresh concrete. Figure 2.2 demonstrates the mechanism of self-sealing cracks using SAP. As can be seen in the figure 2.2a, during cement hydration, the SAP will lose water and shrink due to the unbalance of moisture

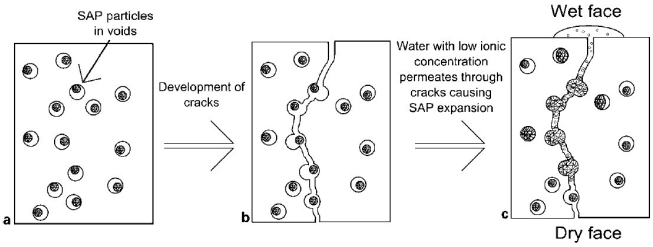

Figure 2.2: Schematic showing potential mechanism of self-sealing cracks using SAP [48].

leaving pores and holes in the cement matrix. When a crack occurs, the pores will act as macro defects and the crack is likely to propagate through them (Figure 2.2b). Once the cracked cementitious materials are exposed to water, the SAP will swell immediately. The swollen SAP can fill the crack and decrease or even stop further water ingress (Figure 2.2c). Despite the influence of SAP inclusion on the mechanical properties, the re-released water from swollen SAP can be used to control self-desiccation and to promote internal curing. It was also found that the application of SAP in cementitious materials can result in a reduction of autogenous shrinkage and cracking [56, 57]. Recently, the potential of applying SAP for self-healing and self-sealing cracks in cementitious materials has also been investigated. Lee et al. [48] reported that, by incorporating 5 vol. % of SAP, the flow rate through a 0.3 mm wide crack was reduced substantially. Kim and Schlangen [58] first demonstrated that using SAP to promote self-healing in Engineered Cementitious Composite (ECC). After that, Snoeck et al. [51] showed that the combined effect of microfibers and SAP enables the cementitious materials to be healed in an environment with a relative humidity of about 60 %. They found that incorporation of 1 % of SAP by cement weight enabled creation of cementitious materials with superior self-sealing capacity without significantly affecting the strength. A recent study showed that, compared to control samples with similar crack widths, the peak flow rate and cumulative flow through SAP embedded samples decreased by up to 85 % and 98 %, respectively [48]. Inevitably, the use of SAP results in a drastic decrease in strength. For example, the addition of 5-13 % SAP by weight of cement was found to reduce compressive strength by 80-87 %. That means the use of 1 % SAP will result in 18 % decrease in strength [48].

Recently, in the HEALCON project (HEALCON is a project funded by EU-FP7 and coordinated by Prof. Nele De Belie(Ghent University), attempts are done to encapsulate SAP so that they do not absorb water during mixing [59]. Then the sealing capacity of SAP can be fully preserved without leaving extra space of holes in the cement matrix caused by water taken up by the SAP during mixing. This improvement not only enhanced the sealing effect of SAP but also increased the strength of the SAP/cement composite.

2.3. Healing agent delivery methods

Physical and chemical conditions present in cementitious materials are complicated and relatively harsh. For instance, the mixing process of cement and aggregate could produce a strong shear force. Following that, in the initial stage of cement hydration, large amounts of $Ca(OH)_2$ may be generated as a hydration product of the tricalcium silicate (C_3S). This $Ca(OH)_2$ dissolves in water, resulting in a fast increase of the pH value ($pH_{max} > 13$). Meanwhile, during the curing and hardening period, water saturated conditions are present. All these factors pose threat to survival of almost all healing agents described. Therefore, in order to deliver the healing agent to the crack effectively, the healing agent has to be preserved until it is needed. Several methods have been developed to protect the healing agent from the influence of the harsh conditions and to deliver the healing agent to where it is needed. In the following paragraphs, three types of typical healing agent delivery methods with their corresponding strengths and weaknesses are presented.

2.3.1. Microencapsulation

Microencapsulation technology has been widely applied in the field of agriculture, drug manufacturing, food processing etc. In recent years, this technology has also been introduced in the field of self-healing materials. The first application of microcapsules as a vessel to protect and deliver the healing agent was in self-healing polymers. There, microcapsules with urea-formaldehyde (UF) shell containing dicyclopentadiene (DCPD) were synthesized by the in-situ polymerization technique [33, 60]. Later, the microcapsule-based self-healing concept also has shown great application potential in extending the lifetime of cementitious materials. Once the incorporated microcapsules are ruptured by stimuli such as mechanical stress [35, 37, 61], ions [62], pH [63, 64], or other, the self-healing is realized through the release and reaction of repairing chemicals in the region of the crack. Figure 2.3 shows the schematic of mechanical trigger microcapsule-based self-healing approach.

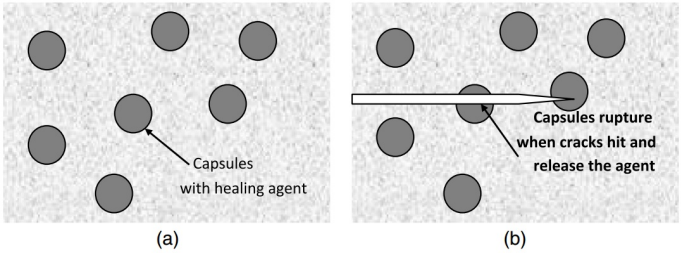

Figure 2.3: Schematic of capsule-based self-healing approach [65].

Properties of microcapsules are important in achieving self-healing in cementitious materials. A good design of microcapsules not only directly determines the self-healing efficiency but also will have a positive influence on the mechanical properties of the cementitious composite. So far, several types of microcapsules have

been particularly developed for self-healing of cementitious materials. Depending on the shell material, the microcapsules for use in self-healing cementitious materials can be grouped in two categories: polymeric microcapsules and inorganic microcapsules. Polymeric microcapsules employ organic materials such as urea-formaldehyde (UF) resin [47], melamine-formaldehyde (MF) resin [66], polystyrene (PS) [64], or other, as shell materials to protect and deliver the healing agent to the crack. Microencapsulation techniques, including spray drying, interfacial polymerization (also named in-situ porlymerization) and polymer phase separation are the most commonly used techniques for polymeric microcapsule fabrication. The benefit of using polymers as shell materials is their ability to seal the healing agent, which is crucial for most healing agents that would lose effect when they encounter the high alkaline solution. Inorganic microcapsules are another category of microcapsules that use inorganic materials such as silica particles [32] and expanded clay [41] as shell materials. The advantage of inorganic microcapsules is the relatively strong bonding between the inorganic shell and the cementitious matrix, which has an great influence on the trigger efficiency of microcapsules.

In general, microencapsulated healing agents have many advantages for use in self-healing cementitious materials. Firstly, the microcapsules have a good dispersibility in the matrix, which enables the self-healing system to have a homogeneous strength and healing effect. Secondly, the round shape of microcapsules enables it to be triggered by cracks from any direction, making the self-healing efficient. However, issues such as the limited amount of the healing agent and sometimes limited triggering efficiency need to be addressed before such systems are put to practical use. To compensate the limitations, some researchers claim that cylindrical capsules and/or vascular systems are more effective than spherical ones. To proof this, a numerical model was built to compare the trigger and healing efficiency of different shapes of capsule systems [67, 68].

2.3.2. Vascular system

The application of vascular system is the oldest method employed for delivering the healing agent to the crack in cementitious materials. In 1994, Dry proposed using hollow fibers containing a chemical healing agent to seal matrix cracks and restore the strength in damaged areas [69]. The vascular self-healing system is illustrated in Figure 2.4. Hollow glass fibers were first embedded in the cementitious matrix. The healing agent and curing agent (only for two channel vascular systems) are stored or injected separately in different fibers. Once the glass fibers are broken by the crack, the healing agent will release and seal the crack.

Joseph et al. [21] designed a vascular healing system that uses embedded borosilicate glass tubes to deliver the healing agent. However, they found that only a small amount of healing agent flowed into the crack after rupture of tubes. To increase the transport distance and amount of healing agent, additional healing agent was provided inside a tank which was connected to the outer end of the hollow fiber [70]. There are two main drawbacks of using glass fiber to form a vascular system. One is the glass fiber may not survive the concrete mixing process. Another is alkali-silica reaction may shorten the long term service of the glass vascular

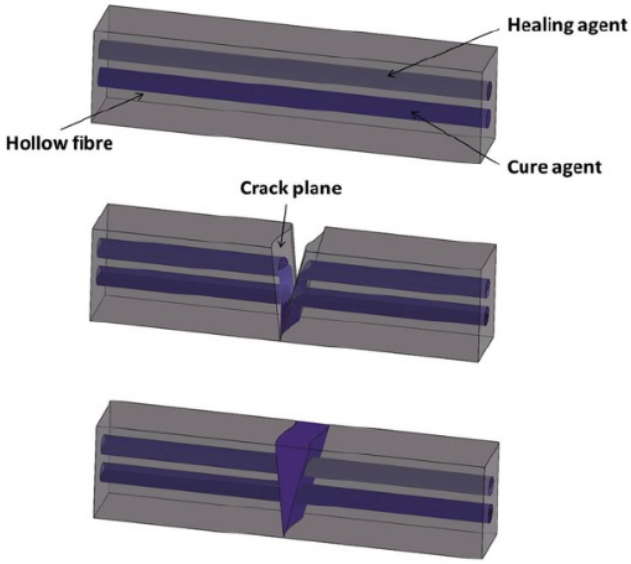

Figure 2.4: Schematic representation of hollow fibers self-healing concept [73].

system. As a replacement, Pareek et al. [71] designed a container free vascular system. To introduce hollow ducts in concrete structures, steel bars with smooth surface were first embedded during casting and then pulled out after the concrete cured for 24 hours. Recently, Minnebo et al. [72] demonstrated using alternative brittle materials: polymethyl methacrylate (PMMA), starch, alumina and inorganic phosphate cement to replace the commonly used vascular material, glass. The results obtained from mechanical testing showed that self-healing can be realized by using such vascular networks.

Overall, to design and optimize the vascular system, researchers need to assess the size (diameter and thickness) of the fiber, in addition to the viscosity and the polymerization kinetics of the healing agent. Meanwhile, the healing agent should be selected based on crack widths that need to be repaired.

2.3.3. Porous network

Taking inspiration of fracture healing of creature's bone, Sangadji and Schlangen proposed the idea of porous network concrete [74]. In porous network concrete, a vascular system is designed and installed without additional delivery methods. The porous network system consists of two parts, the prefabricated porous core and the concrete main body. The porous concrete is embedded in the normal concrete main body. The porous core provides means of transporting the healing agent while the concrete body provides strength and stiffness to the structure. When there is a crack intersecting the porous network, liquid healing agent can be delivered automatically through the porous network to the crack. The schematics of the porous network

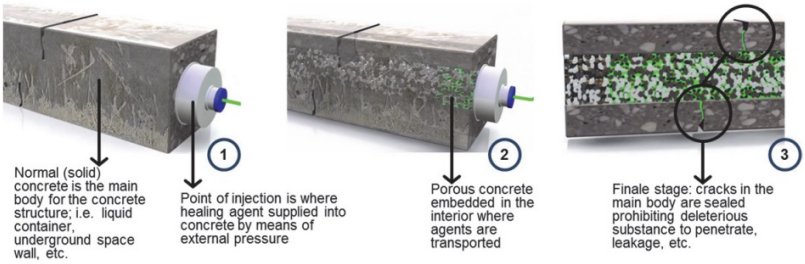

Figure 2.5: Schematics of the conceptual working principle of healing agent transport in the porous network concrete [74].

concrete are shown in Figure 2.5.

Both polymer based healing agents and bacteria based repair solutions were employed as healing agents in their study. When using low viscosity epoxy as the healing agent, the crack zone was sealed and the crack faces were glued, showing a tendency to recover strength and stiffness of cracked specimens. Furthermore, it was also found that the water leakage through the crack can be completely stopped. While applying bacteria as repair solution has a limited effect on strength and stiffness recovery, liquid tightness can be achieved in a cracked porous network system. Still, more research on reusability and upscaling possibility of porous network systems is needed.

2.4. Triggering mechanisms of self-healing systems

The triggering mechanism is a decisive factor in the design and realization of self-healing function in cementitious materials. According to the service environment and possible deterioration mechanisms of cementitious materials, triggering mechanisms can be grouped in three categories.

2.4.1. Mechanical trigger

Mechanical trigger is the most commonly used triggering mechanism in self-healing cementitious materials. As cracking is the main reason for cementitious materials deterioration, crack propagation provides a force to trigger the self-healing action. By mixing the healing agent loaded spherical or tubular microcapsules, a self-healing system can be achieved in cementitious materials.

To practically realize mechanical triggering, two requirements need to be met. First, the crack needs to hit the container with healing agent. To help design such systems, several numerical models have been developed to simulate the crack behaviour of cementitious materials and to calculate the probability of a crack hitting the capsules [75, 76]. Zemskov et al. developed a model that allows to analyze the efficiency of a self-healing material considering the combined influence of crack length, capsule size, and mean intercapsule distance. Lv et al. [77, 78] employed computer simulation to calculate and verify the hitting probability depending on

the dosage, size and shape of capsules. Even though the crack hits the dispersed caspules, there is still possibility that the self-healing function cannot be triggered as the crack may go around rather than rupture the capsules. Therefore, the second requirement is that the container is sensitive to the crack and can be mechanically triggered. At least two factors decide the rupture possibility of healing agent container, (1) the strength and brittleness of the shell material and (2) the bond strength between the shell and the matrix [79]. The strength of the shell material can be controlled by manipulating the preparation conditions or by using different materials. Su et al. [80] found that by changing the core/shell ratio and stirring rate, the size and mechanical properties of microcapsules can be adjusted. Hilloulin et al. [81] presented a healing agent encapsulation method which enables the capsules to break during cracking, but are able to survive the concrete mixing. Three different polymers, poly(lactic acid), polystyrene and poly(methyl methacrylate/n-butyl methacrylate) with a low glass transition temperature were employed as container materials. It was found that the polymeric capsules are able to resist the concrete mixing process and can break when cracks appear.

2.4.2. Chemical trigger system

Although mechanical triggering in self-healing is popular, a significant drawback of this mechanism is that it is hard to ensure that all healing agent containers could be triggered by cracks due to complicated conditions involved. Recently, researchers explored using ions as trigger of the self-healing process. During the service life, cementitious materials are exposed to different ions from the environment. If self-healing can be triggered by certain ions, the trigger efficiency and accuracy can be increased. Xiong et al. developed a novel capsule-based cementitious self-healing recovery system with a chloride ion trigger [62]. Since sodium alginate can be crosslinked with many metal ions (such as Ca^{2+}) to form a hydrogel, they selected Ag^{+} to be coordinated with alginate to form the wall materials of the capsules. When capsules are in contact with chloride ions, the metal ions, Ag^{+}, will react with negative chloride ions and be extracted out to disintegrate the capsules. Dong et al. [63, 64] developed a pH trigger microcapsule system using polystyrene resin (PS) as a shell material. The release of the corrosion inhibitor is a function of time controlled by both pH of the solutions and the thickness of PS shell.

2.4.3. Water and heat trigger system

Some self-healing systems, the healing function can be directly triggered by water ingression. SAP is one of them. Benefiting from its different swelling behaviour in water and in pore solution, SAP can swell to a volume much larger than during the cement hydration process, resulting in almost complete sealing of cracks [82]. Beside the water triggered system, the possibility of heat triggered systems has also been explored by using ethylene-vinyl acetate (EVA) as a repairing component [83]. Although the addition of EVA will cause some decrease of compressive strength, the damaged specimens can be effectively repaired by EVA with a repair efficiency exceeding 100 %.

2.5. Conclusion

In this chapter, literature about self-healing in cementitious materials with diverse triggering mechanisms, healing agents and delivery methods is reviewed. The pros and cons of different healing strategies are analyzed. In general, no healing strategy can be universally applied. When selecting the healing strategy, the environmental conditions and functional requirements need to be considered. In addition, depending on the deterioration mechanism, the crack width in cementitious materials can vary from micro to macro scales. Therefore, to solve the problem as a whole, cracks need to be tackled at different scales.

References

[1] N. Hearn, *Self-sealing, autogenous healing and continued hydration: What is the difference?* Materials and Structures **31**, 563 (1998).

[2] C. A. Clear, *The effect of autogenous healing upon leakage of water through crack initiation and arresting in epoxy,* International Journal of Fracture **55**, 209 (1985).

[3] C. Edvardsen, *Water permeability and autogenous healing of cracks in concrete,* Aci Materials Journal **96**, 448 (1999).

[4] N. Hearn and C. T. Morley, *Self-sealing property of concrete - Experimental evidence,* Materials and Structures **30**, 404 (1997).

[5] K. Van Tittelboom, E. Gruyaert, H. Rahier, and N. De Belie, *Influence of mix composition on the extent of autogenous crack healing by continued hydration or calcium carbonate formation,* Construction and Building Materials **37**, 349 (2012).

[6] K. R. L. Slate and F. 0., *Autogenous Healing of Cement Paste,* Journal Proceedings **52**, 10.14359/11661.

[7] Y. Yang, M. D. Lepech, E.-H. Yang, and V. C. Li, *Autogenous healing of engineered cementitious composites under wet-dry cycles,* Cement and Concrete Research **39**, 382 (2009).

[8] W. Ramm and M. Biscoping, *Autogenous healing and reinforcement corrosion of water-penetrated separation cracks in reinforced concrete,* Nuclear Engineering and Design **179**, 191 (1998).

[9] P. Fidjestol and N. Nilsen, *Field Test of Reinforcement Corrosion in Concrete,* ACI Special Publication **SP 65-12**, 205 (1980).

[10] E. Schlangen, N. ter Heide, and K. van Breugel, *Measuring, Monitoring and Modeling Concrete Properties*, edited by M. S. KonstaGdoutos (2006) pp. 273–+.

[11] S. Qian, J. Zhou, M. R. de Rooij, E. Schlangen, G. Ye, and K. van Breugel, *Self-healing behavior of strain hardening cementitious composites incorporating local waste materials,* Cement & Concrete Composites **31**, 613 (2009).

[12] K. Sisomphon, O. Copuroglu, and E. A. B. Koenders, *Self-healing of surface cracks in mortars with expansive additive and crystalline additive,* Cement and Concrete Composites **34**, 566 (2012).

[13] C. M. Aldea, W. J. Song, J. S. Popovics, and S. P. Shah, *Extent of healing of cracked normal strength concrete,* Journal of Materials in Civil Engineering **12**, 92 (2000).

[14] H. W. Reinhardt and M. Jooss, *Permeability and self-healing of cracked concrete as a function of temperature and crack width,* Cement and Concrete Research **33**, 981 (2003).

[15] M. Sahmaran, S. B. Keskin, G. Ozerkan, and I. O. Yaman, *Self-healing of mechanically-loaded self consolidating concretes with high volumes of fly ash,* Cement & Concrete Composites **30**, 872 (2008).

[16] Z. Jiang, W. Li, and Z. Yuan, *Influence of mineral additives and environmental conditions on the self-healing capabilities of cementitious materials,* Cement and Concrete Composites **57**, 116 (2015).

[17] S. Nagataki and H. Gomi, *Expansive admixtures (mainly ettringite),* Cement and Concrete Composites **20**, 163 (1998).

[18] T. S. Qureshi, A. Kanellopoulos, and A. Al-Tabbaa, *Encapsulation of expansive powder minerals within a concentric glass capsule system for self-healing concrete,* Construction and Building Materials **121**, 629 (2016).

[19] R. Sahamitmongkol and T. Kishi, *Tensile behavior of restrained expansive mortar and concrete,* Cement and Concrete Composites **33**, 131 (2011).

[20] V. C. Li, Y. M. Lim, and Y. W. Chan, *Feasibility study of a passive smart self-healing cementitious composite,* Composites Part B-Engineering **29**, 819 (1998).

[21] C. Joseph, A. D. Jefferson, B. Isaacs, R. Lark, and D. Gardner, *Experimental investigation of adhesive-based self-healing of cementitious materials,* Magazine of Concrete Research **62**, 831 (2010).

[22] L. Sun, W.-y. Yu, and Q. Ge, *Experimental research on the self-healing performance of micro-cracks in concrete bridge,* in *Advanced Building Materials, Pts 1-4*, Vol. 250-253, edited by G. Li, Y. Huang, and C. Chen (2011) pp. 28–32.

[23] C. M. Dry, *Three designs for the internal release of sealants, adhesives, and waterproofing chemicals into concrete to reduce permeability,* Cement and Concrete Research **30**, 1969 (2000).

[24] X. Wang, F. Xing, M. Zhang, N. Han, and Z. Qian, *Experimental study on cementitious composites embedded with organic microcapsules,* Materials **6**, 4064 (2013).

[25] F. Xing, Z. Ni, N. X. Han, B. Q. Dong, X. X. Du, Z. Huang, and M. Zhang, *Self-healing mechanism of a novel cementitious composite using microcapsules,* Advances in Concrete Structural Durability, Proceedings of Icdcs2008, Vols 1 and 2 , 195 (2008).

[26] T. D. P. Thao, T. J. S. Johnson, Q. S. Tong, and P. S. Dai, *Implementation of self-healing in concrete – Proof of concept,* The IES Journal Part A: Civil & Structural Engineering **2**, 116 (2009).

[27] T. Nishiwaki, H. Mihashi, B.-K. Jang, and K. Miura, *Development of Self-Healing System for Concrete with Selective Heating around Crack,* Journal of Advanced Concrete Technology **4**, 267 (2006).

[28] W. Li, Z. Jiang, Z. Yang, N. Zhao, and W. Yuan, *Self-healing efficiency of cementitious materials containing microcapsules filled with healing adhesive: mechanical restoration and healing process monitored by water absorption.* PloS one **8**, e81616 (2013).

[29] C. Dry and W. McMillan, *Three-part methylmethacrylate adhesive system as an internal delivery system for smart responsive concrete,* Smart Materials & Structures **5**, 297 (1996).

[30] C. M. Dry, *<title>Improvement in reinforcing bond strength in reinforced concrete with self-repairing chemical adhesives</title>,* in *Smart Systems for Bridges, Structures, and Highways - Smart Structures and Materials 1997*, Vol. 3043, edited by N. Stubbs (1997) pp. 44–50.

[31] K. Van Tittelboom, N. De Belie, D. Van Loo, and P. Jacobs, *Self-healing efficiency of cementitious materials containing tubular capsules filled with healing agent,* Cement and Concrete Composites **33**, 497 (2011).

[32] Z. Yang, J. Hollar, X. He, and X. Shi, *A self-healing cementitious composite using oil core/silica gel shell microcapsules,* Cement and Concrete Composites **33**, 506 (2011).

[33] E. N. Brown, S. R. White, and N. R. Sottos, *Microcapsule induced toughening in a self-healing polymer composite,* Journal of Materials Science **39**, 1703 (2004).

[34] W. Yuan, K.-Y. Yuan, L. Zou, J.-M. Yang, J.-W. Ju, W. Kao, L. Carlson, B. Edgecombe, and T. Stephen, *DCPD resin catalyzed with Grubbs catalysts for reinforcing pothole patching materials,* in *Nondestructive Characterization for Composite Materials, Aerospace Engineering, Civil Infrastructure, and Homeland Security*, Vol. 8347, edited by A. L. Gyekenyesi (SPIE, San Diego, California, 2012) pp. 83471D–83471D–12.

[35] J. Gilford, M. M. Hassan, T. Rupnow, M. Barbato, A. Okeil, and S. Asadi, *Dicyclopentadiene and sodium silicate microencapsulation for self-healing of concrete,* Journal of Materials in Civil Engineering **26**, 886 (2014).

[36] M. Araujo, S. Van Vlierberghe, J. Feiteira, G. J. Graulus, K. Van Tittelboom, J. C. Martins, P. Dubruel, and N. De Belie, *Cross-linkable polyethers as healing/sealing agents for self-healing of cementitious materials,* Materials and Design **98**, 215 (2016).

[37] F. A. Gilabert, K. Van Tittelboom, J. Van Stappen, V. Cnudde, N. De Belie, and W. Van Paepegem, *Integral procedure to assess crack filling and mechanical contribution of polymer-based healing agent in encapsulation-based self-healing concrete,* Cement and Concrete Composites **77**, 68 (2017).

[38] U. Gollapudi, C. Knutson, S. Bang, and M. Islam, *A new method for controlling leaching through permeable channels,* Chemosphere **30**, 695 (1995).

[39] H. M. Jonkers, A. Thijssen, G. Muyzer, O. Copuroglu, and E. Schlangen, *Application of bacteria as self-healing agent for the development of sustainable concrete,* Ecological Engineering **36**, 230 (2010).

[40] H. M. Jonkers, *Self Healing Concrete: A Biological Approach,* in *Self Healing Materials: An Alternative Approach to 20 Centuries of Materials Science*, Vol. 100, edited by S. VanderZwaag (2007) pp. 195–204.

[41] V. Wiktor and H. M. Jonkers, *Quantification of crack-healing in novel bacteria-based self-healing concrete,* Cement and Concrete Composites **33**, 763 (2011).

[42] W. De Muynck, N. De Belie, and W. Verstraete, *Microbial carbonate precipitation in construction materials: A review,* (2010).

[43] J. Dick, W. De Windt, B. De Graef, H. Saveyn, P. Van Der Meeren, N. De Belie, and W. Verstraete, *Bio-deposition of a calcium carbonate layer on degraded limestone by Bacillus species,* Biodegradation **17**, 357 (2006).

[44] W. De Muynck, D. Debrouwer, N. De Belie, and W. Verstraete, *Bacterial carbonate precipitation improves the durability of cementitious materials,* Cement and Concrete Research **38**, 1005 (2008).

[45] K. Van Tittelboom, N. De Belie, W. De Muynck, and W. Verstraete, *Use of bacteria to repair cracks in concrete,* Cement and Concrete Research **40**, 157 (2010).

[46] J. Y. Wang, K. Van Tittelboom, N. De Belie, and W. Verstraete, *Use of silica gel or polyurethane immobilized bacteria for self-healing concrete,* Construction and Building Materials **26**, 532 (2012).

[47] J. Y. Wang, H. Soens, W. Verstraete, and N. De Belie, *Self-healing concrete by use of microencapsulated bacterial spores,* Cement and Concrete Research **56**, 139 (2014).

[48] H. X. D. Lee, H. S. Wong, and N. R. Buenfeld, *Self-sealing of cracks in concrete using superabsorbent polymers,* Cement and Concrete Research **79**, 194 (2016).

[49] G. Hong and S. Choi, *Rapid self-sealing of cracks in cementitious materials incorporating superabsorbent polymers,* Construction and Building Materials **143**, 1 (2017).

[50] D. Snoeck, S. Steuperaert, K. Van Tittelboom, P. Dubruel, and N. De Belie, *Visualization of water penetration in cementitious materials with superabsorbent polymers by means of neutron radiography,* Cement and Concrete Research **42**, 1113 (2012).

[51] D. Snoeck, K. Van Tittelboom, S. Steuperaert, P. Dubruel, and N. De Belie, *Self-healing cementitious materials by the combination of microfibres and superabsorbent polymers,* Journal of Intelligent Material Systems and Structures **25**, 13 (2014).

[52] M. Maes, K. Van Tittelboom, and N. De Belie, *The efficiency of self-healing cementitious materials by means of encapsulated polyurethane in chloride containing environments,* Construction and Building Materials **71**, 528 (2014).

[53] O. M. Jensen and P. F. Hansen, *Water-entrained cement-based materials,* Cement and Concrete Research **31**, 973 (2001).

[54] K. Friedemann, F. Stallmach, and J. Kärger, *Carboxylates and sulfates of polysaccharides for controlled internal water release during cement hydration,* Cement and Concrete Composites **31**, 244 (2009).

[55] N. Nestle, A. Kühn, K. Friedemann, C. Horch, F. Stallmach, and G. Herth, *Water balance and pore structure development in cementitious materials in internal curing with modified superabsorbent polymer studied by NMR,* Microporous and Mesoporous Materials **125**, 51 (2009).

[56] D. Snoeck, O. M. Jensen, and N. De Belie, *The influence of superabsorbent polymers on the autogenous shrinkage properties of cement pastes with supplementary cementitious materials,* Cement and Concrete Research **74**, 59 (2015).

[57] A. Pourjavadi, S. M. Fakoorpoor, P. Hosseini, and A. Khaloo, *Interactions between superabsorbent polymers and cement-based composites incorporating colloidal silica nanoparticles,* Cement and Concrete Composites **37**, 196 (2013).

[58] J. S. Kim and E. Schlangen, *Self-healing in ecc stimulated by sap under flexural cyclic load,* ICSHM 2011: Proceedings of the 3rd International Conference on Self-Healing Materials, Bath, UK (2011).

[59] E. Gruyaert, B. Debbaut, D. Snoeck, P. Díaz, A. Arizo, E. Tziviloglou, E. Schlangen, and N. De Belie, *Self-healing mortar with ph-sensitive superabsorbent polymers: testing of the sealing efficiency by water flow tests,* Smart Material Structures **25**, 084007 (2016).

[60] E. N. Brown, M. R. Kessler, N. R. Sottos, and S. R. White, *In situ poly(urea-formaldehyde) microencapsulation of dicyclopentadiene,* **20**, 719 (2003).

[61] J. Y. Wang, K. Van Tittelboom, N. De Belie, and W. Verstraete, *Use of silica gel or polyurethane immobilized bacteria for self-healing concrete,* Construction and Building Materials **26**, 532 (2012).

[62] W. Xiong, J. N. Tang, G. M. Zhu, N. X. Han, E. Schlangen, B. Q. Dong, X. F. Wang, and F. Xing, *A novel capsule-based self-recovery system with a chloride ion trigger,* Scientific Reports **5**, 10866 (2015).

[63] B. Q. Dong, Y. S. Wang, G. H. Fang, N. X. Han, F. Xing, and Y. Y. Lu, *Smart releasing behavior of a chemical self-healing microcapsule in the stimulated concrete pore solution,* Cement and Concrete Composites **56**, 46 (2015).

[64] Y. Wang, G. Fang, W. Ding, N. Han, F. Xing, and B. Dong, *Self-immunity microcapsules for corrosion protection of steel bar in reinforced concrete.* Scientific reports **5**, 18484 (2015).

[65] G. Souradeep and H. W. Kua, *Encapsulation technology and techniques in self-healing concrete,* Journal of Materials in Civil Engineering **28**, 04016165 (2016).

[66] J. F. Hu, H. Q. Chen, and Z. B. Zhang, *Mechanical properties of melamine formaldehyde microcapsules for self-healing materials,* Materials Chemistry and Physics **118**, 63 (2009).

[67] H. Huang, G. Ye, and Z. Shui, *Feasibility of self-healing in cementitious materials – By using capsules or a vascular system?* Construction and Building Materials **63**, 108 (2014).

[68] S. V. Zemskov, H. M. Jonkers, and F. J. Vermolen, *An Analytical Model for the Probability Characteristics of a Crack Hitting an Encapsulated Self-healing Agent in Concrete,* in *Computer Algebra in Scientific Computing: 12th International Workshop, CASC 2010, Tsakhkadzor, Armenia, September 6-12, 2010. Proceedings*, edited by V. P. Gerdt, W. Koepf, E. W. Mayr, and E. V. Vorozhtsov (Springer Berlin Heidelberg, Berlin, Heidelberg, 2010) pp. 280–292.

[69] C. Dry, *Matrix cracking repair and filling using active and passive modes for smart timed release of chemicals from fibers into cement matrices,* Smart Materials and Structures **3**, 118 (1994).

[70] C. Dry and M. Corsaw, *A comparison of bending strength between adhesive and steel reinforced concrete with steel only reinforced concrete,* Cement and Concrete Research **33**, 1723 (2003).

[71] S. Pareek, K. C. Shrestha, Y. Suzuki, T. Omori, R. Kainuma, and Y. Araki, *Feasibility of externally activated self-repairing concrete with epoxy injection network and Cu-Al-Mn superelastic alloy reinforcing bars,* Smart Materials and Structures **23** (2014).

[72] P. Minnebo, G. Thierens, G. De Valck, K. Van Tittelboom, N. D. Belie, D. Van Hemelrijck, and E. Tsangouri, *A novel design of autonomously healed concrete: Towards a vascular healing network,* Materials **10** (2017).

[73] M. D. Banea, L. F. M. da Silva, R. D. S. G. Campilho, and C. Sato, *Smart Adhesive Joints: An Overview of Recent Developments,* The Journal of Adhesion **90**, 16 (2014).

[74] S. Sangadji and E. Schlangen, *Self Healing of Concrete Structures - Novel Approach Using Porous Network Concrete,* Journal of Advanced Concrete Technology **10**, 185 (2012).

[75] H. H. Zhu, S. Zhou, Z. G. Yan, J. W. Ju, and Q. Chen, *A two-dimensional micromechanical damage-healing model on microcrack-induced damage for microcapsule-enabled self-healing cementitious composites under tensile loading,* International Journal of Damage Mechanics **24**, 95 (2015).

[76] S. V. Zemskov, H. M. Jonkers, and F. J. Vermolen, *Two analytical models for the probability characteristics of a crack hitting encapsulated particles: Application to self-healing materials,* Computational Materials Science **50**, 3323 (2011).

[77] Z. Lv, H. Chen, and H. Yuan, *Quantitative solution on dosage of repair agent for healing of cracks in materials: Short capsule model vs. two-dimensional crack pattern,* Science and Engineering of Composite Materials **18**, 13 (2011).

[78] Z. Lv, H. S. Chen, and H. F. Yuan, *Analytical solution on dosage of self-healing agents in cementitious materials: Long capsule model,* Journal of Intelligent Material Systems and Structures **25**, 47 (2014).

[79] F. A. Gilabert, D. Garoz, and W. Van Paepegem, *Stress concentrations and bonding strength in encapsulation-based self-healing materials,* Materials and Design **67**, 28 (2015).

[80] J. F. Su, E. Schlangen, and J. Qiu, *Design and construction of microcapsules containing rejuvenator for asphalt,* Powder Technology **235**, 563 (2013).

[81] B. Hilloulin, K. Van Tittelboom, E. Gruyaert, N. De Belie, and A. Loukili, *Design of polymeric capsules for self-healing concrete,* Cement and Concrete Composites **55**, 298 (2015).

[82] H. Lee, *Potential of superabsorbent polymer for self-sealing cracks in concrete,* Advances in Applied Ceramics **109**, 296 (2010).

[83] X. Yuan, W. Sun, X. Zuo, and H. Li, *The Crack Self-healing Properties of Cement-based Material with EVA Heat-melt Adhesive,* Journal of Wuhan University of Technology-Materials Science Edition **26**, 774 (2011).

3

Synthesis and characterization of PF microcapsules for micro-scale self-healing in cementitious materials

A little fire is quickly trodden out.

William Shakespeare

This chapter presents works towards development of a new type of polymeric microcapsule with phenol–formaldehyde (PF) resin as shell and dicyclopentadiene (DCPD) as healing agent for self-healing microcracks in cementitious materials. The PF/DCPD microcapsules are synthesized via in-situ polymerization and characterized by means of optical microscope (OM), scanning electron microscope (SEM) and thermal analysis (TGA). The chemical stability of synthesized microcapsules and the trigger performance are studied respectively in simulated concrete pore solution and hardened cement paste specimens. The relationship between the physical properties of the synthesized microcapsules and its micromechanical properties are investigated using nanoindentation. X-ray computed tomography (XCT) is applied to observe the status and fracture behaviour of microcapsules inside the cement paste matrix.

Parts of this chapter have been published in Construction and Building Materials **487**, 105 (2016) [1] and Materials **9**, 1025 (2016) [2].

3.1. Introduction

As described in Chapter 1, cracking related deterioration of cementitious materials is one of the most serious threats to the safety, integrity and durability of concrete structures. Once micro-cracks formed in cementitious materials, they are difficult to detect and repair by conventional methods before they show on the surface of the structure, which has long been an extremely difficult question to the maintenance of buildings and infrastructures. Although better structural design, raw material selection and proportion can help to reduce the probability of cracking, further study in searching for a more efficient and automatic way to reduce the maintenance/repair frequency and improve the service life of concrete structures is essentially needed.

In recent years, inspired from biological self-healing phenomena, the microcapsule based [3–8] self-healing concept began to show its great application potential in cementitious materials. Once the incorporated microcapsules are ruptured by the cracks or other stimuli, self-healing is realised through the release and reaction of repairing chemicals in the region of damage. As an essential part in self-healing composites, the properties of the microcapsule (e.g. the shell materials) are believed to have a great influence on the self-healing performance and the mechanical properties of the cementitious composite [9, 10]. Up to date, a wide range of materials have been explored as the shell in microencapsulation [8, 11–13]. Inorganic compounds such as alginate, silica gel and expanded clay [3, 14, 15] have been described to be an effective shell material in fabricating microcapsules for self-healing cementitious materials. Owing to the similar chemical properties, microcapsules with an inorganic shell are generally considered more compatible with the cementitious matrix and may produce a stronger bond between the two phases. However, some of the microcapsules could be ruptured by mechanical mixing during the preparation of cement mixtures and/or the later curing stage due to the loose crumb structure of the inorganic shell. Additional concerns could be the leaching out of healing agent from the mesh structural shell over the long service life of concrete structures and consequently the loss of healing effectiveness and the rising risk of pollution posing on the surrounding environment. Organic compounds such as polystyrene, polyurethane and urea-formaldehyde resin [4, 8, 16] have also been used for encapsulating healing agents in the past decade, while the reliability over time and the trigger sensitivity of capsules have not attracted sufficient attention. Melamine-based organic compounds have been studied as a promising type of shell materials to encapsulate bacterial spores for self-healing concrete [17]. It was illustrated that the synthesised microcapsules can survive the mechanical mixing during the preparation of cement mixtures and the later curing stage. Meanwhile, the microcapsules were demonstrated to rupture under certain tensile force, while the probability for practical application was greatly hindered due to the rigorous requirement for the incubation condition of the bacterial healing agent.

To develop microcapsules which are practically applicable to provide effective self-healing capacity for cementitous materials, three specific requirements need to be met:

(1) the microcapsules are chemically stable in the high alkaline environment of

cement mixtures,

(2) the microcapsules can survive the mechanical mixing while not influencing the trigger sensitivity to cracking and

(3) the diameter of microcapsules is tunable in order to heal cracks in different width ranges.

Thanks to its excellent water, thermal and chemical resistance as well as a low flammability and toxicity, phenol–formaldehyde (PF) resin has been suggested as an promising component of the polymer-cement composites [18, 19]. Compared to other commonly used organic shell materials such as urea-formaldehyde (UF) resin and melamine-formaldehyde (MF) resin, PF resin possesses higher stiffness, brittleness and better tunability of mechanical properties, which make the capsules with a PF resin shell have higher possibility to be triggered during crack propagation.

As for the healing agent, it has been reported that dicyclopentadiene (DCPD) is an effective healing agent for polymers [20] and concrete [21]. When DCPD encounters the Grubbs' catalyst, a transition metal catalyst, the process of opening metathesis polymerization (ROMP) occurs. Owing to its unique properties such as low initial viscosity, high toughness after curing and all-weather applicability, DCPD could pass through and seal the cracks, and further restrain the permeation of external aggressive species with water into cementitious materials [22].

Meanwhile, it is known that the realization of the self-healing function is largely depending on the trigger mechanism of the microcapsules, which will further influence the self-healing efficiency of the system [9, 10]. A good understanding of the mechanical properties of microcapsules is crucial in order to fully understand the trigger behaviour and their performance in their target service environment. In previous studies, mechanical characterization of microcapsules is normally performed by using a cone tip or two parallel plates [23–25]. While, in most cases, microcapsules inside the cement paste are not ruptured by compression stress, but by the tensile stress which initiates the propagating crack. Thus, the data acquired by using a flat tip indenter cannot be used to evaluate the mechanical properties and rupture behaviour of microcapsules that fail due to a mechanical trigger. A method to mimic and analyse the performance of microcapsules that are hit by a sharp crack tip is still necessary.

Accordingly, this chapter presents a new type of polymer microcapsules with excellent chemical/mechanical stability and trigger sensitivity for self-healing of microcracks in cementitious materials using phenol-formaldehyde resin as shell material and dicyclopentadiene (DCPD) as core material (i.e. healing agent). The microencapsulating process, surface morphology and thermal properties of synthesized capsules were investigated using optical microscope (OM), scanning electron microscope (SEM) and thermogravimetric analyser (TGA). The diameter of microcapsules was successfully controlled and further graded into a multiple distribution range without overlapping. The chemical stability of synthesized PF/DCPD microcapsules and the self-healing performance were investigated respectively in simulated concrete pore solution and hardened cement paste. Nanoindentation was applied to measure the micromechanical properties of single microcapsule. In addition, X-ray Computed Tomography (XCT) was used to visualize the distribution

and the rupture process of microcapsules. It is expected that the PF/DCPD microcapsules can provide a new alternative approach for self-healing microcracks in cementitious materials.

3.2. Materials and experimental methods

3.2.1. Materials

Phenol, formaldehyde (37%) and poly(acrylic acid sodium salt)(PAA-Na) (M_w=1200) were obtained from Tianjin Damao Co. (China). Dicyclopentadiene (DCPD) used as the healing agent was purchased from Shanghai Aladdin Co. (China). Sodium hydroxide (NaOH) and hydrochloric acid (HCl) were provided by Tianjin Forever Chemical Reagent Co. (China). Deionized water prepared by Milli-Q 185 system (Millipore, USA) was used for all experiments. All chemicals were of analytical grade without further purification. An ordinary Portland cement (CEMI 42.5N) was supplied by ENCI B.V. (The Netherlands).

3.2.2. Synthesis of PF/DCPD microcapsules

The PF/DCPD microcapsules were prepared by an in situ polymerization procedure following three steps:

(1) Addition reaction of PF prepolymer. 5.0 g phenol and 6.5 g 37 % formaldehyde solution were mixed at room temperature in a 100 ml three-necked flask equipped with a reflux condenser. The three-necked flask was suspended in an oil bath in which a temperature control probe was set. 5 wt% NaOH was added to adjust the pH of the solution to be around 9. The solution was then stirred at 90 °C under a stirring rate of 350 rpm for 90 min until a red transparent PF pre-polymer solution was obtained.

(2) Emulsion and agitation. 7.0 g DCPD was added to 50 g surfactant aqueous solution containing 7 g PAA-Na under a stirring rate of 1000 rpm. The resulting suspension was continually agitated at 65 °C for 20 min to separate the DCPD from the water. Upon the completion of emulsion, the PF pre-polymer solution and the emulsion was transferred to a 250 ml three-necked flask and mixed for 10 min under a stirring rate of 350 rpm.

(3) Condensation reaction of PF resin. 50 g 2 wt% HCl was added to adjust the pH of the reaction system to be around 1. Then the system was heated at a rate of 1 °C min^{-1} till it reached the polycondensation temperature of 90 °C and maintained for 3.5 h. After the reaction has completed, the suspension containing microcapsules was cooled down to room temperature. The microcapsules were then collected by filtration and dried in air for 5h until obtaining a sand-like free-flowing powder.

3.2.3. Characterization of PF/DCPD microcapsules

Morphology and shell thickness determination

The morphology and the core/shell structure of the synthesized PF/DCPD microcapsules were characterized by an environmental scanning electron microscope (ESEM) (XL30, Philips, the Netherlands). All imaging were performed in low vacuum. The

rupture pattern and its trigger behaviour of the PF microcapsules were observed using an optical stereoscopic microscope (OM) (VHX-600K, Keyence, Japan).

The shell thickness and diameter of microcapsules were determined from the optical microscope (OM) graphs of the cross-section of microcapsules using a commercial dimensional measurement software. Firstly, the diameter of single microcapsule was recorded under the microscope. After that, the microcapsule of which the diameter has measured in advance was then compressed to rupture between two glass sheets. The shell thickness of this microcapsule was determined from the debris of the shell. In this test, a total of 50 microcapsules were randomly selected and the measurements were performed 2 times on each microcapsule at a different position.

Size distribution analysis and gradation

The mean size and size distribution of synthesized microcapsules, produced under different stirring rate, was determined using a laser particle size analyzer (LPSA, BT-9300ST, Bettersize Instruments Ltd., Dandong, China). Before the test, microcapsules were washed with deionized water and then placed in a drying box at 60°C for 24 hours. Then 1g microcapsules was dispersed by 50ml deionized water in the analysis box. The value of volume-based mean diameter ($D_{4,3}$) and the value of distribution span (SPAN) were calculated automatically by the instrument. The $D_{4,3}$ and SPAN are defined by the following equations:

$$D_{4,3} = \frac{\sum_{i=1}^{n} d_i^4}{\sum_{i=1}^{n} d_i^3} \tag{3.1}$$

$$SPAN = \frac{D_{90} - D_{10}}{D_{50}} \tag{3.2}$$

Where D_{90}, D_{10}, D_{50} represent the diameter when the cumulative volume fraction of the measured particles is 90, 10 and 50 %, respectively; d_i is the diameter of a single microcapsule and n is the number of microcapsules which is measured. The gradation of microcapsules was realized through sieving the microcapsules with different mesh sizes (30, 40 and 70). The size distribution of the microcapsules after sieving was then measured from the OM images of microcapsules using a commercial dimensional measurement software. For each diameter range, at least 50 samples were randomly recorded.

3.2.4. Stability investigation

Thermal stability

The thermal stability of the synthesized microcapsules as well as the healing agent (DCPD) and the PF resin shell of the microcapsules were measured using a TGA analyser (Q50, TA Instruments, USA) under flowing nitrogen (40 ml/min) at a heating rate of 8 °C/min from 25 to 600 °C.

Chemical stability

The chemical stability of the PF/DCPD microcapsules was investigated by exposing them to simulated concrete pore solution. As described in Reference [26], a saturated Calcium hydroxide solution (pH ≈ 13) was used to simulate the highly alkaline concrete pore solution. After being immersed in the saturated Calcium hydroxide solution for 3 h and 48 h, the microcapsules were collected by filtration and washed thoroughly by de-ionized waster. Afterwards, the microcapsules were put in between two parallel glass plates and compressed to rupture allowing the release of the microencapsulated healing agent.

3.2.5. Micromechanical properties of PF microcapsules

Elastic modulus measurement

Nanoindentation was use to obtain the elastic modulus of the shell material and the mechanical response of microcapsules. For the measurement of pure shell material, a large block of pure PF resin was made in advance by exactly the same reaction condition as for the preparation of PF microcapsules. Then the synthesized PF resin block was placed in microtome to cut into a regular flat piece. Before the nanoindentation test, the surface of the sample is ground by four different grinding papers (500#, 800#, 1200#, 4000#). Then the sample was polished by hand on a lapping table using diamond paste with particle diameter of 6 m, 3 μm, 1 μm and 0.25 μm. During the measurement, a total of 15 points were selected to test and the indentation depth was set to 2000 nm. The Continuous Stiffness Method was adopted to run the test [27]. The average elastic modulus was determined in the displacement range between 1000 and 1800 nm.

Then the punching test was performed on microcapsules by nanoindentation. Before the test, microcapsules with different diameter were selected and glued on a glass sheet by a heat-softening glue. To be more specific, the glass slide was first placed on a heated plate of 70 °C. Then the heat-softening glue was smeared on the glass slide and a blade was used to make a thin and uniform glue layer. The microcapsules were then carefully scattered on the slide. After the slide was removed from the heated plate, the glue hardened and the microcapsules were fixed. A diamond Berkovich tip was used for this nanoindentation test. The geometrical characteristics can be found from the referred work of Oliver and Pharr [27]. A quartz standard was indented before and after each test to ensure the accuracy. In this test, the allowable drift rate was 0.15 nm/s, the surface approach velocity was 20 nm/s. The indentation depth was 1000 nm. In this study, the elastic modulus of the shell microcapsule was defined at the linear phase of load-displacement curve as the mean value in the displacement ranging from 600 to 900 nm.

Rupturing force measurements

In order to investigate the required rupture force of the microcapsules under the strike of a crack, a diamond Berkovich tip was used here as a mechanical trigger. In this test, total 50 microcapsules with different size range were selected and fixed on the sample holder using the aforementioned method. Before the test, each micro-

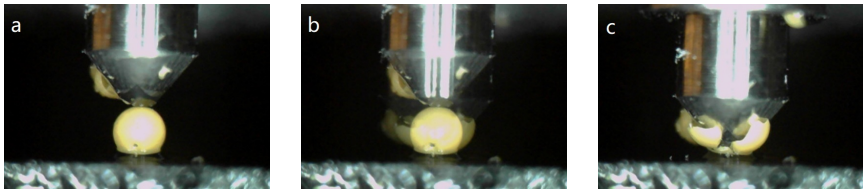

Figure 3.1: Dynamic process of a microcapsule under the rupturing-force measurement.

capsule was photographed from the top by the inset camera of the nanoindentation equipment. The obtained images were used to measure the diameter of each microcapsule. The indent test was performed at the selected physical centre of the microcapsules. To ensure the rupture of the microcapsule, the indentation depth was set to 5000 nm. To visualize the rupture process, a video camera was attached to the sample holder. After the test, the images of ruptured microcapsules were taken again from the top. Figure 3.1 shows the rupture process of a microcapsule under the hit of a Berkovich indenter.

3.2.6. Investigation in cement paste

Sample preparation

The cement paste specimens were prepared with a water-to-cement ratio of 0.4. In which, 4 % of cement mass was replaced by PF/DCPD microcapsules. The microcapsules were first dry mixed with cement in a mixer for 1 min, and then deionized water was added and stirred for one minute to achieve a good workability. After mixing, the fresh mixture was cast in cylindrical moulds (diameter 6.7 mm and length 13.4 mm) for XCT imaging. Then they were carefully compacted on a vibrating table for 30 seconds to reduce the entrapped air. The specimens were demoulded after curing under room temperature (RT) and local lab environment for 48 h and cured in a wet chamber at 25 °C and 95 % relative humidity. After curing for 28 days, samples were taken out from the curing room. A notch was made at half of the hight of sample. The cylinders were fractured by a uniaxial tension testing machine to generate a crack in the middle of the specimens. To keep the original position of the fractured sample, before the test, the cylindrical sample was wrapped by plastic membrane.

Trigger behaviour of microcapsules

X-ray computed tomography (XCT) (Nanotom, GE Inspection Technologies, LP, Lewistown, USA) was applied to investigate the status of microcapsules within hardened cement paste. The raw XCT images were acquired at an acceleration voltage of 50 kV with an exposure time of 4 s and X-ray power of 8 W. The resolution of CT scans is set to 7.5 µm. The final data set of XCT consisted of 720 radiographs of which each image was acquired with a 0.5 ° rotation. Then phase retrieval and tomographic reconstruction were performed to improve the boundaries and signals using the software supplied by the manufacturer. A series of reconstructed tomographic images (X-Z plane) were consequently imported into a commercial software

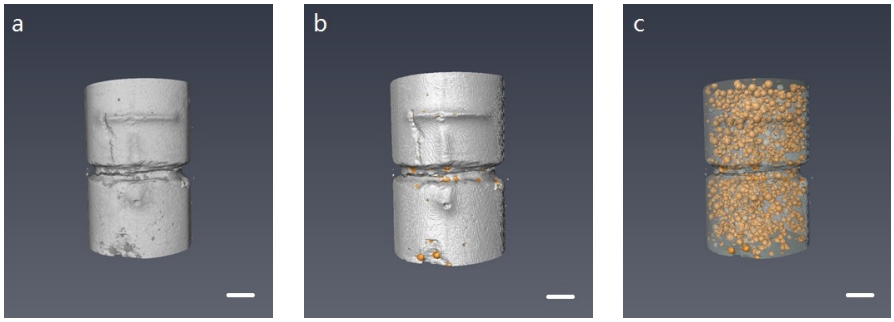

Figure 3.2: XCT visualization process of microcapsules' embedded cement paste cylinder including (a) volume construction; (b) surface generation; and (c) transparent adjusting. The scale bar is 2 mm for all three images.

(Avizo 9.0) for segmentation and 3D visualization. The first step of the visualization involves converting the 2D image into the software and generating a 3D volume (Figure 3.2a). After that, a surface generation step is performed on the volume to separate the sample into 2 materials with different color: cement matrix (gray), microcapsules (yellow) (Figure 3.2b). The cement part was then set as transparent so that the status of microcapsules can be clearly seen (Figure 3.2c). To calculate the trigger ratio of microcapsules on the crack surface, the upper half of the crack zone was manualy isolated from the ROI (region of interest) in the software.

3.3. Results and discussion

3.3.1. Formation mechanism of PF/DCPD microcapsules

The formation process of PF/DCPD microcapsules and relevant chemical reactions are illustrated in Figure 3.3. Poly(acrylic acid sodium salt) (PAA-Na) is a linear water soluble polymer. In this study, low molecular weight PAA-Na (M_w = 1200) was applied as an emulsifier to form a stable oil-in-water (O/W,DCPD/water) emulsion. Due to its special chemical structure, the long carbon chains of PAA-Na tend to aggregate on the surface of oil drops stabilizing the emulsion. This further prevents the amalgamation of DCPD droplets by forming a colloid film [28]. As shown in Figure 3.3a, under mechanical stirring, the DCPD core is wrapped by linear PAA-Na of which the hydrophilic carboxylic groups (–COONa) stretch out as a result of the effect of ion exclusion. Then PF pre-polymers are added and the PF oligomers are attracted to the O/W interface via electrostatic force between the methylene group ($–CH_2^-$) of the PF pre-polymer and the carboxylate group of PAA-Na. Upon acidification by adding 2 wt% HCl solution, the condensation reaction (i.e., dehydration) occurs between the methylol groups of PF pre-polymers on the oil surface resulting in the formation of a hard and brittle PF resin shell. Figure 3.3b describes the possible mechanism of the interactions between carboxylic group and hydroxymethyl group and the in situ condensation reaction of PF shell on the surface of emulsified DCPD oil droplets.

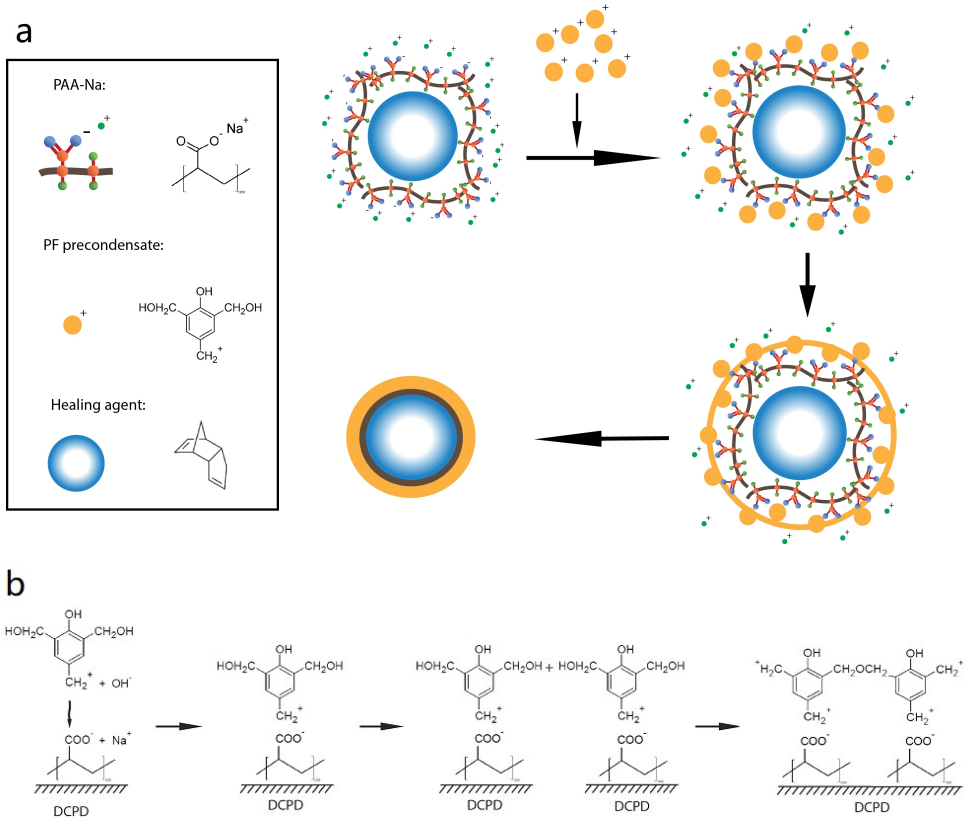

Figure 3.3: Schematic illustration of (**a**) the synthesis route of PF shell/DCPD core microcapsules via in situ polymerization and (**b**) the possible mechanism of the interactions between the carboxylic group and hydroxymethyl group and the condensation process of PF resin.

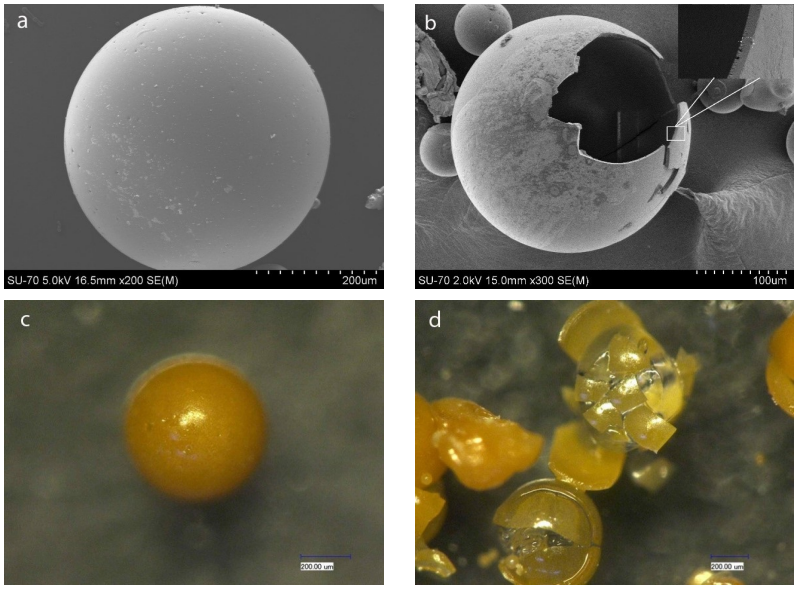

Figure 3.4: SEM of (**a**) surface morphology of the microcapsule, (**b**) ruptured microcapsule and wall thickness and OM images of (**c**) a single microcapsule and (**d**) broken microcapsules compressed by two parallel glass sheets.

3.3.2. Morphology of PF/DCPD microcapsules

Figure 3.4 shows the typical SEM and OM images of an intact and a ruptured PF/DCPD microcapsules. As can be seen from Figure 3.4a that the microcapsule possesses a regular globe shape and smooth surface. Figure 3.4b shows that the shell of the microcapsules is homogeneous with a brittle rupture pattern. In addition, a distinctively low shell thickness/diameter ratio of the synthesized microcapsules offers an ideal storage capacity for retaining the healing agent. The brittle rupture pattern and the high storage capacity of the microcapsules are believed to be of critical importance for self-healing applications in cementitious materials [9]. The OM images as shown in Figure 3.4c indicate that microcapsules are separated from each other with limited agglomeration featuring a PF resin shell with a clear brown color. As shown in Figure 3.4d, the healing agent (DCPD) was detected in the core when the microcapsules were pressed to rupture by compressive force. The combined information from SEM and OM clearly suggests that the PF shell/DCPD core microcapsules with regular globe shape and smooth surface have been successfully synthesized.

3.3.3. Size study

Shell thickness

The shell thickness and diameter of microcapsules were determined from ESEM images of the cross-sections and then calculated by a commercial dimensional measurement software. Due to the brittle nature of the PF resin, after the microcapsules

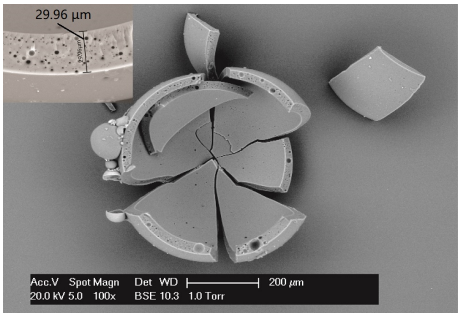

Figure 3.5: Morphology of a ruptured PF microcapsule. Insert is an enlarged image showing the thickness and structure of the shell of synthesized PF microcapsules.

were ruptured by compression, a clear image of a core-shell structure of the microcapsule can be observed under the microscope. A typical morphology of ruptured microcapsules is shown in Figure 3.5. A distinctively low shell thickness/diameter ratio of the microcapsules is obtained. This low ratio offers an ideal storage capacity for the healing agent, which is believed to be a desired feature for self-healing in cementitious materials. The insert image in Figure 3.5 is a magnified image of the shell. It shows that the shell thickness of this microcapsule is 29.96 µm. Meanwhile, it was found that the shell is porous. The pores on the shell are believed to have already formed during the synthesis process. While, as can been see from the Figure, the vast majority of these pores are all embedded pores and the size is very small compared to the thickness. Therefore it will not result in a leakage of healing agent. Figure 3.6 summarizes the relationship between shell thickness and diameter. The result demonstrates that, although the shell thickness to diameter ratio does not show an obvious linear relation and the coefficient of variation is up to 41.24 %, the distribution interval of shell thickness is still found to have an increasing trend with the increase of capsule's diameter. It should be mentioned that, for better expressing the relationship between the shell thickness and the diameter, those data points obtained from microcapsules with shell thickness to diameter ratio at the top or at the bottom 5 % of total data were not included in this calculation.

Size distribution analysis

The size distribution of synthesized microcapsules was measured and analyzed by a particle size analyzer. The typical size distribution curves of microcapsules prepared at different stirring rates (300, 350, 400 and 500 rpm) is shown in Figure 3.7a. Then the effect of stirring speed in the synthesizing process on the mean size ($D_{4,3}$) and size distribution width (SPAN) of the microcapsules prepared at different stirring rates (300, 350, 400 and 500 rpm) was studied. As can be clearly seen from Figure 3.7b, with the increase of stirring rate, the volume-based mean diameter ($D_{4,3}$) of the synthesized microcapsules decreased significantly from 352.2 to 218.5 µm. Simultaneously, the size distribution becomes narrow when the stirring rate increases, which can be reflected from the decrease of SPAN value from 1.667 to 0.831. These results indicate that the mean diameter and the size distribution of

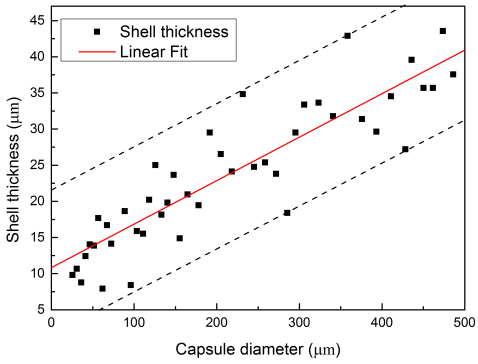

Figure 3.6: Relationship between the diameter and shell thickness of microcapsules.

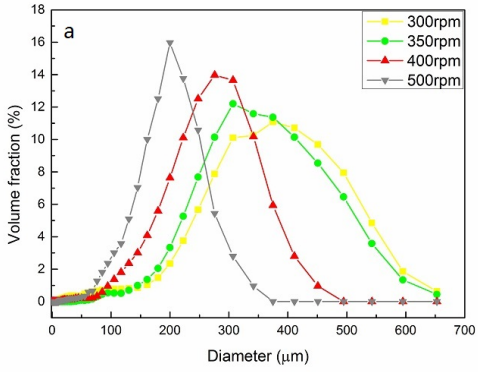

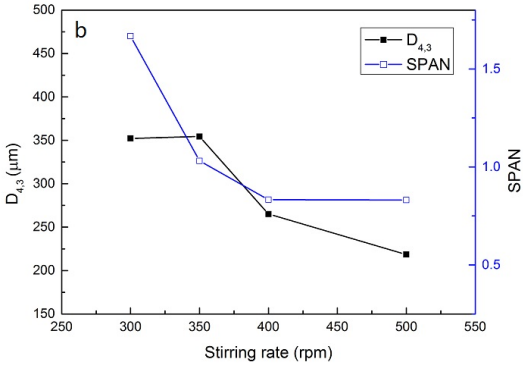

Figure 3.7: Size distribution of PF microcapsules prepared at various stirring rates (300, 350, 400 and 500rpm) (**a**) and its corresponding $D_{4,3}$ and SPAN values (**b**).

microcapsules can be controlled by varying the stirring speed during the polymerization process. Similar results can also be found in previous report in a literature by Junfeng et al. [29].

3.3.4. Stability investigation

Thermal stability

The thermal properties of the synthesized microcapsules as well as the shell material (PF resin) and core material (i.e. healing agent, DCPD), were investigated by thermogravimetric analysis (TGA). The thermal stability of the microcapsules can be reflected from the temperature of decomposition. The measured curves are represented in Figure 3.8. For synthesized microcapsules (Figure 3.8a), two major mass losses of 25 % from 125 to 250 °C and 35 % beyond 410 °C can be observed. A similar trend of mass loss including two major effects was observed for the hardened shell material (i.e. polymerized PF resin) (Figure 3.8b). The first weight loss of 5 % in the range of 125 – 250 °C can be attributed to the partial degradation of the phenolic backbone with the evaporation of residual phenol from the PF matrix. The second weight loss beyond 408 °C corresponds to the complete decomposition of PF resin. The higher percentage of the first mass loss for microcapsules which was about 4 times higher (25 % vs 5 %) with respect to the pure PF shell material, is attributable to the partial decomposition of PF resin shell and the subsequently flowing out and evaporation of the encapsulated healing agent (DCPD). This is further evidenced by the occurrence of several small stepwise mass losses in the first major mass loss stage of the synthesized microcapsules (Figure 3.8a) and the TGA curve of pure healing agent (DCPD) (Figure 3.8c) which shows a complete weight loss between 30 and 120 °C. Nevertheless, the measured three TGA curves as show in Figure 3.8 imply that the healing agent (DCPD) has been successfully encapsulated in the synthesized microcapsules and the thermally stable temperature of the microcapsules is 125 °C, which is much higher than the temperature (80 °C) occurred during the cement hydration [30]. Obviously, the high thermal stability of the PF/DCPD microcapsules essentially ensures their application in cementitious materials and can properly prevent the leaking of healing agent from the microcapsules.

Chemical stability

At the initial stage of cement hydration, there is a large amount of $Ca(OH)_2$ generated as a hydration product of the tricalcium silicate (C_3S). The produced $Ca(OH)_2$ can dissolve in the water of cement paste, resulting in a fast increase of the pH value (pH_{max} > 13). Consequently, this high alkalinity of concrete pore solution could become a threat to the survival of any type of microcapsules that are used in cementitious materials. In this study, the chemical stability of PF microcapsules in simulated concrete solution (saturated calcium hydroxide solution) was investigated at ambient temperature. As can been in Figure 3.9a, after 48 h immersion, the microcapsule maintained its original shape while the surface of the microcapsule was covered with a layer of granular substance. The formation of this granular layer is believed to result from the adsorption of the airborne carbon dioxide by the

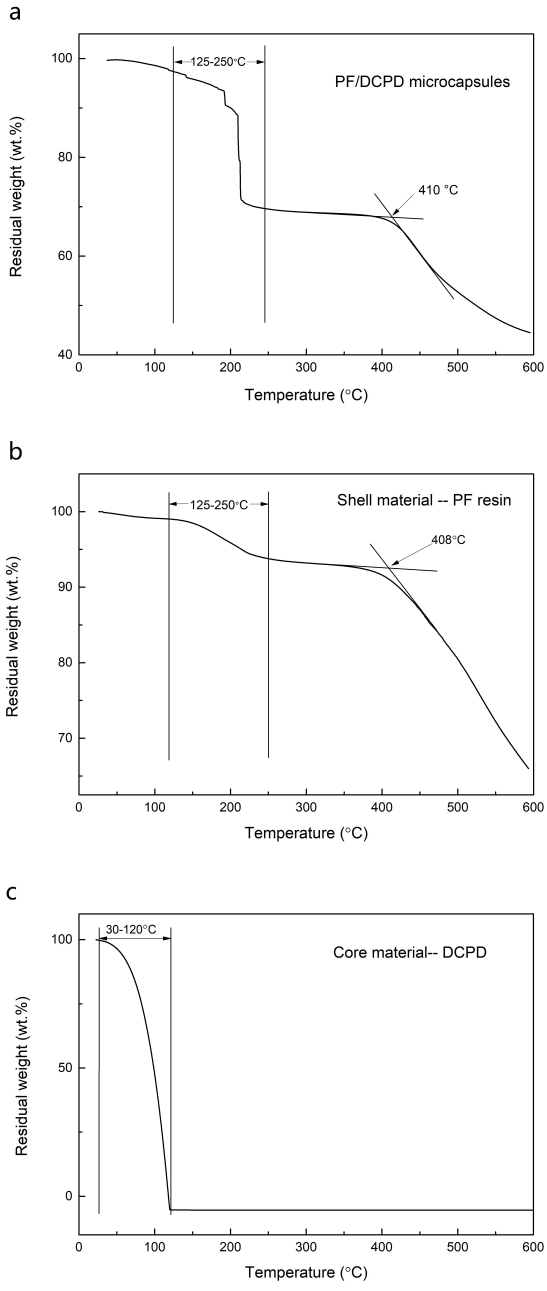

Figure 3.8: TGA curves for (**a**) synthesized PF/DCPD microcapsules, (**b**) PF resin and (**c**) DCPD healing agent.

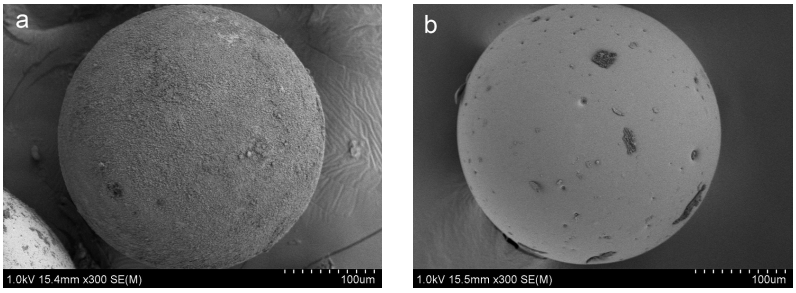

Figure 3.9: SEM images of (a) microcapsule immersed in simulated concrete pore solution for 48 h and (b) microcapsules washed with deionized water after 48 h immersion in simulated concrete pore solution.

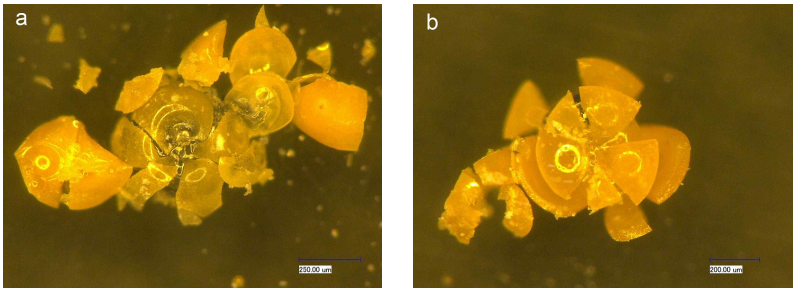

Figure 3.10: OM images of ruptured PF/DCPD microcapsules after immersed in simulated pore solution for (**a**) 3 h and (**b**) 48 h.

calcium hydroxide in the solution, which consequently produced a layer of calcium carbonate depositing on the surface of the microcapsule. The microcapsule was then washed by deionized water. As can be seen from Figure 3.9b, the cleaned microcapsule maintained its regular round shape indicating that the $CaCO_3$ deposits had no negative effect on the microcapsules.

The status and availability of the encapsulated healing agent were investigated by rupture of the microcapsules through compression. Figure 10a and Figure 10b give respectively the OM images of the microcapsules ruptured after 3 h and 48 h immersion in simulated concrete pore solution. As can be seen in these figures, the shell of the microcapsule was uniform and the healing agent (DCPD) was clearly detected in the core of the microcapsule. No difference could be found in appearance of microcapsules comparing with fresh prepared microcapsule and apparently the healing agent was protected properly by the shell material. In summary, the combined observation from both SEM and OM suggests that the highly alkaline environment has no or minor influence on the synthesized microcapsules and the encapsulated healing agent can be released upon rupture of the microcapsules.

3.3.5. Mechanical properties study of a single microcapsule

For mechanically triggered microcapsules, the understanding of the micromechanical properties of a single microcapsule is a fundamental and crucial aspect. In previous reports, the parallel plate compression apparatus [31] is commonly used to investigate the mechanical properties. Parameters about the shell such as elastic modulus have been calculated using the data obtained by the compression force profiles with fractional deformation. While in the real case of cementitious material cracking, the tip of a crack is normally regarded as a point of concentrated stress. Therefore, the fracture force (or bursting force) of microcapsules acquired by parallel plate compression cannot be used to simulate and investigate the trigger behaviour of microcapsules under the strike of a crack. To understand the mechanical properties and trigger behaviour of microcapsules in a more realistic way, a Berkovich indenter and nanoindentation technology is used to characterize the mechanical properties of a single microcapsules in this study. The elastic modulus of the shell and the rupture force of microcapsules is calculated directly by the software of the nanoindentation system.

Elastic modulus

The elastic modulus of the shell material and the PF microcapsules was obtained by performing nanoindentation tests on surface-polished shell material and on a single microcapsule, respectively. Figure 3.11 shows the mean E modulus of microcapsules and shell materials. No relationship was found between the E-modulus of microcapsules and its diameter. The mean E modulus of microcapsules is 2.2 $\pm$ 0.8 GPa which is significantly lower than that of pure shell materials with the value of 5.5 $\pm$ 0.8 GPa. The possible reason for this difference can be attributed to the deformation of microcapsules during the measurement and can also be partly attributed to the microcapsule being pushed into the glue. More information on structural effects when testing capsules with nanoindentation can be found in reference [32, 33]. In this test, the Continuous Stiffness Method developed by Oliver and Pharr [27] was used. The basic idea of this method consists of superimposing small displacement on the primary loading signal and in real time analyse the response of the system by using a frequency-specific amplifier. The E modulus is obtained by a continuous measure of contact stiffness (S) as a function of indentation depth (h). While, when the nanoindentation test performed on the microcapsule, the indent force which imposed on microcapsules will not only results in the Berkovich tip penetrating into the surface, but also makes the microcapsule having a deformation, which will finally increase the indentation depth and further decrease the value of elastic modulus. The porosity of the shell will also result in differences in properties of the microcapsules, which is for instance reflected by a scatter in E-modulus. To better understand the correlation between the E-moduli and the properties of microcapsule such as diameter and shell thickness, numerical modeling method will be used in a later stage.

Rupture force and trigger sensitivity investigation

It is expected that each microcapsule which embedded in self-healing cementitious materials will fracture when a crack encounters that microcapsule. The fact

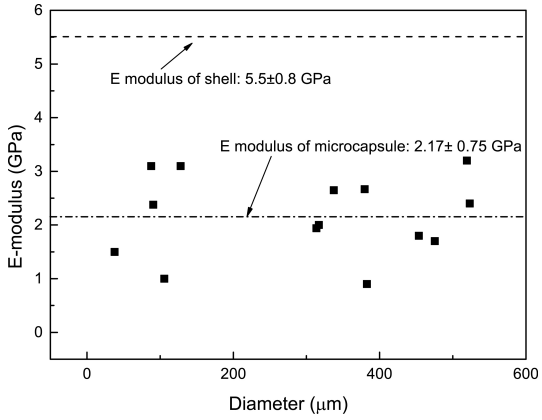

Figure 3.11: Elastic modulus of shell material and PF microcapsules, and its relationship with the diameter of the microcapsules.

is that in practice the trigger force which is imposed on the microcapsules can vary due to the nature and the width of crack. To increase the healing efficiency and prolong the working life, it is ideal that the microcapsules have a different trigger sensitivity based on the crack width. So that, microcapsules can be triggered accordingly to cracks with different crack opening. From previous research, it is known that the bursting force of microcapsules is related to their diameter [31]. In this respect, to achieve the multi-scale trigger function of cementitious materials, the application of microcapsules with different diameters is essential. In this study, a sieve method was used to grade the synthesized microcapsules into several interval scales. Thanks to the excellent dispersibility and mechanical properties of the synthesized PF microcapsules, a gradation of microcapsules was successfully achieved. Figure 3.12 shows the size distribution of the PF/DCPD microcapsules after sieving made at a stirring rate of 400 rpm. As can be seen from the figure that, by passing the microcapsules through a series of sieves with mesh sizes of 30, 40, 70 (590, 420 and 210 μm in diameter), the particle size of the synthesized microcapsules ranging from 50 to 550 μm, has been isolated into three intervals, small size (50-200 μm), medium size (200-400 μm) and large size (400-600 μm), respectively. Inserts gives the OM images of the sieved microcapsules. They are in accordance with those three size distribution regions shown below.

For further investigation of the trigger sensitivity of microcapsules at different size gradation, the rupture force of single microcapsules was measured by nanoindentation. Before the test, the diameter of single microcapsules was measured under the built-in microscope. Figure 3.13a shows the relationship between the rupture force and the diameter of microcapsules. Specifically, the mean rupture force for small size (50-200 μm) microcapsules is 68.5 $\pm$ 41.6 mN. This number goes up to 96.8 $\pm$ 23.5 mN for medium size (200-400 μm) microcapsules. With the increase of diameter to the range of large size (400-600 μm), the rupture force of microcapsules increased continuously. The mean rupture force of large size mi-

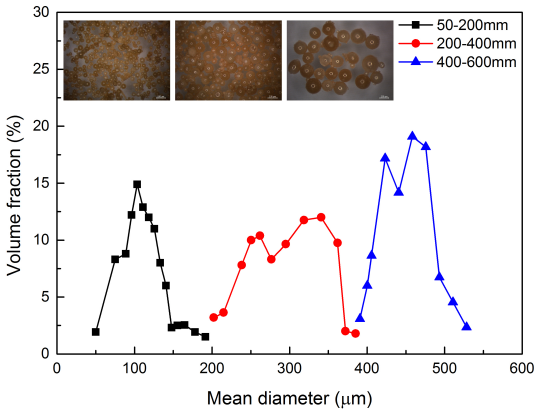

Figure 3.12: Size distribution of the PF microcapsules screened by sieves with various mesh size (30, 40 and 70).

crocapsules is 198.5 $\pm$ 31.6 mN. Despite the scatter, the rupture force shows a increasing trend with the diameter, a similar behaviour can be found in a previous study for thin-shell PMMA microcapsules [31].

After the indentation test, the shell thickness of the ruptured capsules was measured by optical microscopy. Then the relationship between the rupture force and the shell thickness of microcapsules was determined. Figure 3.13b shows the relationship between the rupture force and the shell thickness. As we can see from the figure, the rupture force which is required to break the capsules increases with the capsule shell thickness. In general, it can be concluded that both the increase of capsule size and shell thickness do have influence on the trigger sensitivity of microcapsules. The bigger the size or the thicker the shell of the capsule is, the larger force will be needed to break it. These properties of the synthesized microcapsules can be used for self-healing systems, in which the microcapsules can react according to the strength of the material or the width of the crack.

Finally, the rupture force was tried to correlate with shell thickness/diameter ratio (Figure 3.13c). Unlike previous research for MF microcapsules [29], a heavily scattered decreasing trend was observed between the rupture force and shell thickness/diameter ratio. The possible reason for this decrease comes from the different growth rate of shell thickness and diameter. With the increase of microcapsules capsule diameter, bigger capsule will normally have a relative low shell/diameter ratio. As it has been proofed from figure 3.13a that, for this type of microcapsules, bigger size need a larger force to be ruptured. Therefore, for a microcapsule with low shell/diameter ratio, it is reasonable to have a higher rupture force and vice versa.

3.3.6. Investigation in hardened cement paste

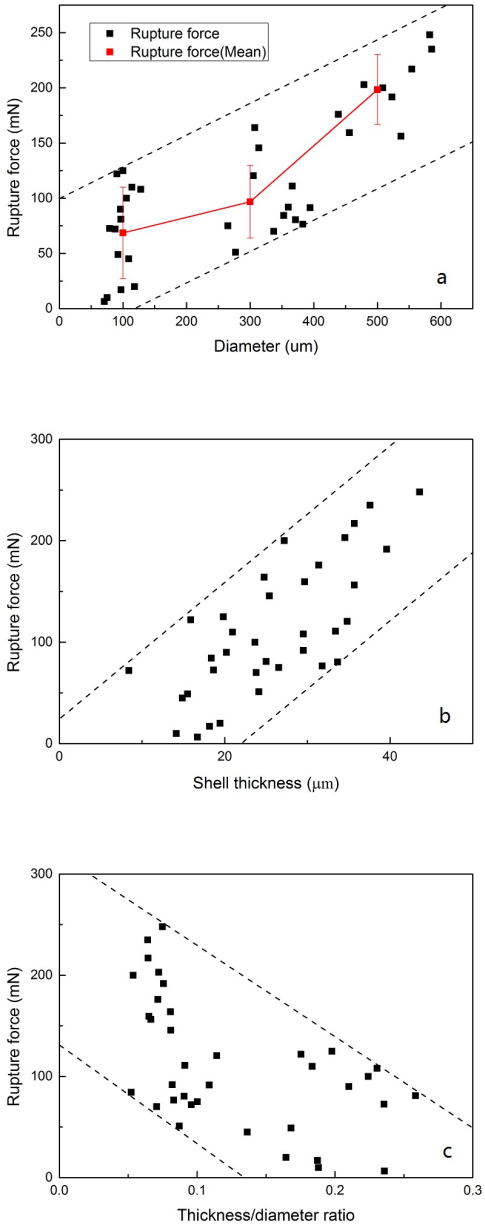

Figure 3.13: The relationship between the rupture force of PF microcapsules and its (**a**) diameter (**b**) shell thickness and (**c**) thickness/diameter ratio

Crack-Zone investigation

XCT is a versatile inspection technique which has been widely applied in numerous fields of research [34, 35]. Recently, the application of this technique has also been extended to the field of civil engineering [36, 37]. As a non-destructive imaging technique, XCT provides an approach to obtain the internal information of a material [38]. In this study, the XCT imaging technique combined with data reconstruction and image segmentation software was used to visualize the trigger behaviour of the microcapsules incorporated hardened cement paste specimens which are tested in tension. To investigate the rupture behaviour of microcapsules along the crack zone, a small region of the cylinder adjacent to the crack was selected as ROI (Region of interest). Then different materials of the reconstructed segments were color labeled. Figure 3.14a shows the 3D representation of the ROI, where the microcapsules, the crack and the cement were defined as yellow, blue and grey color, respectively. The spatial dispersion of microcapsules along the crack demonstrates that the synthesized PF microcapsules can not only be well dispersed but also kept stable in cement paste specimens. For further visualizing the crack surface of the ruptured sample, the upper half of the crack zone was selected form the ROI. Figure 3.14b shows the top-down view of the segmented crack surface. As can be seen from the figure that, when the crack goes through, a portion of the microcapsules was mechanically triggered by the crack. Meanwhile, there are still a large amount of microcapsules which cannot be triggered, leaving voids and untriggered microcapsules at the crack. It is believed that the voids come from the microcapsules which do not break but are pulled out of the matrix, where the crack goes around rather than through the microcapsules.

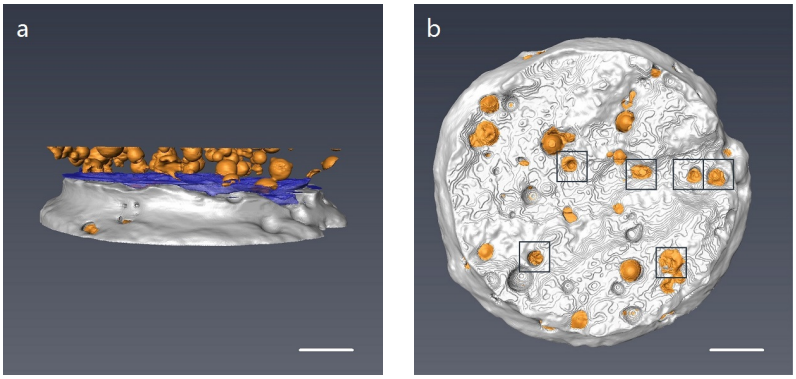

Figure 3.14: 3D reconstructed images of the segmented raw data showing the crack(blue), microcapsules(yellow) and cement(grey); (**a**) a selected section of fractured cement paste in the vicinity of the crack (**b**) a top-down view of crack surface. Ruptured microcapsules are indicated by black square box. The scale bar is 1 mm for both images.

By inspecting the crack surface of XCT reconstructed samples containing (1) large size (400-600 µm), (2) medium size (200-400 µm) and (3) small size (50-200 µm) microcapsules, the number the triggered, untriggered microcapsules (MC) and the voids were counted manually and the statistic results were shown in ta-

Table 3.1: Trigger ratio microcapsules along the crack of cement paste with a diameter (1) 400-600, (2) 200-400 and (3) 50-200 µm

Sample No.	Ruptured MC	Unruptured MC + Voids
1	8.6%	91.4%
2	20.7%	79.3%
3	34.7%	65.3%

ble 3.1. It was found from the table that, for large size microcapsules (400-600 µm) embedded in cement paste samples, only 8.4 % of those microcapsules were triggered on the path of the crack. With the decreasing of diameter from large size to medium size (200-400 µm), the trigger ratio of microcapsules increased sharply from 8.4 % to 20.7 %. This number goes up to 34.7 % when the size of embedded microcapsules decreases from 200-400 µm to 50-200 µm. This results together with the relationship between rupture force and diameter obtained above demonstrates that, the size distribution of microcapsules will influence the trigger efficiency of capsule-based self-healing systems. Smaller size of the synthesized PF microcapsules (50-200 µm) tend to be easier to be ruptured by the crack in cement paste.

Fracture surface investigation

The self-healing function of mechanical trigger microcapsules in cementitious materials is finally realized through the rupture of microcapsules followed by the release of healing agent to the cracks. OM image of a ruptured microcapsule captured on the fracture surface of the paste specimen was shown in Figure 3.15. It can be clearly seen from this image that the microcapsules was ruptured by the crack with the rest of this microcapsules tightly embedded in paste matrix. This image indicates that the synthesized PF/DCPD microcapsules are able to be mechanically triggered by cracking.

For further examination of the feasibility of the synthesised PF/DCPD microcapsule, a preliminary test was carried out to testify the release behaviour of the healing agent (i.e., DCPD) in cement paste. To do this, a microcapsule containing cement paste specimen was bent to fracture and subjected to 30 °C heating in order to speed up the visualization of the flowing of DCPD out of the microcapsules. The newly formed fracture surface with the ruptured microcapsules of this cement paste sample was recorded immediately by OM. As can be observed in Figure 3.16a, the healing agent indeed flew out of the microcapsules around which a dark area was clearly noted. This cement paste sample was then kept heated for ten more minutes and the OM image was recorded again as shown in Figure 3.16b. It was noted that there was an obvious contrast between the rupture surface before and after the sample was kept heated for 10 min featuring the gradual disappearance of the surrounding dark (Figure 3.16b). The main reason for this phenomenon can be attributed to either the absorption of DCPD by the cement matrix or the evaporation of DCPD into the air. This result together with information obtained in Figure 3.14 revealed that the self-healing function of the embedded PF/DCPD mi-

Figure 3.15: OM image of fracture surface with a ruptured microcapsule triggered by crack propagation.

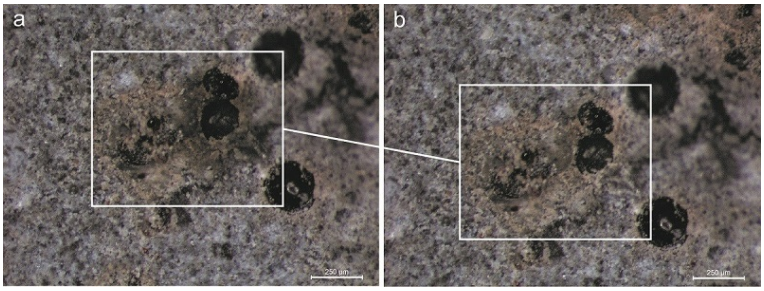

Figure 3.16: OM images of fractured surface of a cement paste specimen incorporated with PF/DCPD microcapsules (**a**) upon heating at 30°C and (**b**) after 10 min heating at 30°C. The scale bar is 250 µm for both images.

crocapsules could be triggered by cracking and the healing agent could be released simultaneously to heal the cracks.

3.4. Conclusion

In this chapter, a new type of phenol-formaldehyde resin (PF resin) shell / dicyclopentadiene (DCPD) core microcapsule for self-healing microcracks in cementitious materials was synthesized via in situ polymerization. The microencapsulating process, surface morphology and shell thickness of synthesized capsules were investigated using optical microscope (OM) and scanning electron microscope (SEM). Thermogravimetric analysis was employed to study the thermal property of the synthesized PF/DCPD microcapsules. The chemical stability of PF/DCPD microcapsules was studied in saturated calcium hydroxide solution. The relationship between the physical properties of the synthesized microcapsules and its micromechanical properties were investigated using nanoindentation. A berkovich tip was used to mimic the behaviour of cracking to get the rupture force of PF microcapsules. The trigger

behaviour of the PF microcapsules was observed and analyzed using XCT based on a microcapsule-embedded cement paste sample. Finally, the crack surface of the sample was inspected by OM. Based on the above findings, the following conclusion can be drawn:

- The synthesized microcapsules possess a regular spherical shape and smooth surface with a distinctively shell thickness/diameter ratio.
- The mean diameter and the distribution of microcapsules could be controlled through adjusting the agitation rate during the synthesis.
- Thermogravimetric analysis showed that the microcapsules had a high thermal stability against the heat that can be generated during cement hydration.
- The chemical stability results revealed that the PF/DCPD microcapsules exhibited excellent stability in both simulated pore solution and real cement environment.
- The mechanical result shows that with the increase of the mean size of microcapsules and the decrease of shell thickness, the mechanical force which is required to trigger the breakage of the microcapsules increased correspondingly.
- Segmentation and 3D rendering of the reconstructed data obtained from XCT showed that the microcapsules had a good dispersibility and could be triggered by the crack. The result demonstrated that smaller sized PF microcapsules tend to be more easily triggered by the crack.
- The OM investigation of a fractured surface of a cement paste incorporated with microcapsules confirms the result of XCT demonstrating that the self-healing function of the incorporated microcapsules could be triggered by cracking and the healing agent could be released.

This study sheds light on the feasibility of self-healing cementitious composites using a new type of synthesized polymeric microcapsule and contributes to search for effective measures to reduce microcrack-induced damage of cement-based structures. Meanwhile, with the data obtained above, a numerical simulation of the failure mechanism will be adopted to give more insight into the relation between rupture force, capsule diameter and shell thickness.

References

[1] L. Lv, Z. Yang, G. Chen, G. Zhu, N. Han, and E. Schlangen, *Synthesis and characterization of a new polymeric microcapsule and feasibility investigation in self-healing cementitious materials,* Construction and Building Materials **105**, 487 (2016).

[2] L. Lv, E. Schlangen, Z. Yang, and F. Xing, *Micromechanical properties of a new polymeric microcapsule for self-healing cementitious materials,* Materials **9** (2016), 10.3390/ma9121025.

[3] Z. Yang, J. Hollar, X. He, and X. Shi, *A self-healing cementitious composite using oil core/silica gel shell microcapsules,* Cement and Concrete Composites **33**, 506 (2011).

[4] B. Q. Dong, Y. S. Wang, G. H. Fang, N. X. Han, F. Xing, and Y. Y. Lu, *Smart releasing behavior of a chemical self-healing microcapsule in the stimulated concrete pore solution,* Cement and Concrete Composites **56**, 46 (2015).

[5] S. G. Ge, F. W. Wan, J. J. Lu, and J. H. Yu, *Molecular self-assembled microcapsules prepared by in situ polymerization technology for self-healing cement materials,* Journal of Inorganic and Organometallic Polymers and Materials **21**, 841 (2011).

[6] M. Maes, K. Van Tittelboom, and N. De Belie, *The efficiency of self-healing cementitious materials by means of encapsulated polyurethane in chloride containing environments,* Construction and Building Materials **71**, 528 (2014).

[7] K. Van Tittelboom, N. De Belie, D. Van Loo, and P. Jacobs, *Self-healing efficiency of cementitious materials containing tubular capsules filled with healing agent,* Cement and Concrete Composites **33**, 497 (2011).

[8] J. Y. Wang, K. Van Tittelboom, N. De Belie, and W. Verstraete, *Use of silica gel or polyurethane immobilized bacteria for self-healing concrete,* Construction and Building Materials **26**, 532 (2012).

[9] B. A. Young, A. M. K. Fujii, A. M. Thiele, A. Kumar, G. Sant, E. Taciroglu, and L. Pilon, *Effective elastic moduli of core-shell-matrix composites,* Mechanics of Materials **92**, 94 (2016).

[10] K. Van Tittelboom and N. De Belie, *Self-healing in cementitious materials-a review,* Materials **6**, 2182 (2013).

[11] J.-F. Su, X.-Y. Wang, and H. Dong, *Micromechanical properties of melamine–formaldehyde microcapsules by nanoindentation: Effect of size and shell thickness,* Materials Letters **89**, 1 (2012).

[12] H. Sawalha, K. Schroen, and R. Boom, *Biodegradable polymeric microcapsules: Preparation and properties,* Chemical Engineering Journal **169**, 1 (2011), 770IB Times Cited:19 Cited References Count:94.

[13] T. Makuta, K. Kadoya, H. Izumi, and M. Miyatake, *Synthesis of cyanoacrylate-covered xylitol microcapsules for thermal storage,* Chemical Engineering Journal **273**, 192 (2015).

[14] W. Xiong, J. N. Tang, G. M. Zhu, N. X. Han, E. Schlangen, B. Q. Dong, X. F. Wang, and F. Xing, *A novel capsule-based self-recovery system with a chloride ion trigger,* Scientific Reports **5**, 10866 (2015).

[15] V. Wiktor and H. M. Jonkers, *Quantification of crack-healing in novel bacteria-based self-healing concrete,* Cement and Concrete Composites **33**, 763 (2011).

[16] F. Xing, Z. Ni, N. X. Han, B. Q. Dong, X. X. Du, Z. Huang, and M. Zhang, *Self-healing mechanism of a novel cementitious composite using microcapsules,* Advances in Concrete Structural Durability, Proceedings of Icdcs2008, Vols 1 and 2 , 195 (2008).

[17] J. Y. Wang, H. Soens, W. Verstraete, and N. De Belie, *Self-healing concrete by use of microencapsulated bacterial spores,* Cement and Concrete Research **56**, 139 (2014).

[18] J. Wolfrum and G. W. Ehrenstein, *Interdependence between the curing, structure, and the mechanical properties of phenolic resins,* Journal of Applied Polymer Science **74**, 3173 (1999).

[19] M. Hasegawa, T. Kobayashi, and G. K. D. Pushpalal, *A new class of high-strength, water and heat-resistant polymer-cement composite solidified by an essentially anhydrous phenol resin precursor,* Cement and Concrete Research **25**, 1191 (1995).

[20] E. N. Brown, S. R. White, and N. R. Sottos, *Microcapsule induced toughening in a self-healing polymer composite,* Journal of Materials Science **39**, 1703 (2004).

[21] J. Gilford, M. M. Hassan, T. Rupnow, M. Barbato, A. Okeil, and S. Asadi, *Dicyclopentadiene and sodium silicate microencapsulation for self-healing of concrete,* Journal of Materials in Civil Engineering **26**, 886 (2014).

[22] W. Kao, L. Carlson, J. Yang, and J. Ju, *Application of high toughness, low viscosity nano-molecular resin for reinforcing pothole patching materials in asphalt and concrete base pavement,* (2011), uS Patent App. 13/096,750.

[23] M. Koopman, G. Gouadec, K. Carlisle, K. K. Chawla, and G. Gladysz, *Compression testing of hollow microspheres (microballoons) to obtain mechanical properties,* Scripta Materialia **50**, 593 (2004).

[24] G. Sun and Z. Zhang, *Mechanical properties of melamine-formaldehyde microcapsules,* Journal of Microencapsulation **18**, 593 (2001).

[25] J. F. Hu, H. Q. Chen, and Z. B. Zhang, *Mechanical properties of melamine formaldehyde microcapsules for self-healing materials,* Materials Chemistry and Physics **118**, 63 (2009).

[26] S. Goni and C. Andrade, *Synthetic concrete pore solution chemistry and rebar corrosion rate in the presence of chlorides,* Cement and Concrete Research **20**, 525 (1990), dv459 Times Cited:71 Cited References Count:19.

[27] W. C. Oliver and G. M. Pharr, *An improved technique for determining hardness and elastic modulus using load and displacement sensing indentation experiments,* Journal of Materials Research **7**, 1564 (2011).

[28] C. Ponzoni, M. Cannio, R. Rosa, and C. Leonelli, *Stabilization of bismuth ferrite suspensions in aqueous medium with sodium polyacrylate characterized by different molecular weights,* Materials Chemistry and Physics **149-150**, 246 (2015).

[29] J.-F. Su, S.-B. Wang, Y.-Y. Zhang, and Z. Huang, *Physicochemical properties and mechanical characters of methanol-modified melamine-formaldehyde (mmf) shell micropcms containing paraffin,* Colloid and Polymer Science **289**, 111 (2010).

[30] J. Gajda and M. Vangeem, *Controlling temperatures in mass concrete.* Concrete international **24**, 58 (2002).

[31] X. M. Pan, R. Mercade-Prieto, D. York, J. A. Preece, and Z. B. Zhang, *Structure and mechanical properties of consumer-friendly pmma microcapsules,* Industrial and Engineering Chemistry Research **52**, 11253 (2013).

[32] J. Jakes, C. Frihart, J. Beecher, R. Moon, P. Resto, Z. Melgarejo, O. Suárez, H. Baumgart, A. Elmustafa, and D. Stone, *Nanoindentation near the edge,* J. Mater. Res. **24**, 1016 (2009).

[33] J. E. Jakes, C. R. Frihart, J. F. Beecher, R. J. Moon, and D. S. Stone, *Experimental method to account for structural compliance in nanoindentation measurements,* J. Mater. Res. **23**, 1113 (2008).

[34] A. Astolfo, F. X. Qie, A. Kibleur, X. J. Hao, R. H. Menk, F. Arfelli, L. Rigon, T. M. Hinton, M. Wickramaratna, T. W. Tan, and T. C. Hughes, *A simple way to track single gold-loaded alginate microcapsules using x-ray ct in small animal longitudinal studies,* Nanomedicine-Nanotechnology Biology and Medicine **10**, 1821 (2014).

[35] S. D. Mookhoek, S. C. Mayo, A. E. Hughes, S. A. Furman, H. R. Fischer, and S. van der Zwaag, *Applying sem-based x-ray microtomography to observe self-healing in solvent encapsulated thermoplastic materials,* Advanced Engineering Materials **12**, 228 (2010).

[36] S. Fan and M. Li, *X-ray computed microtomography of threedimensional microcracks and self-healing in engineered cementitious composites,* Smart Materials and Structures **24**, 015 (2015).

[37] E. Gallucci, K. Scrivener, A. Groso, M. Stampanoni, and G. Margaritondo, *3d experimental investigation of the microstructure of cement pastes using synchrotron x-ray microtomography (μct),* Cement and Concrete Research **37**, 360 (2007).

[38] E. N. Landis and D. T. Keane, *X-ray microtomography,* Materials Characterization **61**, 1305 (2010).

4

Experimental and numerical study of microcapsule-based self-healing cementitious materials

A road of a thousand miles begins with one step.

Lao Zi

A 2D lattice model is constructed to simulate the crack process of the shell-interlayer-cement paste (SIC) zone at the microscale. The simulated tensile strength was validated by an experimental uniaxial tensile test and used as an input for the 3D lattice fracture model. A 3D lattice model is constructed to perform mechanical analysis based on a series of XCT images. The fracture behaviour of the 3D lattice model with assigned mechanical properties shows a similar crack pattern and tensile strength compared to the real cementitious structure. This study provides a feasible approach for simulating and evaluating the fracture and trigger behaviour of capsule-based self-healing cementitious material.

Parts of this chapter have been published in Construction and Building Materials **219**, 156 (2017) [1].

4.1. Introduction

As an essential step in the self-healing process, the crack-induced rupture behaviour of microcapsules plays a decisive role in realizing the self-healing function. It is generally believed that the bond strength, the size parameter and the mechanical properties (e.g. elastic modulus, strength) of microcapsule are among the important factors greatly influencing the self-healing performance as well as the mechanical properties of cementitious composites [2, 3]. Thus, a proper selection and design of the microcapsules could offer a higher healing efficiency with lower degradation of mechanical properties of the cementitious systems.

In general, there are two available routes to design/optimize the synthesis process of microcapsules with desired properties. The first route is using an experimental method. Some experimental methods including morphology observation, crack surface inspection and mechanical recover rate calculation, have been performed on microcapsule-embedded cementitious materials [4–6]. Microcapsules with desired chemical and physical properties could be obtained in such a way on the basis of the experimental results. However, the analysis based on the the experimental data can sometimes only provides limited information. It cannot give an indication on what properties the microcapsules should have in order to be prone to rupture by concrete cracking and to further predict how the embedded microcapsules will influence the self-healing behaviour in a broader sense. The second route is predicting the relevant parameters of the microcapsules through simulation approaches. There already exists a wide range of micromechanical models for predicting the optimal dosage and parameters of the microcapsules as well as the mechanical properties of the cementitious composites. Most of these models use a continuum approach to predict the elastic properties of this three-component composite [7, 8], it is inherently incapable when dealing with fracture process for this type of materials. Moreover, the bond strength between shell materials and cement paste is often ignored resulting in an overestimation of the simulated values.

In order to simulate the fracture behaviour of microcapsule-embedded cementitious materials in a more realistic way, two points should be considered: The first point is related to obtaining the mechanical parameters of the components of the self-healing composite, corresponding to the shell, cementitious matrix and interlayer, respectively. These data can be used directly as input for the 3D modelling of the self-healing system. Similar to the fact that the interfacial transition zone (ITZ) in concrete has a great influence on the mechanical properties of concrete [9], the interlayer properties between shell materials of microcapsules and the cementitious matrix also significantly affect the stability of the microcapsules, the potential self-healing efficiency and the mechanical properties of cementitious structure. However, studies regarding micromechanical properties of the interlayer between microcapsules and matrix such as bond strength and elastic modulus are very limited. In this context, fundamental and practical research is essentially needed for the application of capsule-based self-healing cementitious materials. The second point is obtaining a real 3D microstructure of microcapsule-embedded cementitious materials, in which the shell thickness, particle size and distribution of microcapsules should be correlated with the real situation. Micro X-ray computed tomogra-

phy (XCT) offers a non-destructive experimental technique, which has already been used to collect the microstructure information of cement paste in terms of digitized voxels [10]. By segmenting the phases and defining the local mechanical properties to individual phases, a 3D lattice model can be formed [11].

In this study, the nanoindentation method was used for mapping the mechanical properties of complex surfaces of shell-interlayer-matrix. The measured properties were directly applied as input for constructing a 2D numerical model. A direct tension test was simulated and the bond strength and the elastic modulus of the interlayer between shell and matrix were obtained based on the 2D model. The XCT technology was further used to get the 3D volume images of an actual cementitious material in which capsules were incorporated. Based on these images and the mechanical information obtained from the 2D model, a 3D lattice model of a capsule-based self-healing cementitious material was formed. The crack pattern and the self-healing behaviour of the microcapsule-based self-healing cementitious materials were discussed accordingly.

4.2. Materials and methods

4.2.1. Materials

CEM I 42.5N Portland cement in accordance with the European standard EN-197-1 and deionized water were used. The phenol-formaldehyde (PF) microcapsules (mean diameter 201 μm) were prepared and graded according to our previous study [12].

4.2.2. Sample preparation

Sample preparation for 2D shell-interlayer-cement (SIC) zone study

The shell material i.e., PF resin as shown in Figure 4.1a, was synthesized under the same condition as that of the microcapsules. After that, the PF resin bulk was cut into small pieces of 10 × 10 × 3 mm. Cement paste with water-to-cement ratio of 0.4 was prepared and cast into 10 × 10 × 10 mm prismatic mould. Then a piece of shell material (10 × 10 × 3 mm) was placed on top of fresh cement paste. A vibration plate was used to minimize the amount of entrapped air in the cement paste and the area between cement paste and PF piece and to maximize the contact area between the two materials. After curing at room temperature in the lab for 24 h, the specimens were moved to a curing room at 23 °C and over 95% relative humidity. After curing for 28 days, the samples were taken out from the fog room and demoulded. Four samples were prepared in total, in which 3 samples were prepared for tensile testing and the one was sealed by epoxy resin for nanoindentation to obtain the local mechanical properties of shell-interlayer-cement paste (SIC) zone. One of the side surfaces of the epoxy sealed sample containing both shell material and cement paste was then ground with No. 2000 and 4000 emery paper and subsequently polished with 6 μm, 1 μm and 0.25 μm diameter paste on a lapping table. The samples were further cleaned in an ultrasonic bath to remove any residues. Figure 4.1b shows the prepared specimen for the nanoindentation test.

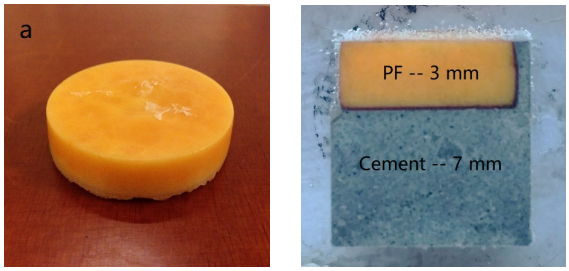

Figure 4.1: Samples used for the shell-interlayer-cement paste (SIC) zone study. (**a**) Synthesized PF resin – shell material of microcapsules (left) and (**a**) specimen of SIC zone for nanoindentation (right).

Sample preparation for 3D crack behaviour study

The microcapsules-embedded cement paste specimens for the XCT study were prepared with a water-to-cement ratio of 0.4 and contained 4% PF/DCPD microcapsules (mean diameter 201 µm) of cement mass. The microcapsules were blended with cement and deionized water and mixed for 1 min to achieve a good workability. After mixing, the fresh mixture was cast into a plastic cylindrical mould (6.7 hight with a diameter of 13.4 mm). Then they were carefully compacted on a vibrating table to reduce the entrapped air. The specimens were demoulded after curing at room temperature (RT) and local lab environment for 48 h. Then they were cured in a wet chamber at 23 °C and over 95% relative humidity. After curing for 28 days, samples were taken out from the curing room. Four samples were prepared in total, in which three samples for tensile test and one sample for XCT scanning. Figure 4.2 shows an optical microscopy images of the microcapsules used in this study.

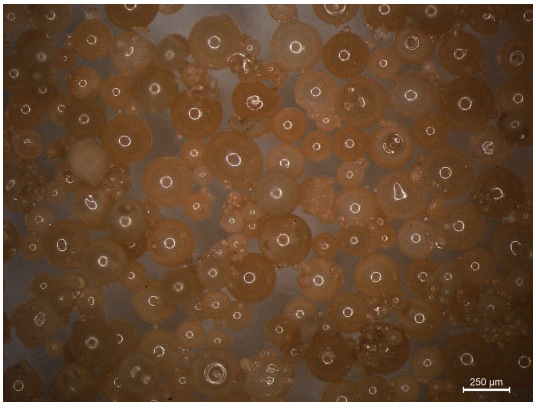

Figure 4.2: OM image showing PF microcapsules which were used in this study.

4.2.3. Test methods

Nanoindentation

Nanoindentation tests were performed to obtain the local micromechanical properties of SIC complex using an Agilent Nano Indenter (G200, Keysight, USA) with a diamond Berkovich tip. The continuous stiffness method (CSM) developed by Oliver and Pharr [13] was used in this study. By using this method, a small oscillation is imposed on the primary loading signal and the response of the system is analysed by means of a frequency-specific amplifier, so that a continuous measure of contact stiffness as a function of indentation depth can be achieved. Therefore, the E modulus and hardness are obtained as a continuous function of the depth of surface penetration. Before each of the tests, quartz standard was indented to ensure the accuracy of the measurement. The indentation depth was defined at 1000 nm, the allowable drift rate was 0.25 nm/s and the surface approach velocity was 10 nm/s. Due to the scatter of results at low indentation depths, the E modulus and hardness were determined from the indentation depths range between 600-1000 nm. Then a tightly spaced matrix of 20 × 20 indents was taken randomly crossing the area from shell material to cement paste, spacing of 10 µm on both parallel and perpendicular direction to the interface. Due to the large heterogeneity of cement paste on the microscale, in this preliminary research, the minimum sampling number for statistical confidence of results was not considered. After the nanoindentation test, the surface of sample was examined with optical microscope (Leitz DMRXP, Leica, Germany).

Tensile test

In order to compare the numerical tensile strength result with the experimental result, a direct tensile test was performed respectively on the SIC zone specimens prepared and the capsule-embedded cementitious material specimen prepared as described in section 4.2.2. A meso-scale mechanical test apparatus (developed by Kammrath & Weiss, Germany), as shown in Figure 4.3, was used to impose a tensile load on the shell end and cement end of the SIC specimen and two ends of cylinder specimen of capsule-embedded cementitious material. Before the test, two component instant adhesive, Plex 7742 and Pleximon 801 (Evonik Rohm GmbH, Darmstadt, Germany), was used to glue the sample on the holder of the apparatus. The tensile test was performed under deformation control with a step speed of 0.01-mm/s. The load and displacement are recorded by inset software automatically.

XCT scanning

XCT images used as the input for the 3D simulation were obtained by XCT scanning (Nanotom, GE Inspection Technologies, Lewistown, LP, USA). In this study, a capsule-embedded paste cylinder was scanned by XCT before and after it was fractured, so that the rupture behaviour could be observed. Upon finishing prior-fracture XCT scanning, the cement cylinders were glued in an Axial Tension-Compression Systems (8872, Instron, High Wycombe, UK) to generate a crack in the middle of the specimens. The loading speed was set to 0.01 mm/s. The load-displacement curve was recorded by an in-set software. Then the fractured two cylinder-ends were wrapped together by plastic tape with their original position for the after-fracture XCT scanning. The raw XCT images were acquired at an acceleration voltage of

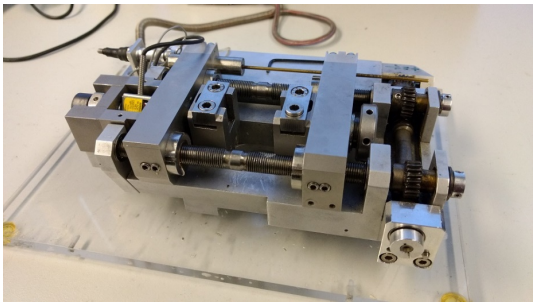

Figure 4.3: Meso-scale compression-tension test setup.

50 kV with an exposure time of 4s and X-ray power of 8W. The final data set of XCT consisted of 1440 images of which each image was acquired with a 0.25° rotation. Then phase retrieval and tomographic reconstruction were performed on the obtained raw data to improve the boundaries and signals using the software supplied by the manufacturer. A commercial software was used to segment and visualize the 3D structure based on a series of reconstructed tomographic images (X-Z plane).

4.2.4. Modelling procedure

The fracture process of microcapsule-embedded cementitious materials can be simulated by a lattice model [14, 15]. In this study, the lattice model which developed by our lab was first used to investigate the tensile strength of the interlayer based on the 2D mechanical map of SIC zone. After that, the fracture behaviour of 3D capsule-embedded paste cylinders was studied by the lattice model under the same principles. In this model, the material is schematized as a mesh of beam elements which connected at the ends and all individual elements are defined having linear elastic behaviour. To achieve crack growth, unit prescribed displacement is imposed on the lattice system and only one element with the highest stress/strength ratio is removed from the mesh at every loading step. As this method can express the physical process of fracture behaviour, a realistic crack pattern as well as the stress-strain response will be obtained. The uniaxial tensile simulation test was achieved by applying uniform displacement at one side of the specimens and restraining the movement and rotation of the opposite edge. The lattice element can only fail in tension.

The procedure of 3D spatial discretization of the cylindrical domain is performed as follows: first, a cubic domain (1.5 × 1.5 × 1.5 mm) is divided into a cubic grid with a cell size of 30 μm^3. Then, a sub-cell can be defined within each cell in which a node is randomly placed. The ratio between the length of the sub-cell and the cell is defined as randomness. Since the simulated crack patterns are highly influenced by the orientation of meshes, the choice of randomness affects the simulation for the fracture behaviour of materials. More information about the influence of randomness can be found elsewhere [16]. In order to avoid big

variations in the length of elements and geometry disorder of material texture, a randomness of 0.5 is adopted. The next step is to erase the nodes outside the cylinder. Afterwards, Delaunay triangulation is performed to connect the 4 nodes which are closest to each other with lattice elements.

The heterogeneity is realized by employing the overlay procedure. In this procedure, different mechanical properties are assigned to different phases. For this purpose, the material structure obtained by XCT scanning is used here. In order to reduce the computing time and to avoid the possible wall effect, a cylindrical region of interest (ROI) with a diameter of 1500 µm and thickness of 1500 µm at a resolution of 30 µm is extracted from the center of the 3D volume where the capsule-based cementitious material is considered to be the most homogeneous. Each beam is assigned mechanical properties depending on its location. What has to be noted here is the elements that connect both shell material and paste matrix are regarded as the interface element. The properties of these elements are derived from 2D fracture simulation of the interface zone.

The mesh method also works for 2D simulation of the SIC zone. In this thesis, the interface properties are defined as material properties. While since local micromechanical properties of the interface performance and bulk materials obtained by nanoindentation do not provide any information about the interface performance and its strength, they need to be linked in a structure where all the individual local tests are assembled. By overlapping the measured properties on a 2D lattice mesh, their spatial distribution was used as input for numerical modelling. In the 2D lattice fracture model, a square with a side of length 200 µm is meshed into a lattice network. A 1.0 µm square cell size and a randomness of 0.5 are applied in this step. Unlike 3D lattice simulation, the heterogeneity is taken into account by overlapping the mechanical properties of nanoindentation results on top of nodes which belong to corresponding indented locations. The properties of elements are ascribed with mean values from these two nodes. The overlapped elastic modulus is considered equal to the measured modulus of elasticity. Meanwhile, a value of 300 times lower than the hardness is taken as an approximation of the tensile strength, since no data from literature was found defining this ratio in cement-based material.

4.3. Results and discussion

4.3.1. Local mechanical properties of the SIC zone

The mechanical properties of SIC zone including the shell material, cement paste and the interlayer in between were measured by nanoindentation. Figure 4.4a shows the image of the prepared SIC sample for SIC zone study, as descried in 4.2.2. The morphology of the tested area was imaged by optical microscope (Figure 4.4b) and then correlated to the results of micromechanical measurement which is measured by nanoindentation (Figure 4.4c). The hardness distribution among the shell material, cement paste and interlayer in between can be clearly seen from this image. According to the study carried out by Lukovic et al. [16], the interface properties are defined as materials properties. To visually represent the different phases, the hardness of the different phases was defined by colour ranging from

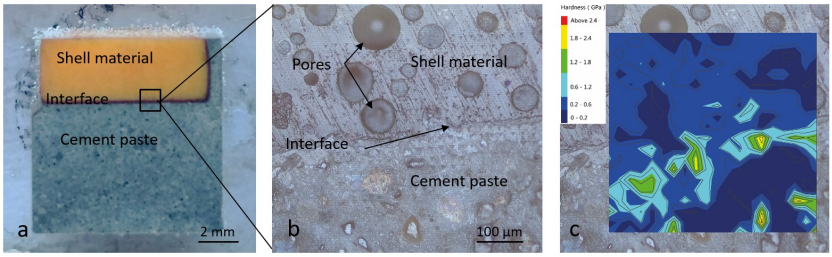

Figure 4.4: Photomicrographs of the (**a**) prepared SIC zone specimen, (**b**) test area of nanoindentation(left) and (**c**) the corresponding hardness (right).

below 0.2 GPa (navy) to above 1.2 GPa (red). As we can see that the upper area of the map has a blue and navy colour, representing that the hardness of the shell materials is lower than 0.6 GPa. The cement paste at lower part of this figure shows a more complicated mechanical distribution likely due to the heterogeneous nature and different mechanical properties of the phases in the cement paste, especially at the contact area with the interlayer.

4.3.2. 2D Modelling of interfacial zone

Upon completion of the micromechanical properties evaluation, the fracture behaviour and tensile strength at the SIC zone were investigated on a 2D lattice model. In a simulated uniaxial tensile test, the micromechanical response of this 2D lattice model, made as described in section 4.2.4, can be indirectly evaluated. This enables the assessment of the fracture properties of the interfacial zone at the microscale, while taking into account its intrinsic heterogeneity.

The 2D lattice mesh with assigned properties and boundary conditions is presented in Figure 4.5. Those locations of which the mechanical properties could not be obtained were regarded as pores. Accordingly, the elements which belong to these pores in the lattice model were removed. In order to check the influence of the adopted randomness and cell size on simulated results, the meshes were generated 5 times. The simulated load-displacement diagrams are shown in Figure 4.6. Since the simulated load-displacement diagrams are similar, a cell size of 1 µm and randomness of 0.5 were selected to study the fracture behaviour of the simulated interlayer zone.

Figure 4.7 illustrates the crack development of the simulated SIC zone. The snapshots a, b and c correspond to the points a, b and c which are represented in the simulated load-displacement curves in Figure 4.6. As can be seen from Figure 4.7a, due to the nature of heterogeneity in the SIC zone, the existence of pores would introduce stress concentration to the microstructure. When the uniaxial tensile force was applied on the simulated model, the stress concentration in the microstructure produced a localization of the cracks before the load reached the peak. Then, with the increase of displacement, those microcracks started to propagate at certain points, and this led to the softening post-peak behaviour (Figure 4.7b). By connecting its way through the nearby weak spots, a critical crack

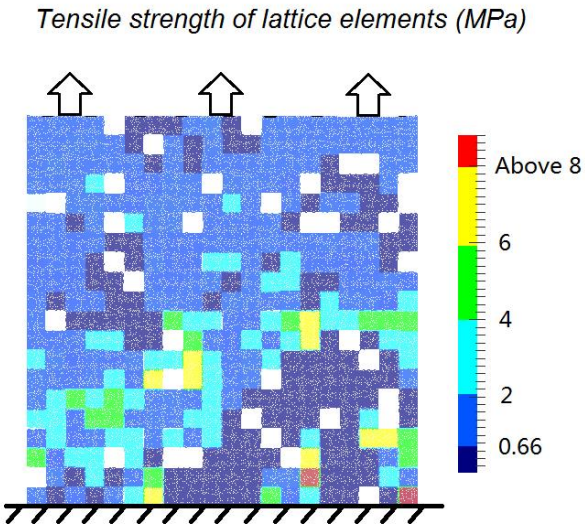

Figure 4.5: The applied lattice mesh with assigned properties and boundary conditions.

formed which is located across the interlayer and cement paste zone, resulting in a so-called crack-face bridge which is still capable of carrying some limited load (Figure 4.7c).

To calculate the required mechanical properties such as tensile strength and E modulus of this zone, the peak load in Figure 4.6 and the initial slope of the curve are used. The calculated results are listed in Table 4.1. It was found that the simulated tensile strength, 0.125 $\pm$ 0.009 MPa, is consistent with the tensile strength value obtained experimentally by meso-scale tensile test as described in chapter 4.2.3, 0.091 $\pm$ 0.006 MPa. The result demonstrates that the used method of obtaining the mechanical properties of SIC zone and the formulated lattice model can be used to simulate the mechanical properties of SIC zone. On the other hand, due to the limitation of measuring device in the experiment, the displacement of the interface zone cannot be measured accurately, which means that the obtained modulus of elasticity cannot be verified in this test. Therefore, the simulated results of the mechanical properties of SIC zone will be used as the input for 3D modelling in the following section to represent the bond element between the shell material and the matrix of cement paste.

4.3.3. 3D modelling of cracking behaviour

The mechanical properties of different phases which were used as input for the structure-informed lattice model are listed in Table 4.2. According to a previous study, the tensile strength (f_t) and Young's modulus of cement paste are taken as 3 Mpa and 16 Gpa [17]. The E modulus of the shell material was derived from the mean value of the nanoindentation measurements on the shell side of the SIC

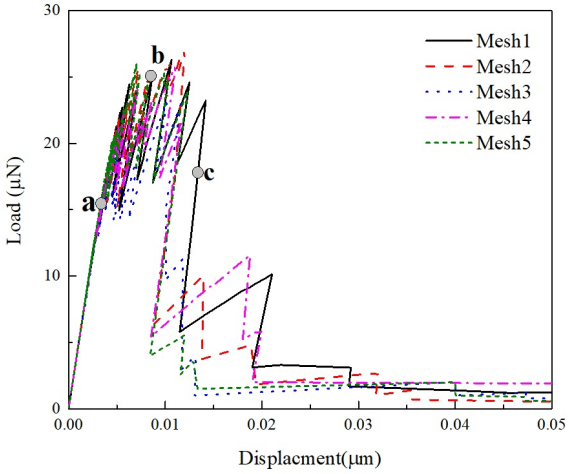

Figure 4.6: The simulated load-displacement curves for five different meshes (cell size 1 μm).

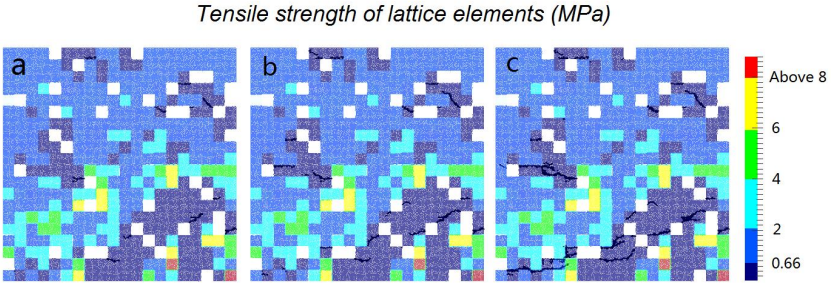

Figure 4.7: Cracking history of the SIC specimen in the simulated direct tensile test.

Table 4.1: Simulated results of the tensile strength and E modulus of the simulated SIC zone

Mesh number	Tensile strength (MPa)	E modulus (GPa)
1	0.116	4.77
2	0.135	4.72
3	0.116	4.76
4	0.130	4.73
5	0.130	4.76
Mean value	0.125 ± 0.009	4.75 ± 0.02

Table 4.2: Mechanical properties of different phases

Phases	E modulus (GPa)	f_t (GPa)
Paste matrix	16.0	3.00
Shell material	5.5	1.10
Interlayer	4.75	0.12

zone while the tensile strength (f_t) was defined as three hundredths of the measured hardness value. The properties of interlayer elements which connect the shell material and the cement matrix were obtained from the 2D simulation results in section 4.3.2. Based on these abovementioned data, a 3D lattice cylinder (1.5 mm long with a diameter of 1.5 mm) consisting of 98057 nodes and 738640 beam elements was generated from a selected volume within the reconstructed XCT images. Figure 4.8a shows the numerically simulated specimen in which the cement paste, shell material and the interlayer are defined as grey, red and purple respectively. Then the simulated uniaxial tensile test was performed by applying a uniform displacement on top of the round surface in the direction perpendicular to the loading surface. The final cracked specimen is presented in Figure 4.8b. As can be seen from the figure that a critical crack (in black) goes through the middle of the cylindrical specimen. To observe the main crack surface more clearly, the crack surface in the middle of the specimen is given in Figure 4.8c. It can be seen that microcapsules along the crack were partly triggered, leaving a cloud with a few spherical shell elements (in red) in paste matrix.

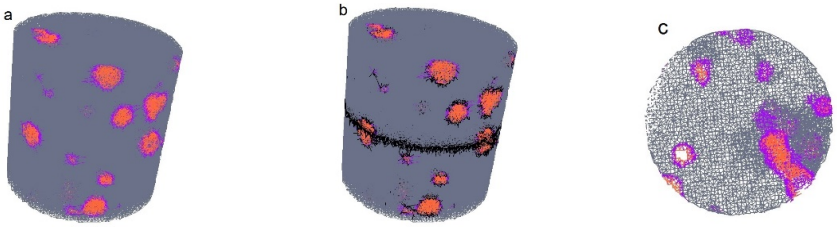

Figure 4.8: The initial state (**a**) and final fracture pattern (**b**) of the generated 3D lattice mesh under uniform tensile test and the corresponding crack surface (**c**). The grey elements are defined as the cement paste matrix, the red elements are defined as the shell material and the purple elements are defined as the interlayer.

To further investigate the cracking behaviour of the microcapsules-containing cement paste, the simulated stress-strain curve and crack evolution history are shown in Figure 4.9 and Figure 4.10, respectively. Each snapshot in Figure 4.10 corresponds to the points (a, b, c and d) which are indicated in the stress-strain curve (Figure 4.9). Only cracked elements are shown in these snapshots. As we can see from Figure 4.10a that, due to the relatively lower tensile strength of the interlayer, partial microcracks were firstly initiated at the interlayer around the capsules.

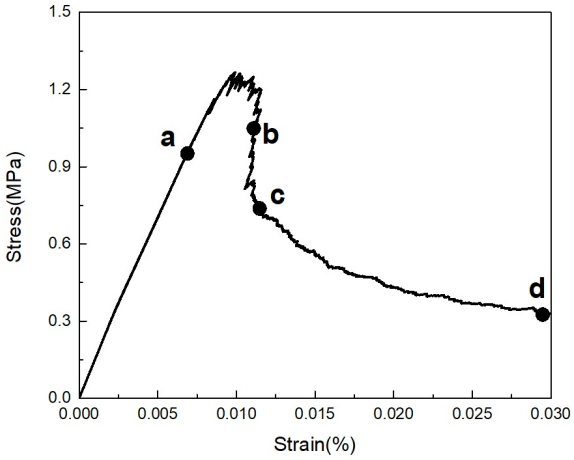

Figure 4.9: Stress-strain diagram of the lattice mesh sample under tension.

Once the fracture zone nucleated from the weakest spots along the circumference, the stiffness of the simulated 'specimen' decreased, which resulted in a softening post-peak regime of the stress-strain curve. During this period, microcapsules in the vicinity of the crack tip are "triggered" (Figure 4.10b and c). Based on this simulated load displacement curve, the tensile strength and E modulus are evaluated as 1.25-MPa and 14.9 GPa, respectively. Comparing with numerical simulation results, the experimental results of tensile strength (1.05 ± 0.15 MPa) obtained from larger size cylinder specimens prepared as described in section 4.2.2 shows a slightly lower value while in the same range. A possible explanation of this difference is that no initial defect is considered in this simulation. However, initial defects are inherent to cement based material, which have a great influence on the strength of such materials [18]. In addition, size effect cannot be avoided in which the theoretical strength of a quasi-brittle material increases as the sample size decreases [19].

4.3.4. Parametric analysis

It is known that a proper design of the properties of microcapsules could offer a higher trigger efficiency of microcapsules with lower degradation of mechanical properties of microcapsules-embedded cementitious materials [8, 20]. To provide a good instruction for synthesizing microcapsules, the influence of interlayer strength and shell strength were studied based on the proposed numerical lattice model. Then two specimens acquired at different locations in the volume of XCT images were used to validate this model. Only one variable is changed for each parametric study and other parameters are kept unchanged. Table 4.3 shows the studied specimens with different input parameters. Here, 'H' stands for 5 time higher and 'L' stands for 5 times lower than the 'Standard' value. The prefix 'inter' and 'shell' refer to the variables, interlayer and shell, going to be changed. P-1 and P-2 represent

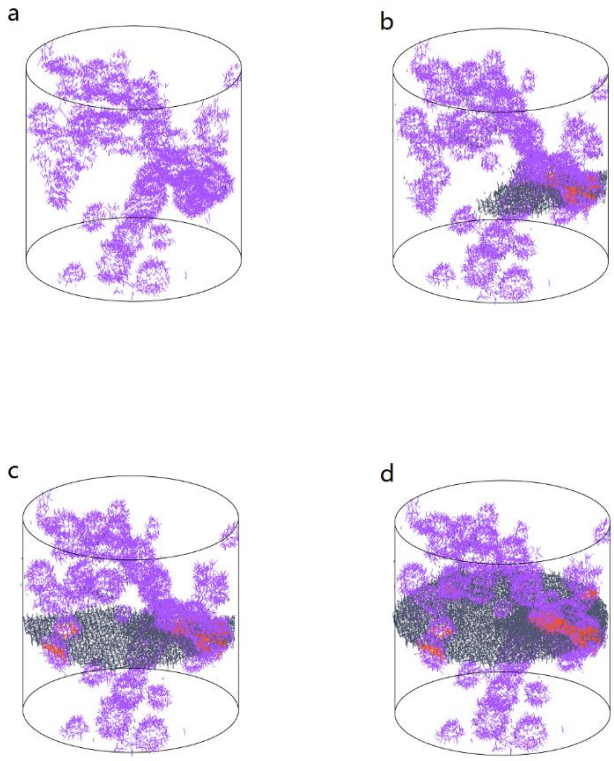

Figure 4.10: Cracking evolution of the microcapsules-embedded cement paste specimen in a simulated direct tensile test. The grey elements are defined as the ruptured cement paste matrix, the red elements are defined as the ruptured shell material and the purple elements are defined as the ruptured interlayer.

Table 4.3: Input parameters of the simulated microcapsule - embedded paste specimens.

Specimen	Interlayer strength (MPa)	Shell strength (MPa)
Standard	0.12	1.10
H-inter	0.60	1.10
L-inter	0.024	1.10
H-shell	0.12	5.50
L-shell	0.12	0.22
P-1	0.12	0.22
P-2	0.12	0.22

another two locations selected randomly within the volume of XCT images.

Influence of interlayer strength

By varying the interlayer strength from 5 times higher (1.2 MPa, H-inter) to 5 times lower (0.05 MPa, L-inter) than the data (0.24 MPa, Standard) obtained from real experiments, the influence of the interlayer strength on the mechanical properties and trigger efficiency were studied. The stress-strain curve under different interlayer strengths are shown in Figure 4.11. As can be seen from the figure, the H-inter specimen yields a higher load response and becomes stiffer in the ascending branch. While no obvious variation is observed between the L-inter and standard specimens. The corresponding crack pattern of the microcapsules-embedded cement paste specimen with different interlayer strength are shown in Figure 4.12. As can be seen from Figure 4.12a that, when the interlayer strength of the specimen is 5 times higher than the standard specimen, only very few elements of interlayer were fractured. It is suggested that higher interlayer strength could confer the microcapsules a better bond with the paste matrix. Meanwhile, compared to the standard specimen in Figure 4.12b, the H-inter specimen has more shell material elements (in red) that cracked in the tensile test. Since the cracking of shell material element can be recognized as the breaking of microcapsules, the more cracked shell elements means the more microcapsules were ruptured. Macroscopically, the main crack goes through the shell material and triggers the microcapsules. As the strength of the interlayer is adjusted to a value that is 5 times lower than the experimental result, more cracked interlayer elements and less cracked shell material can be found (Figure 4.12c). At this condition, it is easier for shell to detach the shell from the paste matrix under the tensile loading. The results illustrate that the strength of the interlayer plays a very important role in controlling the trigger efficiency of microcapsules.

Influence of shell strength

It is known that the strength of the shell is the property of the microcapsule that can be manipulated by adjusting the synthesis process [8, 21]. Many studies have suggested that the trigger efficiency has a close relation with the mechanical properties of shell material [2]. Thus, a good understanding of the influence of shell properties on the self-healing system is another important task. In this thesis, based

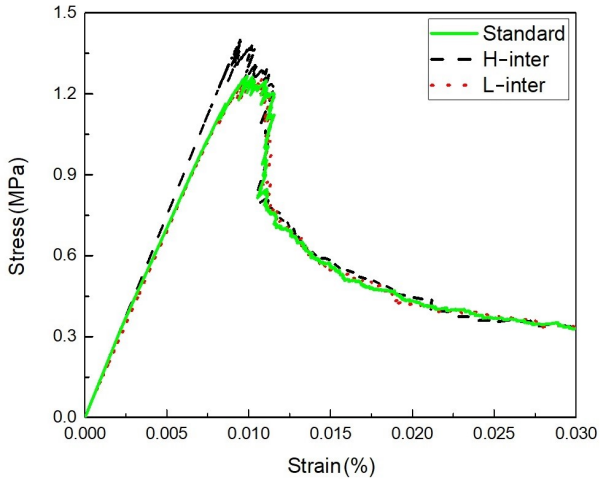

Figure 4.11: Stress-strain diagram of the paste specimens with different interlayer strength.

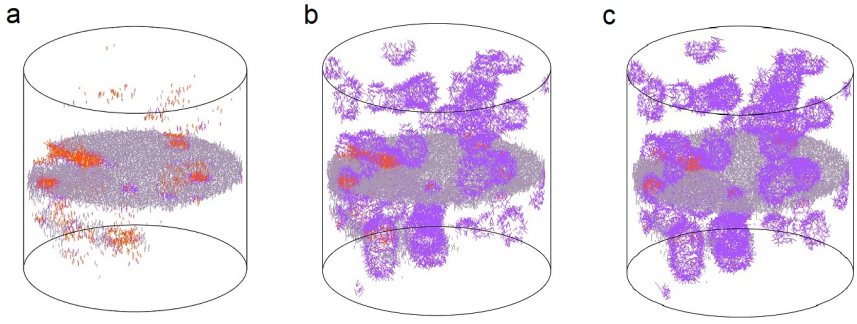

Figure 4.12: Crack pattern of the microcapsules-embedded cement paste specimen with different interlayer strength, (**a**) H-inter, (**b**) standard and (**c**) L-inter. The grey elements are defined as the ruptured cement paste matrix, the red elements are defined as the ruptured shell material and the purple elements are defined as the ruptured interlayer.

on the formulated lattice model, the self-healing specimen with three different shell strengths was investigated. Figure 4.13 shows the influence of shell strength on the load-displacement curve of the self-healing system. As can be seen in Figure 4.13, although the influence of shell strength on the simulated stress-strain response is very small, the H-shell specimen with higher shell strength (5.5 MPa) has a more stable softening regime. On the other hand, the L-shell specimen with the lower shell strength (0.22 MPa) yields a lower peak load compared to the other two specimens. The final crack patterns of the systems are shown in Figure 4.14. It is clear that, when the shell strength is 5 times higher than the standard value, almost no

shell element (in red) was found to be cracked. However, as the strength of shell material decreased to the standard value (1.1 MPa), some of the cracked elements along the main crack are of the shell material. With the continuous decrease of shell strength from 1.1 MPa to 0.22 MPa, more cracked elements were found not only at the main crack but also throughout the specimen.

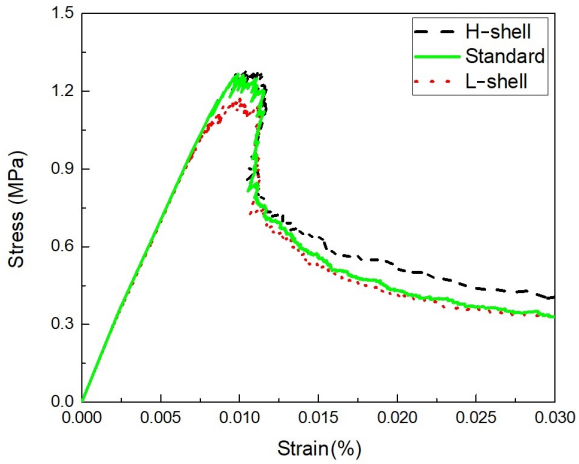

Figure 4.13: Stress-strain diagram of the specimens with different strength of shell material.

Influence of composite structure

To further prove the function and the validity of the proposed model, another two positions (P-1 and P-2) with different composite structure were selected in the volume of XCT images of capsule-embedded cement paste. Low shell strength (0.22 MPa) and normal interlayer strength (0.24 MPa) were assigned to the model. The stress-strain diagram in Figure 4.15 demonstrates that choosing a different location for the microcapsule-embedded cement paste, has a big difference on the stress-strain curve, mainly in the softening regime. The possible reason for this can be attributed to the diverse distribution and content of microcapsules in the selected specimens. Meanwhile, based on the crack pinning and crack deflection mechanisms, the presence of microcapsules and their rupture behaviour will decrease the coalescence of the initial crack and increase the energy for crack development, which will finally influence the propagation of the crack. This can be seen from the different crack patterns in Figure 4.15 b and c, which correspond to the curve of specimens P-1 and P-2 in Figure 4.15a.

Trigger efficiency study and healable volume

Finally, the trigger efficiency of embedded microcapsules in the simulated cement paste specimen under different strength of interlayer and shell materials were investigated. The cracked and uncracked microcapsules of the simulated specimens

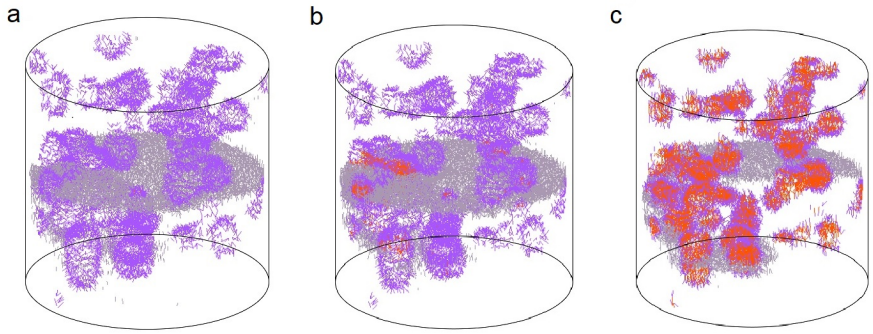

Figure 4.14: Crack patterns of the microcapsule-embedded cement paste specimen with different strength of shell material, (**a**) H-shell, (**b**) standard and (**c**) L-shell. The grey elements are defined as the ruptured cement paste matrix, the red elements are defined as the ruptured shell material and the purple elements are defined as the ruptured interlayer.

were observed and recorded using the software (Paraview 5.2.0). The cracked microcapsules can be recognized as a cloud of red spherical elements in the simulated specimen. The trigger efficiency is defined as the shell cracked microcapsules divided by all the microcapsules which contact with the main crack of the specimen. Based on the results of the trigger efficiency, the available volume of healing agent that can be used to fill a crack and the healable crack width are predicted. In a previous chapter, it was found that there exists a certain relationship between the size and shell thickness of microcapsules. In this study, microcapsules with mean size of 201 μm and shell thickness of 18 μm were embedded in the specimen. The volume of available healing agent (V_h) can be defined as the number of ruptured microcapsules multipling by the average volume of healing agent (Eq (1)). The healable crack width (W_h) can be defined as available healing agent (V_h) divided by the area of crack surface (Eq(2)):

$$V_h = \frac{4}{3}\pi(R_{capsule} - T_{shell})^3 \cdot n \tag{4.1}$$

$$W_h = \frac{V_h}{S_{crack}} \tag{4.2}$$

where n is the number of cracked microcapsules; S_{crack} represent the calculate area of crack surface; $R_{capsule}$ and T_{shell} are the radius and shell thickness of microcapsule, respectively.

As can be seen from Tables 4.4 that, both interlayer strength and shell strength can influence the trigger efficiency of microcapsule-embedded self-healing systems. When the interlayer strength increased from 0.05 to 1.2 MPa, the trigger efficiency rose from 30% to 61%. And the healable volume and crack width increased accordingly from 0.023 to 0.046 mm^3 and from 3.3 to 6.5 μm respectively. Compared to the interlayer strength, the trigger efficiency seems to be more sensitive to shell

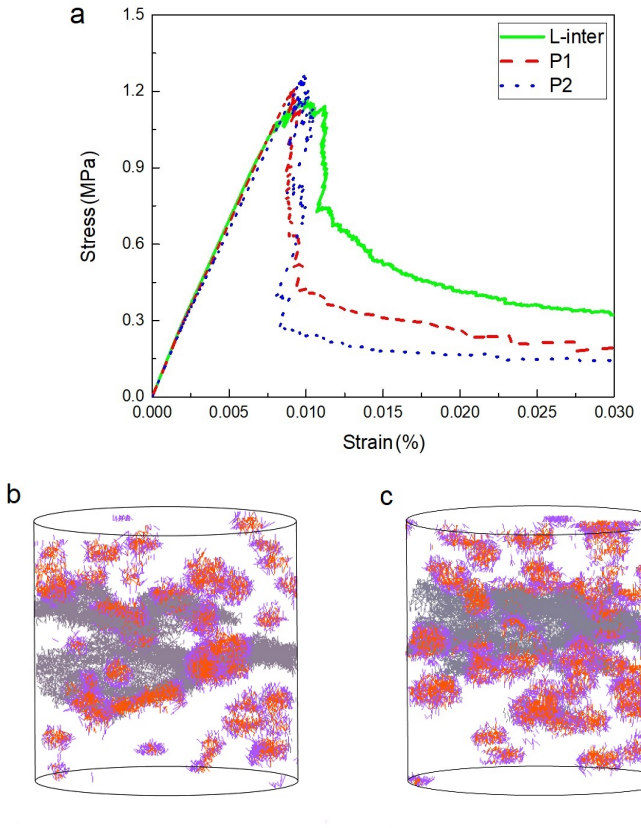

Figure 4.15: Simulated stress-strain diagrams (**a**) and crack pattern (**b,c**) of specimens at different locations in the volume of reconstructed XCT images of microcapsule-embedded cement paste. The grey elements are defined as the ruptured cement paste matrix, the red elements are defined as the ruptured shell material and the purple elements are defined as the ruptured interlayer.

strength. No microcapsules were found to be triggered with a shell strength of 5.5 MPa, while, 100% of microcapsules were triggered by a crack when the shell strength decreased 5 times lower than the standard value obtained from the real experiment. The results can also suggest that, under the condition that cement paste contains 4% microcapsules ($R_{capsule}$ = 125 μm and T_{shell} = 18 μm) and 100% of these microcapsules can be triggered by the crack, a maximum crack width of 10.6-μm can be healed completely.

Table 4.4: Results of the parametric analysis of the simulated microcapsules-embedded cementitious specimens

Specimen	Trigger efficiency	Healable healing agent	Healable crack width
Standard	42 %	0.031 mm^3	4.5 μm
H-inter	61 %	0.046 mm^3	6.5 μm
L-inter	30 %	0.023 mm^3	3.3 μm
H-shell	0 %	0.000 mm^3	0.0 μm
L-shell	100 %	0.075 mm^3	10.6 μm
P-1	100 %	0.072 mm^3	10.2 μm
P-2	100 %	0.060 mm^3	8.6 μm

4.4. Conclusion

In this chapter, a feasible approach was developed for simulating and evaluating of the fracture and trigger behaviour of a microcapsule-based self-healing cementitious material. It provides a promising method for guiding the design of microcapsule-based self-healing cementitious composites towards an ideal self-healing performance.

- A 2D lattice fracture model was built to simulate the fracture performance and to obtain the tensile strength of the SIC zone.
- The tensile strength of the SIC zone which was obtained from the 2D simulation, 0.125 $\pm$ 0.009 MPa, is consistent with the tensile strength value which was obtained by the experiment, 0.091 $\pm$ 0.006 MPa.
- The 3D lattice network which was used for the numerical simulation of the crack behaviour of microcapsule-based self-healing system is constructed based on the XCT microstructure.
- The parametric study of the constructed 3D model shows that both interlayer strength and shell strength can influence the trigger efficiency of microcapsule-embedded self-healing systems.
- When the interlayer strength increased from 0.05 to 1.2 MPa, the trigger efficiency rose from 30% to 61%. The healable volume and crack width increased accordingly from 0.023 to 0.046 mm^3 and from 3.3 to 6.5 μm, respectively.
- Comparing to the interlayer strength, the trigger efficiency of microcapsules seems to be more easily affected by the shell strength.

Some improvements to the proposed study are still needed. Firstly, a better procedure for accurate measurement of bond strength should be developed. The boundary conditions of the tensile test should be well controlled. A LVDT module can be used to record the displacement precisely. In addition, because the ratio between the measured hardness and the tensile strength of cement paste is only an assumed value in this study, further effort will be given to establish an appropriate relationship between local hardness and the fracture strength of the cement paste.

References

[1] L.-Y. Lv, H. Zhang, E. Schlangen, Z. Yang, and F. Xing, *Experimental and numerical study of crack behaviour for capsule-based self-healing cementitious materials,* Construction and Building Materials **156**, 219 (2017).

[2] B. A. Young, A. M. K. Fujii, A. M. Thiele, A. Kumar, G. Sant, E. Taciroglu, and L. Pilon, *Effective elastic moduli of core-shell-matrix composites,* Mechanics of Materials **92**, 94 (2016).

[3] K. Van Tittelboom and N. De Belie, *Self-healing in cementitious materials-a review,* Materials **6**, 2182 (2013).

[4] W. Li, X. Zhu, N. Zhao, and Z. Jiang, *Preparation and properties of melamine urea-formaldehyde microcapsules for self-healing of cementitious materials,* Materials **9**, 152 (2016).

[5] S. Fan and M. Li, *X-ray computed microtomography of threedimensional microcracks and self-healing in engineered cementitious composites,* Smart Materials and Structures **24**, 015 (2015).

[6] D. Palin, H. Jonkers, and V. Wiktor, *Autogenous healing of sea-water exposed mortar: Quantification through a simple and rapid permeability test,* Cement and Concrete Research **84**, 1 (2016).

[7] H. H. Zhu, S. Zhou, Z. G. Yan, J. W. Ju, and Q. Chen, *A two-dimensional micromechanical damage-healing model on microcrack-induced damage for microcapsule-enabled self-healing cementitious composites under tensile loading,* International Journal of Damage Mechanics **24**, 95 (2015).

[8] H. H. Zhu, S. Zhou, Z. G. Yan, W. Ju, and Q. Chen, *A 3d analytical model for the probabilistic characteristics of self-healing model for concrete using spherical microcapsule,* Computers and Concrete **15**, 37 (2015).

[9] D. Bentz, E. Schlangen, and E. Garboczi, *Computer simulation of interfacial zone microstructure and its effect on the properties of cement-based composites,* Materials science of concrete IV , 155 (1995).

[10] M. Zhang and A. P. Jivkov, *Micromechanical modelling of deformation and fracture of hydrating cement paste using x-ray computed tomography characterisation,* Composites Part B: Engineering **88**, 64 (2016).

[11] H. Zhang, B. Savija, S. C. Figueiredo, M. Lukovic, and E. Schlangen, *Microscale testing and modelling of cement paste as basis for multi-scale modelling,* Materials **9** (2016).

[12] L. Lv, Z. Yang, G. Chen, G. Zhu, N. Han, and E. Schlangen, *Synthesis and characterization of a new polymeric microcapsule and feasibility investigation in self-healing cementitious materials,* Construction and Building Materials **105**, 487 (2016).

[13] W. C. Oliver and G. M. Pharr, *An improved technique for determining hardness and elastic modulus using load and displacement sensing indentation experiments,* Journal of Materials Research **7**, 1564 (2011).

[14] E. Schlangen and E. J. Garboczi, *Fracture simulations of concrete using lattice models: Computational aspects,* Engineering Fracture Mechanics **57**, 319 (1997).

[15] E. Schlangen, *Crack development in concrete, part 2: Modelling of fracture process.* Advances in Fracture and Damage Mechanics Vii **385-387**, 73 (2008).

[16] M. Lukovic, B. Savija, H. Dong, E. Schlangen, and G. Ye, *Micromechanical study of the interface properties in concrete repair systems,* Journal of Advanced Concrete Technology **12**, 320 (2014).

[17] M. Z. Zhang, Y. J. He, G. Ye, D. A. Lange, and K. van Breugel, *Computational investigation on mass diffusivity in portland cement paste based on x-ray computed microtomography (mu ct) image,* Construction and Building Materials **27**, 472 (2012).

[18] P. K. Mehta and P. J. Monteiro, *Concrete-microstructure, properties and materials. 2006,* Utilization of palm oil fuel ash in concrete: a review (1976).

[19] Z. P. Bažant and A. Yavari, *Is the cause of size effect on structural strength fractal or energetic–statistical?* Engineering Fracture Mechanics **72**, 1 (2005).

[20] A. Kanellopoulos, P. Giannaros, and A. Al-Tabbaa, *The effect of varying volume fraction of microcapsules on fresh, mechanical and self-healing properties of mortars,* Construction and Building Materials **122**, 577 (2016).

[21] X. M. Pan, R. Mercade-Prieto, D. York, J. A. Preece, and Z. B. Zhang, *Structure and mechanical properties of consumer-friendly pmma microcapsules,* Industrial and Engineering Chemistry Research **52**, 11253 (2013).

5

Quantification of the healing potential of PF microcapsule-based two component healing system

Learn to be what you are,
and learn to resign with a good grace all that you are not.

Henri-Frédéric Amiel

The self-healing potential of the PF capsule-based self-healing system in terms of permeability reduction and mechanical recovery is evaluated under an ideal condition. The healing function and reaction product are characterized by ESEM, EDS and TGA.The water permeability test is employed to characterize the influence of the self-healing system on the reduction of water transportation. The self-healing potential of PF/DCPD capsule-based self-healing system in mechanical regain is measured by means of 3-point bending test, wherein bonding strength is provided by the reacted healing agent.

5.1. Introduction

In chapter 3, PF microcapsules incorporating DCPD healing agent have been synthesized by the in-situ polymerization method. The results showed that the healing agent has been successfully microencapsulated in the PF shell. Synthesized PF microcapsules have a clear shell/core structure and can be partly triggered by the propagation of cracks. The related mechanical properties and the trigger ability of the synthesised microcapsules have also been investigated. Based on that, a numerical model for simulating the crack behaviour of microcapsule-embedded cementitious materials has been proposed. This numerical model helps to understand and design capsule-based self-healing cementitious materials.

Understanding of the optimal healing effect is crucial in designing a self-healing system, as it can provide a prediction to the full potential of the proposed system. Many studies have shown that self-healing can be realized in cementitious materials by incorporating microencapsulated healing agent [1–6]. However, due to the complicated triggering and healing process, the healing function induced by a capsule-based self-healing system has not been characterized clearly in cementitious materials. Furthermore, as the stability of the triggering and mixing of the system is not easy to control, it is difficult to quantitatively evaluate the potential of the capsule-based self-healing system at the moment.

It is known that microcapsule-based self-healing can only be fully realized if both the microcapsules and the catalyst can be triggered and mixed properly. In this chapter, to provide a better way to practically assess the functionality of the synthesised capsule-based self-healing system, a standardized method which can quantitatively evaluate the healing efficiency is developed. A cement paste with an artificial planar crack was used to simulate a cracked specimen. Microcapsules containing the healing agent and catalyst were delivered manually between two cement surfaces with controlled width. Since the healing system is a two-component system, wax protected Grubbs' catalyst was prepared based on an improved procedure reported in [7]. The self-healing potential of the PF capsule-based self-healing system in terms of permeability reduction and mechanical recovery was evaluated under an ideal condition wherein all capsules can be triggered and mixed properly with catalyst. TGA was used to characterize the polymerization of the healing agent. The morphology of the reacted healing agent was observed by environmental scanning electron microscope (ESEM) and the chemical elements were detected by energy dispersive spectroscopy (EDS). Finally, a water permeability test was employed to characterize the efficiency of the self-healing system on the reduction of water transportation. The self-healing potential of the PF/DCPD capsule-based self-healing system in mechanical regain was measured by means of a 3-point bending test, where the bond strength between two halves of the beam specimen was provided purely by the reacted healing agent.

5.2. Materials and experimental procedures

5.2.1. Materials

Ordinary Portland cement, CEM I 52.5 N supplied by ENCI B.V. (The Netherlands) was used for preparation of test samples. Deionized water was used as mixing water. The water to cement ratio was 0.4. Millimeter level PF/DCPD microcapsules with diameter of 618 $\pm$ 38 μm and shell thickness of 40 μm were synthesized and screened according to the procedure described in Chapter 3.

Paraffin wax and 1^{st} generation Grubbs' catalyst purchased from Aldrich Co. (UK) were used to synthesize the wax protected catalyst. Poly(acrylic acid sodium salt) (Mw=1200)(PAA-Na) obtained from Aldrich Co. (UK) was used to enhance and keep the dispersibility of wax drops in the water. Details about the synthesis process of wax-protected catalyst will be given in 5.2.3.

5.2.2. Sample preparation

The healing function of the two component system was quantified by means of visual observation, healing product analysis, mechanical bond measurement and permeability testing. The methods to prepare the test samples are described in the following sections.

Quantification of healing agent delivered by microcapsules

To quantitatively study the crack healing and sealing provided by the microcapsule-based two component system, the amount of healing agent in the crack delivered by the microcapsules is a critical factor. In chapter 3, it has been found that there is a certain relationship between the size and the shell thickness of microcapsules. It is meant that, the average shell thickness can be estimated by understanding the mean diameter of the microcapsules. Therefore, the average amount of healing agent (A_h) delivered by a single microcapsule can be defined with the following equation:

$$A_h = \frac{4}{3}\pi(R_{capsule} - T_{shell})^3 \tag{5.1}$$

Based on this definition, the number of capsules (N_c) required for delivering the healing agent to a crack with certain width (W_h) can be defined as:

$$N_c = \frac{W_h \cdot S_{crack}}{A_h} \cdot V_f \tag{5.2}$$

where V_f [mm^3] is the assumed filling fraction of crack volume by the healing agent; S_{crack} [mm^2] represents the calculated area of crack surface; $R_{capsule}$ and T_{shell} [mm] are the average radius and shell thickness of the microcapsules, respectively. The above mentioned equations mean that, by understanding the average radius of capsules and the corresponding shell thickness and crack volume, the number of capsules required to partially or completely heal a crack can be calculated. In this calculation, it is assume that the microcapsules were completely filled with healing agent.

In the previous chapter, simulation results showed that, for microcapsules with an average diameter of 125 μm, 4 % addition to the cementitious material can

result in complete filling by healing agent of a 4.5 µm crack. The potential of capsule-based healing system should be evaluated on the same scale. However, in laboratory conditions, it is difficult to quantitatively evaluate the healing at such a length scale, as it is difficult to manipulate cracks with a calculated number of micro-size microcapsules. In addition, a certain amount of healing agent can be absorbed by the porous cementitious material within a short time. Therefore, in this part of the study, to practically investigate the healing potential of the capsule-based seal-healing system, millimeter level of PF/DCPD microcapsules ($R_{capsule}$: 618 ± 38 µm and T_{shell}: 40 µm) were employed to investigate the healing potential of artificial planar crack with controllable width (200 and 400 µm). The assumed fraction of the crack volume filled by healing agent was selected as 30, 60 and 100 %.

Sample preparation for water permeability tests

For the water permeability test, cylinders with a diameter of 25mm and thickness of 10mm were cast and then cut into two semi-cylinders using a thin section machine. The cut surfaces of the specimens were carefully ground using sand paper P500, P1200 and P4000. An artificial crack was simulated by putting the ground cutting surfaces of those two semi-circular columns together.

Figure 5.1 shows the schematic of the sample preparation and the test setup. In the first step, to control the crack width, double-faced adhesive tape with different thickness was applied at the ends of the crack as a spacer. Then, PF/DCPD micro-capsules with corresponding ratio of catalyst were placed between the two semi-circular samples (Figure 5.1a). After the microcapsules and catalyst were triggered by pressing those two semi-circular columns together to the required crack width, the healing agent was released and healed in a fast curing environment at 60 °C for 10 mins (Figure 5.1b). Then, samples were placed at room temperature for 24 h for a complete polymerization of the healing agent (Figure 5.1c). The water sealing potential of the prepared specimens with different crack width and volume filling fraction was investigated by the water permeability test (Figure 5.1d).

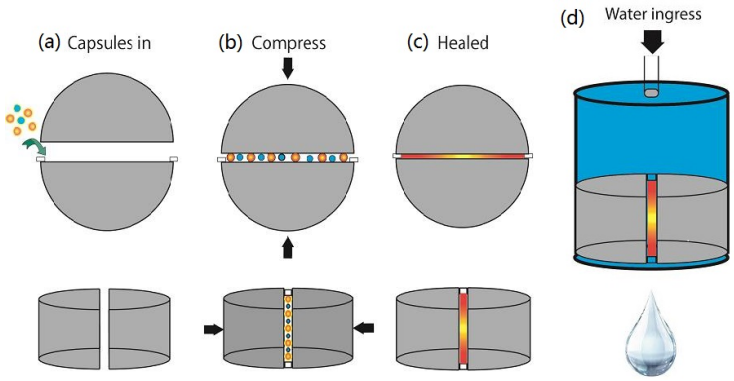

Figure 5.1: Schematic of the sample preparation process (a - c) and the water permeability test (d).

Table 5.1 describes the samples used in the permeability test. The sample name

Table 5.1: Samples used for permeability test.

Sample ID	Crack width (W_h)	Volume fraction (V_f)	Number of capsules (N_c)
S-0.2-0	0.2 mm	0 %	0
S-0.2-30	0.2 mm	30 %	16
S-0.2-60	0.2 mm	60 %	32
S-0.2-100	0.2 mm	100 %	52
S-0.4-0	0.4 mm	0 %	0
S-0.4-30	0.4 mm	30 %	32
S-0.4-60	0.4 mm	60 %	64
S-0.4-100	0.4 mm	100 %	106

(ID), crack width (W_h), the assumed filling fraction of crack volume by healing agent (V_f) and the number of capsules (N_c) used to prepare samples for healing potential investigation are listed. The catalyst to capsule ratio was constant at 0.2.

Sample preparation for mechanical bond measurement

For bond strength measurement, prisms with a size of (10 × 10 × 50 mm) were cast and then cut into two half prisms (10 × 10 × 25 mm) using a thin section machine. The cut surface of the specimens were carefully ground using sand paper P500, P1200 and P4000. An artificial crack (planar crack) was simulated by putting the grounded cutting surfaces of those two half prisms together.

To control the crack width, a simple device was designed, as shown in Figure 5.2a. Figure 5.2b demonstrates the process of sample preparation for the mechanical regain test. In the first step, two half prisms were put together into the mould leaving no space in between. To label the initial position, two limiters were stuck on both sides of the upper prism using double-sided adhesive tape with the bottom of limiter attached on the mould (Figure 5.2a). In the second step, after the limiters were fixed, a certain amount of capsules and wax-protected catalyst were placed in the artificial crack. Spacers (double-sided adhesive tape) with certain thickness were placed on the wall of mould (Figure 5.2b(a)). In the third step, the healing process was simulated as the microcapsules and catalyst were triggered by compressing the two half prisms (Figure 5.2b(b)). After the samples were cured at 60 °C for 10 min, the "healed" prism was taken out from the mould ((Figure 5.2b(c)). The mechanical healing potential which was realized by the bond strength of polymerized healing agent was tested using a meso-scale mechanical testing machine with 3-point-bending setup (developed by Kammrath & Weiss, Germany).

The sample name (ID), crack width (W_h), the assumed filling fraction of crack volume by healing agent (V_f) and the number of capsules (N_c) used to prepare the samples for healing potential investigation are list in table 5.2. The catalyst to capsules ratio was constant at 0.2.

5.2.3. Preparation of wax-protected catalyst

The wax-protected catalyst microspheres were synthesised according to the work of Rule et al. [7]. In a nitrogen protection glovebox, 10 g of paraffin wax (melting

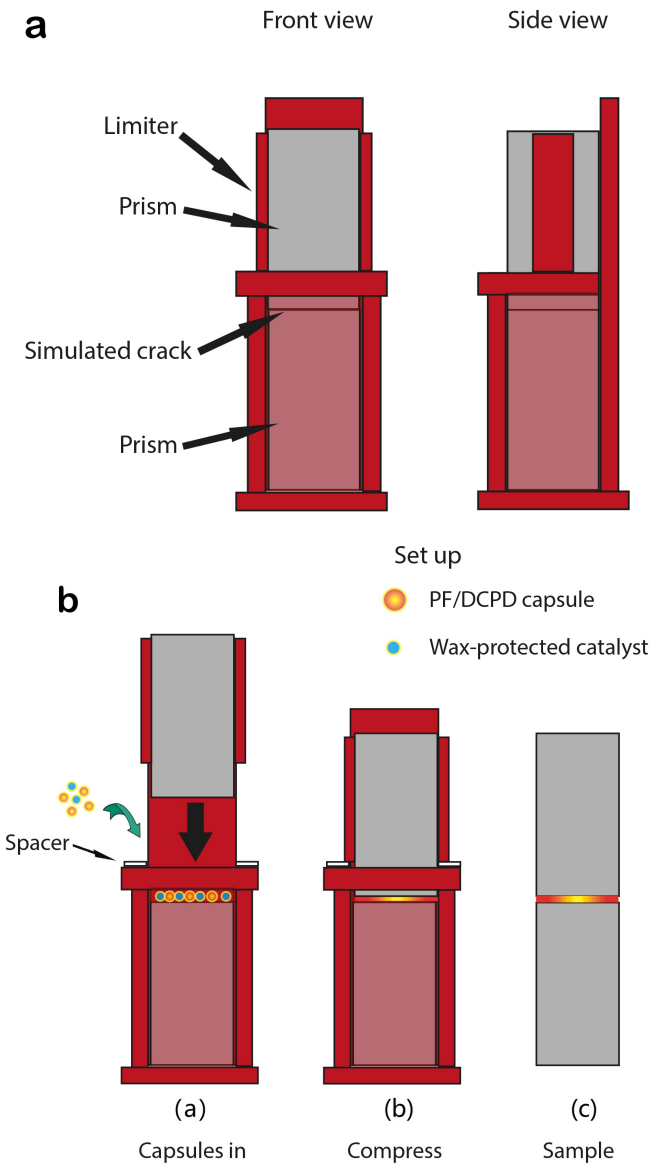

Figure 5.2: Schematic of (a) the device and (b) the process of sample preparation.

Table 5.2: Mixture of samples for mechanical test.

Sample ID	Crack width (W_h)	Volume fraction (V_f)	Applied capsules (N_c)
S-0.2-0	0.2 mm	0 %	0
S-0.2-30	0.2 mm	30 %	8
S-0.2-60	0.2 mm	60 %	16
S-0.2-100	0.2 mm	100 %	26
S-0.4-0	0.4 mm	0 %	0
S-0.4-30	0.4 mm	30 %	16
S-0.4-60	0.4 mm	60 %	32
S-0.4-100	0.4 mm	100 %	53

point = 58-60 °C) and 500 mg of 1^{st} generation Grubbs' catalyst were poured and sealed in a 20ml glass vial. Then the vial was taken out from the glove box and submerged in a thermostatic water bath at 80 °C. A solution consisting of 250 g water and 1 g Poly(acrylic acid sodium salt) (Mw=1200)(PAA-Na) was mixed in a 1L beaker and heated in the same thermostatic water bath at 80 °C. After 10 min (until the wax has melted), the vial was shaken to disperse the catalyst into the melted wax. Then the vial was opened and the catalyst containing the wax was poured immediately into a heated water solution (65-70 °C) while being stirred at 900 rpm. After stirring for 2 min, 600 ml freezing water (0 °C) was quickly poured into the beaker and the stirring machine was stopped at the same time. The final product was sieved by a sieve (D = 1 mm) to screen out big particles and then dried at room temperature.

5.2.4. Characterization of polymerized healing agent

The morphology of the reacted healing agent was observed using an ESEM (FEI XL35, Philips, The Netherlands) and the chemical composition was detected by the built-in EDS. Thermal properties of the polymerized healing agent were studied using a TGA analyzer (STA 449, NETZSCH, Germany) under flowing nitrogen (40-ml/min) at a heating rate of 10 °C/min from 40 to 600 °C.

5.2.5. Water permeability test

The water permeability was tested using a self-made permeability test setup. Figure 5.3 shows an overview of the setup. The permeability cells were first attached to the bottom of the permeability setup. Then water was poured into reservoirs at the top of the setup. To provide a constant water pressure of 0.1 bar, the water level of each permeability setup was manually controlled to a height of 1 meter from the top of water surface to the bottom of the permeability cell. To start the test, the switch of the reservoirs was turned on and timing was started simultaneously. Water flowing through the cracks was collected separately by buckets underneath the testing setups. The weight of the water in the buckets was weighted and recorded two times at two continuous 1 minutes. Permeability of the sample is defined as the water flow per second ($cm^3 \cdot s^{-1}$).

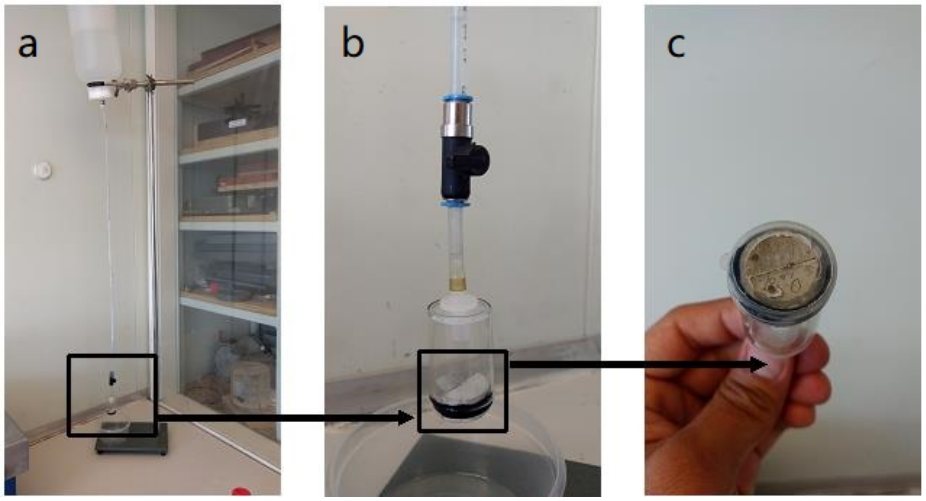

Figure 5.3: Images of the water permeability test setup (a), the permeability cells (b) and the bottom view of the test sample (c).

5.2.6. Three point bending test

The mechanical regain provided by the polymerized healing agent was tested using a meso-scale mechanical testing apparatus (developed by Kammrath & Weiss, Germany) with a three points bending test module, as shown in Figure 5.4. Before the test, the sample was placed in the middle between the two supports with the crack facing the top support. Then the bending test is performed under deformation control with a speed of 0.01mm/s. The load and displacement are recorded by the software automatically.

5.3. Results and discussion

5.3.1. Wax-protected Grubbs' catalyst

The environment in cementitious materials at the early age of hydration is harsh for the survival of sensitive additives. The pH value can rise up to 13. The moisture and air can also destructively influence the activity of sensitive catalyst. To protect the catalyst from being attacked by the harsh environment, paraffin wax is used as a shell to protect the activity of the sensitive Grubbs' catalyst from being influenced by the environment. A series of granular wax-protected catalyst is prepared.

Morphology

Figure 5.5 shows the morphology of the wax-protected Grubbs' catalyst prepared at different stirring rates, 1000 (a), 600 (b) and 400 (c) rpm, respectively. It was found that the stirring rate has a great influence on the size and shape of the particles. With the stirring rate of 1000 rpm, the particles show a regular spherical

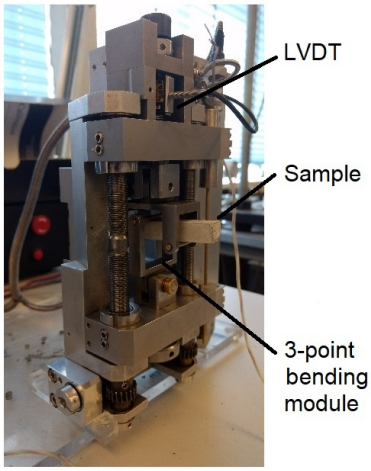

Figure 5.4: Meso-scale mechanical test machine with the 3-point bending test module.

shape. The average diameter of collected wax microspheres was around 115 μm. The majority of catalyst particles seem not be wrapped by wax microspheres properly. As the stirring rate decreased to 600 rpm, the size of the particles increases and agglomeration can be observed. However, the catalyst still has not been properly wrapped by wax. When the stirring rate decreased to 400 rpm, the size of wax granules increased. The shape of wax particles changed from round shape to granular shape. Despite the non-spherical shape, optical micrographs show that catalyst particles are suspended in the colorless wax, giving the granules a speckled appearance. Therefore, to guarantee a maximum healing performance, the wax-protect catalyst prepared at 400 rpm was selected for application in the following study.

Activity of the wax-protected catalyst

Following the successful preparation of wax-protected catalyst particles, the activity of the product in polymerization of DCPD was demonstrated through a simple proof of concept test. The test is shown in Figure 5.6. In this test, the weight ratio of catalyst particles to capsule is set as 0.2. When picking up the sample, it was found the that the glass sheet and cement sheet have been glued together (Figure 5.6d). This preliminary test demonstrates that the prepared wax-protected catalyst can be used to catalyze the microencapsulated healing agent, DCPD.

5.3.2. Identification of polymerized healing agent

The morphology of the healed surface is shown in Figure 5.7. This ESEM image illustrates that the capsules were ruptured by the compressive force and the healing agent flaw out and was polymerized by the catalyst. In order to test the chemical composition of different materials in this image, three different areas were selected

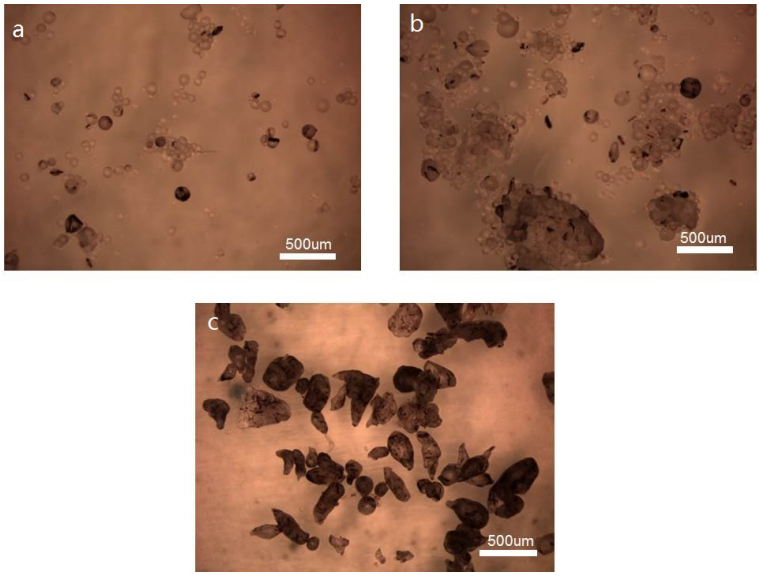

Figure 5.5: Morphology of wax-protected Grubbs' catalyst prepared at different stirring rate, (a) 1000, (b) 600 and (c) 400 rpm.

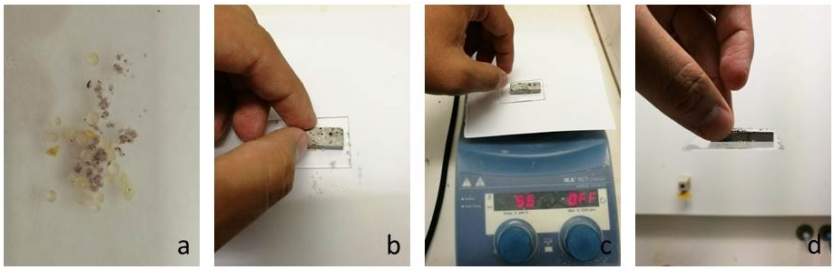

Figure 5.6: Preliminary test of the activity of the wax-protected Grubbs' catalyst. (a) Microcapsules and wax-protected Grubbs' catalyst were first dispersed on a glass sheet. (b) A cement sheet was placed on the capsule/catalyst mixture and a compressive force was imposed on the cement sheet to mechanically trigger the capsules. (c) Heat the sample on a heating plate at 60 °C for 10 min and keep it at room temperature for another 10 min. (d) The sample was left up to check the activity of the catalyst.

to perform EDS scanning. Corresponding EDS results and chemical composition are shown in Figure 5.8 and table 3. The EDS results demonstrate that, in area 1, despite a very weak calcium peak, only carbon can be found. This agrees well with the hydrocarbon chemical structure of the poly(DCPD), which consists of carbon and hydrogen. Since hydrogen cannot be detected by EDS, only the carbon peak can be observed. The energy spectrum of area 2 (Figure 5.8b) shows that, despite the strong peak of carbon, around 22 % of the total volume consists of oxygen. It is estimated that oxygen and carbon can be identified as the oxhydryl group of the phenol-formaldehyde resin. Remaining energy peaks such as calcium and silicon

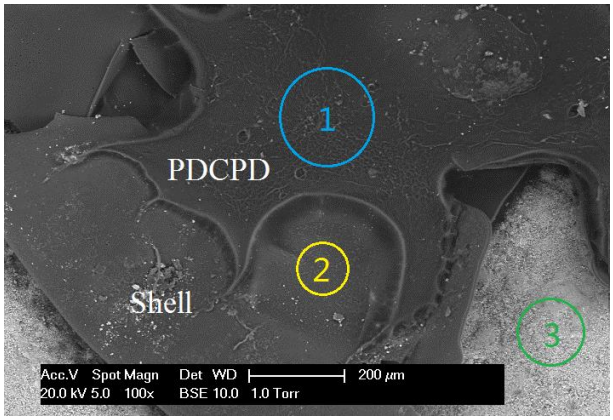

Figure 5.7: ESEM image shows that morphology of three different materials, poly-DCPD, shell and cement respectively. The inset circle areas 1, 2 and 3 are corresponding to the EDS result in Figure 5.8.

Table 5.3: Weight composition of the EDS scanned area. $Area_1$, $Area_2$ and $Area_3$ corresponding to the area 1, 2 and 3 in Figure 5.7.

	C-K	O-K	Na-K	Mg-K	Al-K	Si-K	S-K	Cl-K	K-K	Ca-K	Fe-K
Area_1	99.35									0.65	
Area_2	72.22	26.75				0.12		0.07		0.85	
Area_3	16.79	46.40	0.78	0.61	1.56	3.90	0.18	0.14	0.90	27.32	1.43

might be attributed to the pollution from the cement paste. The energy spectrum of area 3 (Figure 5.8c) is a standard spectrum of cementitious materials.

However, ESEM images and EDS analysis alone do not ensure that the product on the cement surface is the polymerized healing agent, poly-DCPD. To further identify this, the reaction product was then scratch off from the cement surface and thermogravimetry analysis (TGA) was employed to investigate the thermal behaviour of the reaction product. The TGA result of the reaction product was compared with the pure mono-DCPD. As shown in Figure 5.9, two major thermal degradations were observed on the TG curve of the reaction product. In the temperature range between 135 to 280 °C, the weight loss in the first stage was attributed to the decomposition of hydrocarbon compounds of the paraffin wax. The second weight loss of 40% in the range of 375 - 425 °C corresponded to gradual decomposition of the rigid cyclopentyl backbone of poly-DCPD. This result is consistent with the previous report for paraffin wax [8] and poly-DCPD [9]. On the contrary, the TGA curve of the pure healing agent (mono-DCPD) (in dashed line) only shows a steady weight loss between 30 and 120 °C. Obviously, the measured TGA curve implies that reaction product consist of paraffin wax and the polymerized healing agent, poly-DCPD. To be more specific, the healing agent, DCPD, has been polymerized by the wax-protected catalyst.

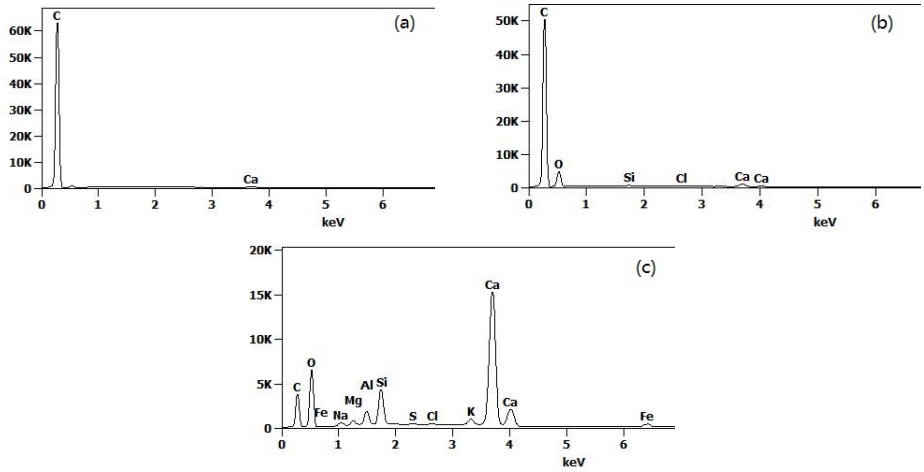

Figure 5.8: EDS results of (a) polymerized healing agent, (b) shell material (crosslinked PF resin and (c) cement paste.

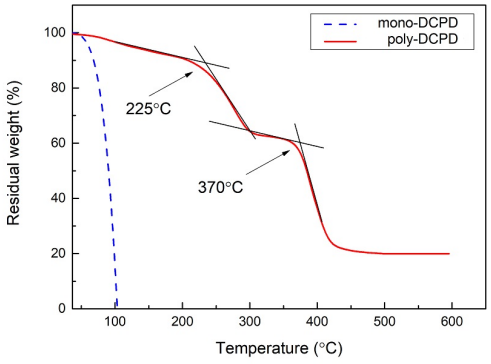

Figure 5.9: TGA results of the assumed reaction product (poly-DCPD) and mono-DCPD.

5.3.3. Quantification of self-healing potential in water blocking

The self-healing potential of the PF capsule-based healing system was first evaluated by means of a water permeability test. Each data point and its deviation is obtained from 3 samples. Figure 5.10 shows the result of samples with two different crack widths and 4 different crack filling fractions by the encapsulated healing agent. As can be seen from the water permeability result in Figure 5.10a, with the increase of volume fraction of healing agent delivered by capsules in the crack space, the permeability of the artificial crack of samples decreases steadily from 7.6 to 0.26 $cm^3 \cdot s^{-1}$ for 0.4 mm width cracks and from 5.5 to 0.17 $cm^3 \cdot s^{-1}$ for 0.2 mm cracks.

Based on the result of the water permeability test, the effect of water blocking as a function of volume filling fraction by the healing agent can be calculated as:

$$e = \left(1 - \frac{p_{(v)}}{p_0}\right) \cdot 100\% \tag{5.3}$$

where $p_{(v)}$ $[cm^3 \cdot s^{-1}]$ is the water permeability after the crack has been filled by v [%] of healing agent and $p_{(0)}$ $[cm^3 \cdot s^{-1}]$ is the permeability of the sample of which the artificial crack has not been filled by the healing agent. Figure 5.10b shows the potential self-healing efficiency of the PF capsule-based healing system in terms of water permeability calculated using the above equation. The result shows that the self-healing potential increased with the increase of volume fraction filled by the healing agent. A wide deviation in calculated healing efficiency can be found when the volume fraction of the healing agent is 30 %. This can be attributed to the heterogeneous distribution of capsules on the crack surface. This deviation is narrower when the filling fraction increased from 30 % to 60 % and even narrower when the filling fraction rose to 100 %. This suggests that, to have a stable self-sealing efficiency of the capsule-based self-healing system, the density and the distribution of capsules on the crack surface is a crucial factor. The figure also demonstrates that, if the crack space can be filled with the same volume of microencapsulated healing agent, more than 96% permeability reduction can be achieved after in-situ polymerization of the healing agent. So, for randomly distributed PF/DCPD capsules, to achieve a complete and stable sealing of a crack, the volume of healing agent which is deliver by capsules has to be equal to the volume of crack space under the condition that all healing agent can be released and polymerized. Additionally, no significant difference in healing efficiency was found with the same volume fraction of healing agent with a different crack width. It means, to achieve the water blocking function of the capsule-based self-healing system, the volume of the healing agent which can be delivered to the crack is a key factor.

5.3.4. Quantification of healing potential in mechanical regain

Following the water permeability test, the self-healing potential of the PF/DCPD capsule-based system was evaluated in mechanical regain. Meso-scale three-point bending tests were employed to impose a bending force on samples prepared as described in section 5.2.2. Figure 5.11a shows typical load-displacement curves

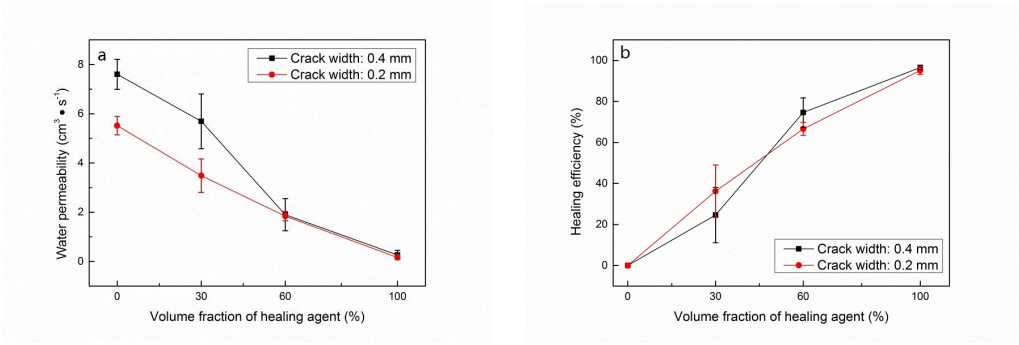

Figure 5.10: The self-sealing potential of the PF capsule-based self-healing system in water blocking. Figure (a) shows the water permeability of artificial cracked sample after the healing process and Figure (b) shows the potential healing efficiency calculated from the water permeability data with equation 5.3.

of representative blank cement sample and capsule healed sample with an artificial crack. It can be seen from the curve that, the peak load of the blank cement sample is much higher than the healed one. Moreover, the healed sample exhibited a nonlinear elastic behaviour. The nonlinearity is assumed to result from the poly-(DCPD) being plasticized by the paraffin wax which was applied to protect the Grubbs' catalyst.

The self-healing potential of the PF capsule-based self-healing system in mechanical regain is shown in Figure 5.11b. The self-healing potential is defined in the current work as the peak of healed sample divided by the peak load of the blank cement paste sample. Experimental results show that a maximum of 6% of the mechanical strength can be regained by applying the PF/DCPD self-healing system on an artificial crack. A wide deviation can be found on the result for each series of samples. Meanwhile, unlike the water permeability test, no obvious increase in the mechanical regain can be found with increases in the volume fraction filled with healing agent. This can be partly attributed to the increase of wax volume with proportional increasing of wax-protected catalyst on the spot of healing agent polymerization that detriment the bonding function of poly-(DCPD). The result demonstrate that, even through under the ideal condition that all healing agent can be released and be polymerized by the catalyst, very limited mechanical regain can be achieved on cementitious materials using the proposed capsule-based healing system.

5.3.5. Crack surface observation

Finally, the healed crack surface was investigated. An ESEM image of the crack surface can be found in Figure 5.12. The image shows that the microcapsules has ruptured and encapsulated healing agent has flown out. Moreover, as can be seen from the magnified figure on the right, the healed surface shows a polymer film on the crack plane with a high surface roughness. It is estimated that the high surface roughness allows for some mechanical bonding between the cement matrix and the

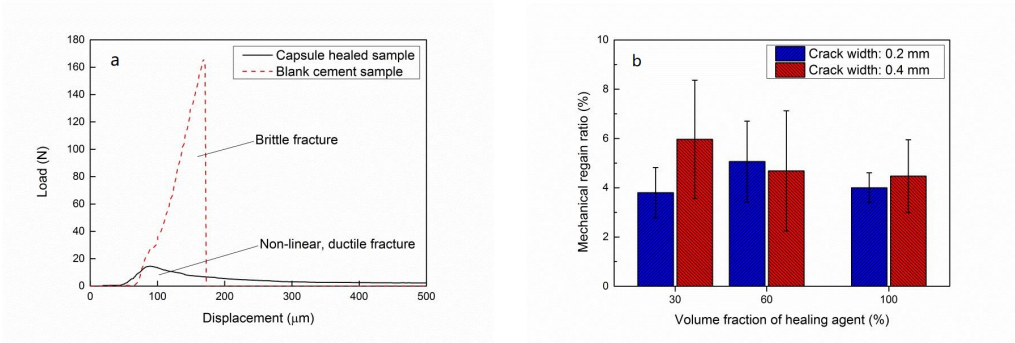

Figure 5.11: The self-healing potential of the PF capsule-based self-healing system in mechanical regain. (a) Typical load-displacement curves of representative blank cement sample and healed sample with artificial crack. (b) The self-healing potential of the PF capsule-based self-healing system in mechanical regain.

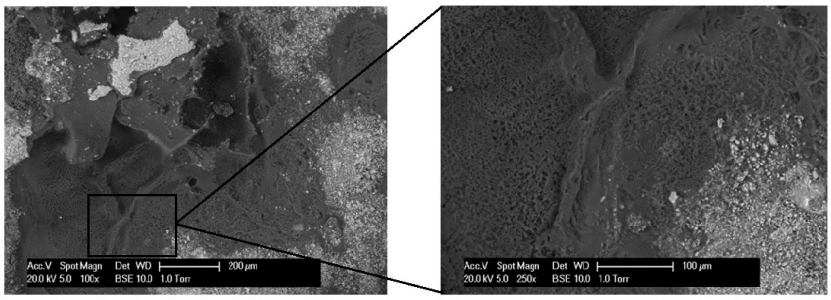

Figure 5.12: Morphology of healed cement surface showing (a) the ruptured microcapsules and (b) the polymerized healing agent.

polymerized healing agent.

5.4. Conclusion

In this chapter, the self-healing potential of the proposed two-component polymeric capsule-based self-healing system is explored and quantified. Granular wax-protected Grubbs' catalyst has been prepared and successfully catalysed the polymerization of DCPD which has been encapsulated in PF capsules. This result confirms that the PF/DCPD capsules and wax-protected catalyst particles system is functional under the condition that the microencapsulated healing agent can flow out and mix properly with catalyst. A series of cement paste samples with artificial planar cracks were used to explore and quantify the self-healing potential in water blocking and mechanical regain. Based on the presented study, the following conclusions can be drawn:

- The prepared granular wax-protected catalyst can be used to catalyze the

microencapsulated healing agent (DCPD).

• Results of the permeability test demonstrate that more than 96% water blocking can be achieved when the volume of available healing agent is equal to the volume of the crack.

• The potential of the self-healing system in mechanical regain is not very promising. A maximum of only 6% strength regain was observed.

The results suggest that the capsule-based self-healing system with PF/DCPD microcapsules and wax-protected catalyst particles have a great potential for crack sealing while they can do very little in terms of mechanical strength regain.

References

[1] N. P. B. Tan, L. H. Keung, W. H. Choi, W. C. Lam, and H. N. Leung, *Silica-based self-healing microcapsules for self-repair in concrete,* Journal of Applied Polymer Science **133** (2016).

[2] T. S. Qureshi, A. Kanellopoulos, and A. Al-Tabbaa, *Encapsulation of expansive powder minerals within a concentric glass capsule system for self-healing concrete,* Construction and Building Materials **121**, 629 (2016).

[3] P. Giannaros, A. Kanellopoulos, and A. Al-Tabbaa, *Sealing of cracks in cement using microencapsulated sodium silicate,* Smart Materials and Structures **25** (2016), Artn 084005 10.1088/0964-1726/25/8/084005.

[4] M. Araujo, S. Van Vlierberghe, J. Feiteira, G. J. Graulus, K. Van Tittelboom, J. C. Martins, P. Dubruel, and N. De Belie, *Cross-linkable polyethers as healing/sealing agents for self-healing of cementitious materials,* Materials and Design **98**, 215 (2016).

[5] B. Q. Dong, G. H. Fang, W. J. Ding, Y. Q. Liu, J. C. Zhang, N. X. Han, and F. Xing, *Self-healing features in cementitious material with urea-formaldehyde/epoxy microcapsules,* Construction and Building Materials **106**, 608 (2016).

[6] J. Y. Wang, H. Soens, W. Verstraete, and N. De Belie, *Self-healing concrete by use of microencapsulated bacterial spores,* Cement and Concrete Research **56**, 139 (2014).

[7] J. D. Rule, E. N. Brown, N. R. Sottos, S. R. White, and J. S. Moore, *Wax-protected catalyst microspheres for efficient self-healing materials,* Advanced Materials **17**, 205 (2005).

[8] L. Sanchez-Silva, J. F. Rodriguez, M. Carmona, A. Romero, and P. Sanchez, *Thermal and morphological stability of polystyrene microcapsules containing phase-change materials,* Journal of Applied Polymer Science **120**, 291 (2011).

[9] B. T. Wang, K. Mireles, M. Rock, Y. Z. Li, V. K. Thakur, D. Gao, and M. R. Kessler, *Synthesis and preparation of bio-based romp thermosets from functionalized renewable isosorbide derivative,* Macromolecular Chemistry and Physics **217**, 871 (2016).

6

Self-sealing concrete by using water-swelling rubber particles

An ant hole can cause a collapse of a great dike.

Han Feizi

In this study, the application of water-swelling rubber particles for providing the cracked concrete a self-sealing function is developed. The feasibility of applying water-swelling rubber particles and the influence of incorporating water-swelling rubber particles on the mechanical properties of concrete is investigated. The self-sealing efficiency of water-swelling rubber particles embedded cementitious material with different content and particle size is quantified through a permeability test. The sealing effect of samples with water swelling rubber particles is monitored by X-ray Computed Tomography (XCT).

Parts of this chapter have been published in Materials **10**, 979 (2017) [1].

6.1. Introduction

Cracks on meso-scale level can cause water leakage, then reducing the functionality of civil structures such as dams, retaining walls, tunnels. Cracks also allow transport aggressive agents by water migration through the crack, which is often detrimental to the service life of reinforced concrete structures. Furthermore, when the ingress of aggressive agents leads to corrosion of the reinforcement, it can even pose a threat to the safety of the structure. Therefore, for meso-scale cracks, they also need a more efficient and automatic way to reduce the hazardous effect it brings.

Up to now, several routes were studied targeting to reduce the permeability of concrete automatically. Polymer water-swelling materials such as superabsorbent polymers (SAP) are found to be a new type of self-healing materials that hold a potential in crack self-sealing [2–5]. The result shows that the application of SAP can provide up to 85 % and 98 % decrease of the peak flow and cumulative flow, leading to the complete sealing of a 0.3 mm crack. However, practical application of SAP in civil engineering structures was rather limited due to its detrimental effect on compressive strength. Recent results show that the addition of 5 % SAP by weight of cement will lead to a reduction of 80 % of compressive strength of mortar [2].

To find a material which is practically applicable of providing a long-term sealing capacity of concrete structures, three requirements should be satisfied: (1) the materials can survive in and have a good bonding with concrete structure; (2) the sealing function of the selected material can be triggered automatically upon water ingress or other stimuli without or with less human intervention; (3) the incorporation of the material should have only limited negative effect on the mechanical properties of concrete, and if possible, even enhance it. Previously, the possibility of applying rubber phases as partial replacement of sand in concrete has been investigated towards making the concrete, a traditional building material, embrace more versatile performances such as higher energy dissipation, ductility, durability, damping ratio, impact resistance and toughness [6–9]. The results of these studies show that waste tire rubber reinforced concrete (RRC) could be an ideal ecological component of concrete when it was applied as a replacement of aggregates and subjected to dynamic loading conditions. While, to our knowledge, no research can be found on the application of rubber with water swelling function to provide the concrete with a combined self-sealing and crack bridging function.

Water swelling rubber is a new type of construction material which has been widely used for sealing of pre-cast concrete elements (e.g. man holes), shaft rings and pipe lead-throughs etc. The matrix of water swelling rubber is butyl rubber, a copolymer of isobutylene with isoprene, also known as Isoprene Isobutylene Rubber (IIR). The expanding property of water swelling rubber results from the irrevocable bonding of polyurethane-based water-expanding polymer resin which has been premixed in the IIR during the fabrication process. Comparing with instant swelling SAP, the benefit of water swelling rubber is that, there will be a swelling delay when it first mixes with water. This is means that only limited volume of can swell up within 24 h. This 24 h swelling delay provides a precious time for the mortar to be hardened. The reason for this delay can be attributed to the IIR rubber prolonging

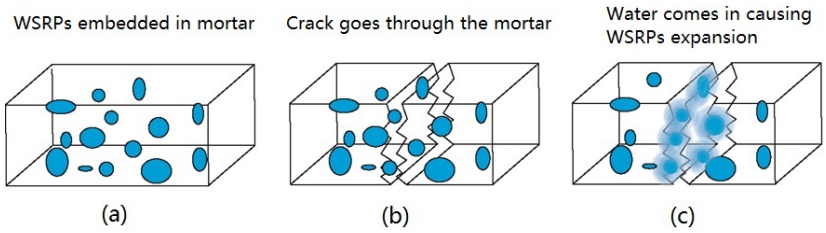

Figure 6.1: Schematic showing the mechanism of self-sealing cracks using WSRPs.

the time for the pre-mixed polyurethane-based water-expanding polymer resin in it from swelling by water. After 7 days contact with water, the water swelling rubber can finally swell up to 250 % of its original volume. Meanwhile, due to the sticky texture and strong surface bond strength of water swelling rubber to cementitious materials, it is expected that the expanded rubber could have a good adhesion to the crack faces, provide some crack bridging effect and keep the cracked pieces together.

Accordingly, the core concept of this work is to utilize water swelling rubber particles (WSRPs) as a new ingredient of cementitious materials to enable the ability of cracked concrete to reduce its permeability and partially regain its deteriorated mechanical properties. Once cracks have formed in the concrete structure and water penetrates, the rubber may swell gradually, expand along the crack and partly seal the crack. Subsequently, the embedded rubber particles can also act as reinforcing particles that provide an extra bond strength and prolong the serviceability of cracked concrete. In this study, the feasibility of applying WSRPs in crack self-sealing was proven by both a simulated crack and XCT technology. The influence of incorporation of WSRPs on the mechanical properties was investigated. Water permeability tests were carried out on a series of WSRPs embedded mortar specimens to study the influence of WSRPs size and content, and crack width on the self-sealing effect. Finally, the capability of crack bridging to the cracked mortar, provided by the embedded WSRPs, was characterized. Figure 6.1 schematically shows the concept.

6.2. Experimental study

6.2.1. Materials

Water swelling rubber (AQUA TACKSEAL) was provided by TPH Bausysteme GmbH, Norderstedt, Germany. To obtain the water swelling rubber particles (WSRPs), the as received materials were first frozen by liquid nitrogen and then crushed immediately in a grinder by hand. Before the mass water swelling rubber was crushed into smaller particles, cement powder was added in the grinder. This cement powder acted as desiccant, sticking on the new formed surface of WSRPs to prevent the new formed particles from sticking together. After that, the crushed WSRPs were screened by a sieve with mesh diameter of 0.5 mm, 1 mm, 2 mm and 4 mm,

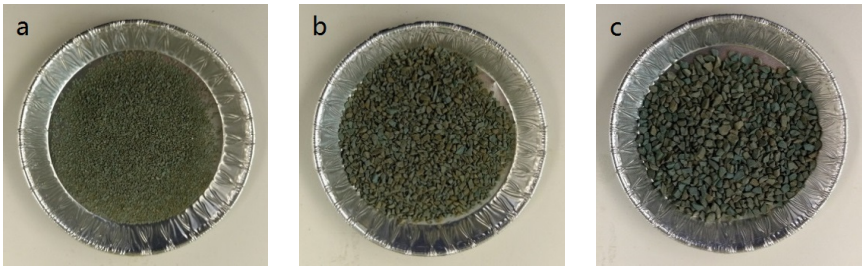

Figure 6.2: Images of WSRP with size range of (**a**) 0.5-1 mm, (**b**) 1-2 mm and (**c**) 2-4 mm.

respectively. Figure 6.2 shows the images of granular WSRPs used in this study highlighting the difference in particle size, (a) S size, (b) M size and (c) L size.

Ordinary Portland cement, CEM I 52.5 N and CEN standard sand was used for the preparation of mortar samples. The grading of the sand is given in Table 6.1, which complies with the requirements of EN 196-1 (§ 5) and ISO 679: 2009 (§ 5). Deionized water was used as batch water.

Table 6.1: The Grading of Standard CEN Sand

Square mesh size (mm)	2	1.6	1	0.5	0.16	0.08
Cumulative (%) retained	0	7	33	67	87	99

6.2.2. Sample preparation

According to the EU standard EN 196-1 [10], the amount of cement was kept constant at 450 g, water to cement ratio was selected as 0.5, and 1350 g filler (standard sand + WSRPs) was used as fine aggregate. Mortar was chosen as a representative material for concrete. The mixture contents of cement mortar are shown in Table 6.2. Four series of specimens including S, M, L, and B were made. For those WSRPs incorporated cement mortar, series S, M and L represent the size of incorporated WSRPs, ranging 0.5–1 mm, 1–2 mm and 2–4 mm. The following numbers 1, 3 and 6 stand for the volume ratio of sand replaced by WSRPs. Series B, as reference, is pure mortar without WSRPs. To avoid any interference and complication in the results, superplasticizer was not used. Mortar mixtures were mixed in a Hobart mixer by a certain order. In the first step, cement, sand and WSRPs were put in the mixer and mixed thoroughly at low gear (60 rpm) for 60 s. Water was then added in the mixer and mixed at low gear (60 rpm) for another 60 s. After the mixing, the mortar mixtures were cast into standard prismatic moulds (40 × 40 × 160 mm^3) and cylindrical moulds (60 mm long and with a diameter of 33.5 mm). Following the work of Palin et al. [11], the cylinder mould has two opposite notches on both side along the height (2 mm wide and 3 mm deep). The casted moulds were then vibrated on a shaking table to remove the voids. All the specimens were de-moulded after 24 hours and then cured in a fog room at normal curing condition

(20 °C, >95 % RH) for 28 days. For each mix (with different ID) , 6 standard prisms and 9 cylinders were casted. Figure 6.3 illustrates images of the mixture prepared for mixing procedure (a), the prisms for mechanical test (b) and the cylinder with notches for water permeability test (c).

Table 6.2: Mix content of cement mortar

Series	ID	Water (g)	Cement (g)	Sand (g)	WSRPs (g)	WSRPs/Sand
S	S1	225	450	1338.9	11.1	1 vol. %
	S3	225	450	1309.5	33.0	3 vol. %
	S6	225	450	1285.7	64.3	6 vol. %
M	M1	225	450	1338.9	11.1	1 vol. %
	M3	225	450	1309.5	33.0	3 vol. %
	M6	225	450	1285.7	64.3	6 vol. %
L	L1	225	450	1338.9	11.1	1 vol. %
	L3	225	450	1309.5	33.0	3 vol. %
	L6	225	450	1285.7	64.3	6 vol. %
B	B	225	450	1350	0	0 vol. %

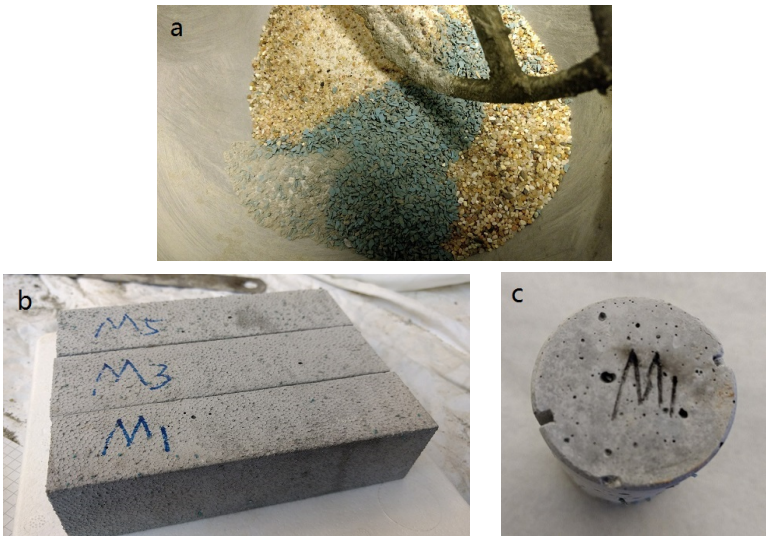

Figure 6.3: Images of (**a**) the mixture prepared for mixing procedure, (**b**) prisms for mechanical test and (**c**) cylinder with notches for water permeability test

6.2.3. Morphology of WSRPs in mortar

The morphology of cement mortar containing L and M sized WSRPs was imaged by a digital camera. The size of specimens that was used for the observations is a 40 ×

40 × 5 mm piece obtained from prism. The microstructure of the WSRP embedded mortar was characterized by environmental scanning electron microscope (ESEM) (XL30, Philips, Amsterdam, The Netherlands). All imaging was performed under low vacuum. Before the test, the surface of the sample is ground by four different grinding papers (500#, 800#, 1200#, 4000#). Then, the sample was polished by hand on a lapping table using diamond paste with particle diameter of 6, 3, 1 and 0.25 µm. The polishing time is 5 min for each step.

6.2.4. Feasibility of applying WSRP in concrete — proof of concept

Swelling effect of WSRPs in simulated crack

The swelling effect of WSRPs in concrete was first investigated using a simulated crack. To clearly see the swelling effect, a glass sheet was used to cover the cross section of WSRPs containing mortar sample. In order to ensure the crack width, a double sided plastic tape with a thickness of 0.8 mm was inserted in between the glass sheet and the section surface of the sample to control the simulated crack width to 0.8 mm. Nomal plastic tape was used to prevent the glass debond from the double side plastic tape by wraping the two end of glass sheet. The swelling effect of the WSRPs was recorded by acquiring images with a digital camera after 0, 3, 7 days of immersion in deionized water.

Sealing effect of WSRP in mortar

XCT (Nanotom, GE Inspection Technologies, Lewistown, LP, USA) was applied to proof the swelling and sealing function of WSRPs within hardened mortar. As a non-destructive imaging technique, XCT provides an approach to obtain internal information of (cementitious) materials [12]. To visualize the sealing effect of WSRP in mortar, the WSRP embedded mortar cylinder was subjected to XCT twice, before and after the sealing process. In between, the cylinder was immersed in deionized water for 7 days. In this study, the raw XCT images were acquired at an acceleration voltage of 120 kV with an exposure time of 4s and X-ray power of 8 W. The resolution of CT scans was set to 20 µm. The final data set of XCT consisted of 1440 radiographs of which each image was acquired with a 0.25 ° rotation. Then, phase retrieval and tomographic reconstruction were performed to improve the boundaries and signals using the software supplied by the manufacturer. A series of reconstructed tomographic images (X–Z plane) were consequently imported into a commercial software (VGStudio MAX 3.0, Volume Graphics GmbH, Heidelberg, Germany) for segmentation and 3D visualization. Section images of the reconstructed 3D volume containing information of the crack and WSRP were compared. The crack self-sealing effect was quantified via an additional analysis of the 3D volume by comparing the volume fraction of WSRP and crack in regions around the healed crack, before and after the healing process. Figure 6.4 shows the setup for non-destructive observation of the self-sealing effect using XCT.

Figure 6.4: XCT setup for the evaluation of sealing effect of WSRP in mortar.

6.2.5. Influence of the WSRP on the mechanical properties of mortar

The flexural and compressive strength of the WSRP embedded cement mortar was measured according to TS EN 1015–11 (2000) [13]. In order to obtain the flexural strength of the mortars, 40 × 40 × 160 mm specimens were used. The specimens were tested after 28 days curing for flexural strength under three-point loading with the span between supports being of 100 mm. The average of results obtained from three prismatic specimens was reported as flexural strength. The two broken parts of the 40 × 40 × 160 mm retained after the flexural strength test were used for determination of the compressive strength. The loading area was 40 × 40 mm. The average of results obtained from six broken pieces was reported as compressive strength. The loading rate was 500 N/s for both flexural and compressive strength test. To investigate the influence of aging on the mechanical properties, the same test was conducted again on the rest three specimens which were stored in lab environment for 28 days after the first 28 days of hydration.

6.2.6. Evaluation of self-sealing ability

Crack calibration

A crack with a certain width was induced on the cylindrical specimens for the evaluation of the water sealing effect. Before the test, a steel rod was placed on above of the upper side of the notch (Figure 6.5a). Then an Instron 8872 servohydraulic testing machine (Instron Corp., Canton, MA, USA) was used to apply a compressive load on the steel rods until the cylinder split diametrically. Spacers with a width of 2.4, 2.7 and 3.0 mm were placed thoroughly in the notches. Since the width of notches is 2 mm, therefore by placing spacers with a width of 2.4, 2.7 and 3.0-mm, cracks widths of 0.4, 0.7 and 1.0 mm can be achieved. Then the spacers were moved to half way of the notches, and a two-component adhesive, Plex 7742 and Pleximon 801 (Evonik Rohm GmbH, Darmstadt, Germany), was mixed and applied on the space of notches. After the adhesive had hardened, the spacers were removed and the rest space of notches was completely filled by adhesive. A wa-

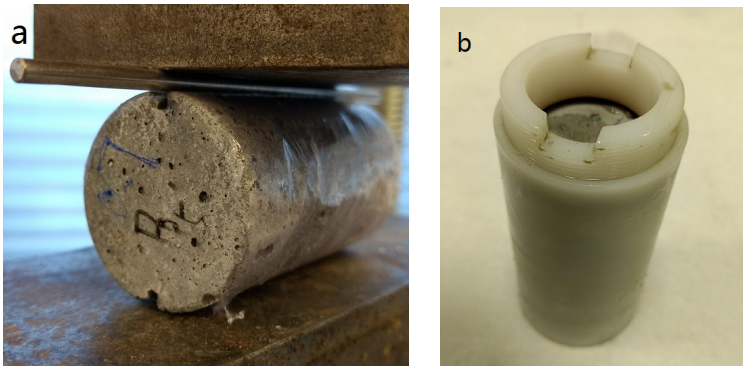

Figure 6.5: Images of (**a**) test setup for crack calibration and (**b**) watertight permeability cell.

tertight permeability cell was used to seal the cylinder specimens and to connect them with the permeability test setup (Figure 6.5b). To prevent the water leakage from pores or defects of cylinders during the permeability test, before the cylinder was placed into the cell, rubber rings were attached on both ends of the cylinder specimen. In the end, stereomicroscope analysis was applied to measure the actual widths of cracks. A tolerable variation was set for those samples with a crack variable higher than a given criteria to be screened out from the permeability test. For the 0.4 mm crack sample, the tolerable variation is 0.05 mm, for 0.7 mm crack sample, the tolerable variation is 0.07 mm and for 1.0 mm crack sample, the tolerable variation is 0.1 mm. This means the variable of those tested sample within the tolerable variation was regarded as and reflected on the standard deviation of water permeability.

Water permeability

The water permeability was tested according to the work of Palin et al. [11]. Briefly, the permeability cells were first attached to the bottom of the permeability setup. Water was then poured into reservoirs at the top of each setup. To provide an almost constant water pressure of 0.1 bar, the water level of each permeability setup was manually controlled to a height of 1 meter from the top of the water surface to the bottom of the permeability cell. To start the test, taps of the reservoirs were released. Water was flowing through the cracks and was collected separately by buckets beneath the testing setups. The weight of the water in the buckets was weighted and recorded two times at two continuous 5 minutes. The permeability test was performed after 0 and 7 days submersion of the crack-induced specimens in tap water. The permeability ($cm^3 \cdot s^{-1}$) is simply defined as the volume of flowed out water from the crack (cm^3) divided by the recorded time (s). For each data point, 3 replicate samples were tested. The image of the permeability setup is shown in Figure 6.5.

6.2.7. Visual Assessment of reinforcement function of WSRPs

The crack bridging function is a unique characteristic of WSRPs which can prevent the crack from fully separating the specimens in two pieces. To visualize the function, a mortar prism with WSRPs embedded was fractured by tensile force using Axial Tension-Compression Systems (8872, Instron Corp., Canton, MA, USA). Then the tensile force was removed, the cracked area of WSRPs embedded mortar was recorded by a digital camera.

6.3. Results and discussion

6.3.1. Morphology of WSRP in mortar

The morphology of mortar with embedded WSRPs is shown in Figure 6.6, highlighting the dispersibility, size and shape of the embedded WSRPs. As can be seen from the figure that both large size and medium size WSRPs (blue) are well dispersed in mortar. No obvious voids can be found around the WSRP, demonstrating that the quartz shape WSRPs have a good connection with the mortar matrix, reminiscent of aggregates. For better understanding the influence of WSRPs on the surrounding microstructure of mortar, the interface zone between WSRPs and mortar matrix at the age of 28 days of the sample was investigated by ESEM. It can be clearly seen from Figure 6.7a that no macro or micro-cracks were found due to the incorporation of WSRPs. Meanwhile, the magnified image in Figure 6.7b tends to show that WSRPs have an effective adhesion with cement paste. All the above-mentioned phenomena suggest that the embedded WSRPs do not change evidently during the process of hydration and the existence of WSRPs will not influence the microstructure of the surrounding mortar.

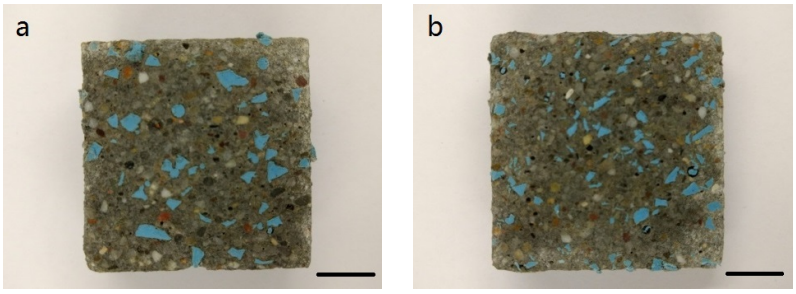

Figure 6.6: Images of the cross section of mortar specimen with WSRPs embedded (**a**) L series (particle size: 2-4 mm); (**b**) M series (particle size: 1-2 mm). The length of scale bar in images is 10 mm.

6.3.2. Proof of concept

Swelling effect of WSRPs at simulated crack

The self-sealing function of the WSRPs in cementitious materials is realized through swelling of WSRPs and expanding into the cracks. To proof the feasibility of applying WSRPs in mortar to reduce the volume of the crack and further decrease the permeability, a preliminary test was carried out. In order to have a direct view of

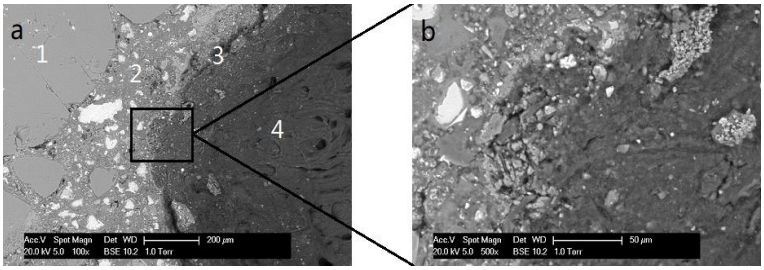

Figure 6.7: ESEM microstructure morphologies of the interface zone between WSRP and mortar matrix at the age of 28 days: (**a**) (1) the aggregate particles, (2) hydrated and unhydrated cement paste, (3) WSRPs and cement paste interface and (4) embedded WSRPs, and (**b**) an enlarged view of the microstructure of the interface.

the swelling process of WSRPs, a glass sheet was used as one side of the crack, covering a slice of WSRPs embedded mortar. Figure 6.8 shows the swelling process of WSRP in the simulated crack. As can be seen from the figure, at the initial stage (0 day), the WSRPs (blue) keep their original shape (Figure 6.8a). After 3 days of immersion in water, the embedded WSRPs begin to swell and expand in the crack space in which some of them join together which partly blocks the crack space (Figure 6.8b). As the immersion time goes to 7 days, the WSRPs expand only a little bit more (Figure 6.8c). The results demonstrate that the self-sealing action of WSRPs can be activated and reach its maximum function within 7 days.

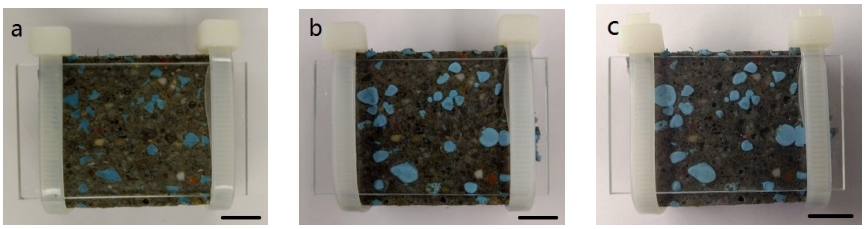

Figure 6.8: Swelling effect of WSR particle in a simulated crack with a crack width of 0.8 mm at (**a**) 0 day, (**b**) 3 days and (**c**) 7 days of the specimens being immersed in water. The length of scale bar in images is 10 mm for all images.

Self-sealing effect of WSRPs in mortar

In this study, XCT was used to study the self-sealing effect of WSRPs on cracks in the hardened mortar specimens. In the first step, the reconstructed 3D volumes of the cracked mortar samples, before and after the water healing process, were coupled by selecting the same rotation angle (Figure 6.9a). In the second step, tomographic slices of a longitudinal cross-section of the reconstructed 3D volumes were selected and compared in detail (Figure 6.9b). Finally, various phases of composite material are differentiated and colored based on the principle of different grey value (result from different molecular weight and density of phases) under the X-Ray. Therefore,

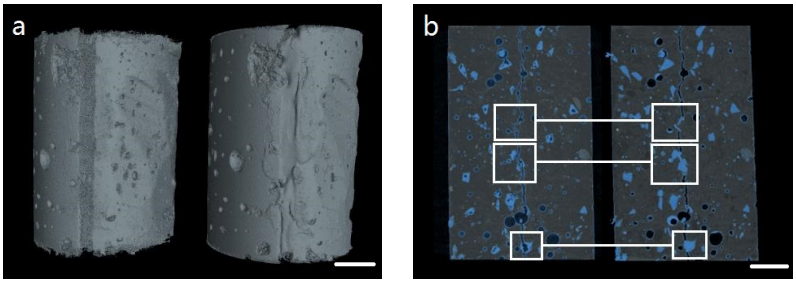

Figure 6.9: Reconstructed XCT images of (**a**) samples with WSRPs embedded cement mortar and (**b**) samples before and after sealing of the crack by WSRPs (blue particles). The length of scale bar in images is 10 mm.

those materials with the same density can be selected. Since the rubber is basically a polymer which has much less density than the cementitious material, all grey value falling into a certain band of grey value chart should be the phase of rubber. So the material within this grey value was selected and then labeled with a blue color. It can be clearly seen that, before the water healing process, the crack runs through the entire specimen. This means that the water can permeate through the crack directly without any obstacle. While, after the healing process, WSRPs (blue) which are located along the crack were swollen in response to water absorption and partially blocked the crack, as can be seen in the white boxed areas. This result revealed that the WSRPs hold a potential to be applied for self-sealing cracks in mortar with the water swelling function.

6.3.3. Influence of WSRPs on the mechanical properties of mortar

It is known that the use of 1 % superabsorbent polymer (SAP) will result in an around 18 % decrease in strength [2, 14]. Similarly, a significant decrease in concrete compressive strength with increasing amount of rubber phase in the mixture can always be detected regardless the different nature, size and composition of tyre rubber [6, 15]. The result shows that the compressive strength of rubberised concrete decreased 20, 28 and 64 % by adding 2, 3 and 6 % of tyre rubber in concrete [16]. In this study, the influence of incorporating 1, 3 and 6 % of WSRPs on the mechanical properties of mortar was evaluated systematically. For each mix 3 replicate prisms were cast. Mortar with 10 % of WSRPs incorporation has also been tried. While since it detrimentally influence on the mechanical properties of mortar, the results have not taken into consideration in this study.

Figure 6.10a shows the relationship between the flexural strength and content of WSRPs. The error bar represents the standard deviation of the test results. It is clear that the addition of WSRPs has a negative effect of the flexural strength of the specimens. For the L series specimens, the flexural strength was decreased by values ranging from 10.5 to 20 % with increasing content of WSRPs from 1 to 6 %. The flexural strength of M series specimens decreased up to 18 % for

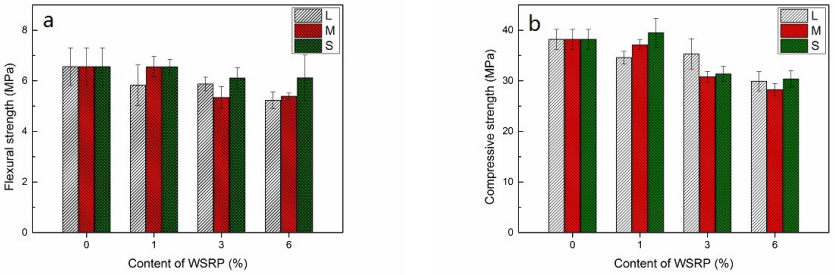

Figure 6.10: Influence of WSRPs incorporation on the flexural strength (**a**) and compressive strength (**b**) of the specimens (with different additions of WSRPs, 0 % (series B), 1 %, 3 %, 6 % of sand by volume percentage, respectively) at the age of 28 days of hydration.

those specimens containing 6 % WSRP. The addition of S size WSRPs has the least influence on the flexural strength. It only decreased 6 % of its flexural strength for a dosage of 6 % WSRPs. As expected, the incorporation of WSRPs also had a negative effect on the compressive strength of the specimens. As shown in Figure 6.10b, by incorporation of 1, 3 and 6 % of WSRPs, the compressive strength for S, M and L series specimens reduced by 0-10 %, 8-18 % and 20-26 %, respectively.

As it is expected that the addition of WSRPs will have a long-term effect on the internal strength and humidity, the mechanical properties of the specimens at a later age (28 days of hydration and then 28 days stored in laboratory environment) were investigated on the L series specimens. The results are shown in Figure 6.11. According to the results, a significant increase was observed for both flexural and compressive strength in each series of specimens. For the flexural strength, a maximum of 38.7 % increase was found for specimens containing 6 % of large size WSRPs at the age of 56 days compared to 28 days. Regarding the compressive strength, an obvious increase was noticed for the R and L1 specimens while only slight increase was found on L3 and L6. It can be seen that longer storage time can enhance the mechanical properties for both of the specimens with and without WSRPs. The main reason for this can be attributed to the further hydration of those unhydrated cement powder. Meanwhile, it is noteworthy that after a 28 days storage in laboratory environment, both flexural strength and compressive strength of WSRPs containing specimens were even higher or similar to the reference specimens with 0 % of WSRP at 28 days of hydration. The possible reason for this enhancement can be partly attributed to the fact that, after a 28 days storage in laboratory environment, the WSRPs in specimens has less swelling pressure than the specimens which were just taken out from the fog room at 28 days of hydration. This will result in a lower stress concentration in the specimens and, therefore, a higher mechanical strength of specimens. Another explanation for this phenomenon is that the absorbed water in WSRPs promoted a further hydration of the cement matrix by yielding their absorbed water into the surrounding cement matrix for the formation of new C–S–H crystals after 28 days of hydration. This

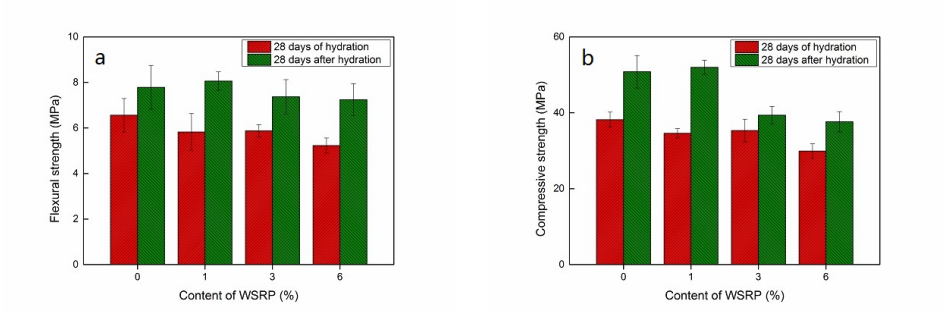

Figure 6.11: Comparison of mechanical properties of WSRPs embedded specimens at different ages (28days of hydration and 28 days storage at lab environment after 28 days of hydration) .

can be deduced from the obviously slightly higher increase of flexural strength in the specimens with WSRPs than the reference specimen with 0 % of WSRPs after a 28 days storage in laboratory environment. While the details of further hydration function is beyond the scope of this thesis and will be analyzed and described in the future.

6.3.4. Self-sealing effect

The permeability of specimens before and after the healing process was measured and plotted. Figure 6.12 shows the data of the permeability tests with different content of WSRPs (0 % (R), 1 %, 3 %, 6 % of sand by volume percentage) and different sample crack widths (0.4, 0.7 and 1.0 mm).

For 0.4 mm crack width samples, the permeability decreased within the range of 13 - 27 % with the addition of 1 - 6 % of small size rubber filler (S series). In this particular experimental setup, reductions caused by 1 % concentration of medium size (M) and large size (L) rubber fillers were negligible. However, the performance of specimens containing 3 - 6 % of both medium (M) and large (L) size rubber fillers were more advanced compared to the small size particles (S) series with 18 - 42 % and 38 - 45 % reduction in permeability, respectively. Despite the permeability reductions due to the addition of WSRPs, only few percentage points of self-sealing capability can be found on most of the 0.4 mm crack width samples by comparing the permeability before and after the healing process. For 0.7 mm crack width samples, the S series still shows limited effect with only maximum 18 % decrease of permeability. While medium size (M) and large size (L) rubber systems showed much better performance in permeability reductions, ranging from 17 - 56 % and 16 - 64 % consecutively for WSRPs concentrations of 1 - 6 %. Although the value of the flow rate is much higher than for samples with 0.4 and 0.7 mm cracks, samples with 1.0 mm crack width had a similar trend of permeability reductions. A permeability reduction of 22 - 58 % and 23 - 61 % can be found for the medium size (M) and large size (L) rubber systems with 1.0 mm crack width. While there is no significant decrease of permeability for the small size (S) rubber system.

Moreover, a noticeable improvement could be found by comparing the perme-

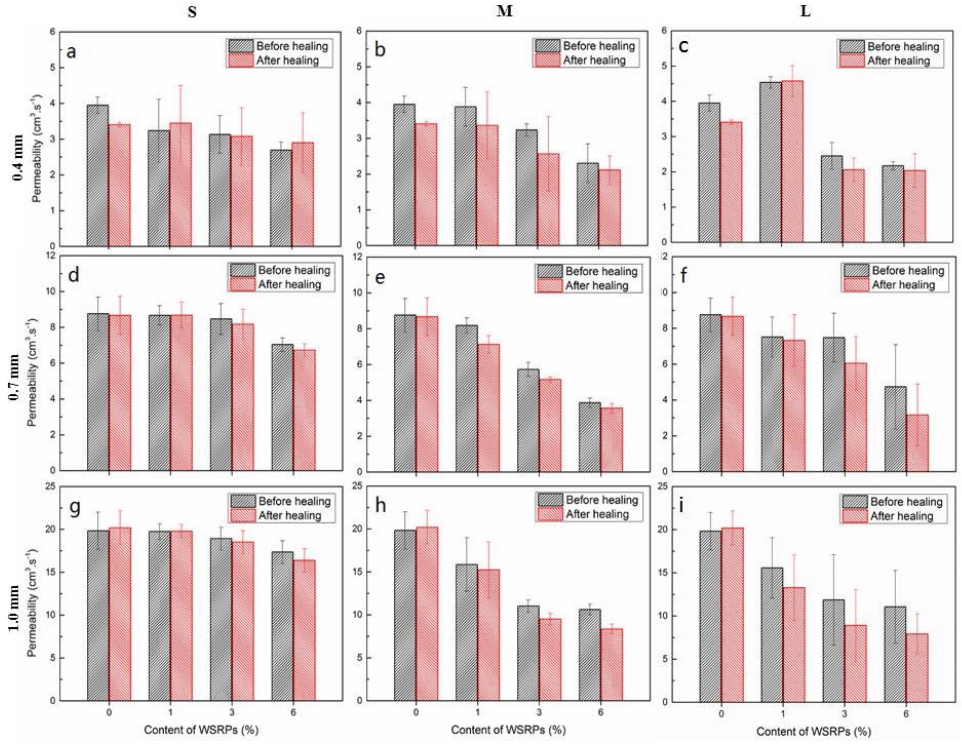

Figure 6.12: Data of permeability test of series S, M, L and B comparing the permeability at 0 day and after 7 days of water healing process in the form of 9 bar chart graphs. Graphs **a**, **d** and **g** show the permeability data of S series samples with different crack width (0.4, 0.7 and 1.0 mm). Graphs **b**, **e** and **h** show the permeability data of M series samples with different crack width (0.4, 0.7 and 1.0 mm). Graphs **c**, **f** and **i** show the permeability data of L series samples with different crack width (0.4, 0.7 and 1.0 mm).

ability decreases before and after the rubber was allowed to swell for 7 days of immersion (self-sealing process). This self-sealing effect became more prominent for the samples with crack widths of 0.7 mm and 1 mm as they showed relatively steeper decrease in permeability. In general, samples which were prepared with higher concentration and larger particles size seemed to show more significant further permeability reduction by the self-sealing effect of WSRPs. For 0.7 mm crack width samples, the swollen rubber for medium series (M) samples could lower the permeability to about 6 - 12 % compared to the sample before immersion. While, the swollen rubber of large series (L) rubber could generate further reduction of about 3 - 20 % with the rubber concentration of 1 - 6 %. In addition, in 1.0 mm crack width samples the permeability can be further lowered in the range of 3 - 22 % and 12 - 24 %, respectively for both medium (M) and large (L) particles.

In general, based on the results of water permeability test of the mortar specimens, the reduction in water permeability in this study can be attributed to two reasons. The first reason that the existance of WSRPs on the crack partly block the path of water flow. This can be reflected from the immediate decrease of permeability for those "before healing" sample with WSRPs embedded. The second reason is that the swelling effect of WSRPs further enlarge the volume of WSRPs which block the crack that enable the permeability to further decrease. This can be reflected by the further decrease of permeability after 7 days water immersion healing process. Meanwhile, the large series (L) samples performed almost similar to the medium series (M) samples for both 0.7 mm and 1 mm crack widths. These occurrences can be attributed to the balance between limitations of rubber expansion and the spatial availability within the cracked sample. This means that the swelling of large size particles is more difficult since the dimensions of the spaces in which it has to squeeze through are smaller in comparison. Another matter to consider is the significantly higher scatter in the data collected for the large particles series (L) compared to the medium particle samples (M) due to the lower probability of particle homogenisation. Since, comparing with small and medium particles, less number of large particles are needed to keep the the same volumetric ratio, which causes uneven particle distribution within the mortar samples. Then it ultimately causes L series particles to have a lower probability to be homogenously present in the crack path. Therefore, although L and M size particles may seem to produce the same average permeability reduction in this study, there are chances in which the self-sealing function of L series samples may be underestimated because of the inferior particle distribution.

6.3.5. Visual assessment of the reinforcement function of WSRPs

The crack bridging function is a unique characteristic of WSRPs. The embedded WSRPs can provide the concrete with a bridging effect to prevent the crack from fully separating the specimen. Typical images of the crack area of the WSRPs embedded samples were examined by a digital camera and are shown in Figure 6.13. As can be seen from Figure 6.13a, after the tensile load was first imposed and then removed from the cracked sample loaded with 4 % of WSRPs, the blue rubber

Figure 6.13: Typical images showing the crack bridging function function of WSRPs in mortar. Figure (a) shows the cracked sample under a tensile strengh, Figure (b) shows the prism sample ruptured by fracture strength test and Figure (c) is an enlarged image showing the crack surface and the bridging function of the WSRPs

particles become visible inside the crack. It is clear that the cracked specimen halves were kept together by the WSRPs and the specimen is not separated into two parts. This phenomenon indicates that the embedded rubber has the ability to bridge the cracked faces of the specimen. Figure 6.13b and c shows the internal crack surface of a sample with only 1 % of WSRPs. It can be seen that, even if the specimen was completely broken, the remnant of rubber particles were still binding to the mortar and the original grainy rubber was stretched into a fiber-like structure. This observation demonstrates that the rubber has a good bonding strength with the mortar matrix, which corresponds well with the result of the microstructure study by ESEM in Section 6.3.1.

6.4. Conclusions

In this chapter, granulated water swelling rubber (WSRP) was used for reducing the permeability of meso-scale cracks (width: 0.4 to 1 mm) through volume blocking and volume expansion triggered by water absorption. The sealing function of WSRPs in mortar was studied for cracks of 0.4 mm, 0.7 mm and 1.0 mm wide. Based on the result described above, the following conclusions can be drawn:

- The XCT result shows that the WSRPs have an obvious self-sealing effect in the cracked mortar.
- The incorporation of WSRPs into the system lowered the compressive strength by maximum of 19 % with addition of 6 % of large size WSRPs, and the flexural strength by maximum of 20 % with incorporation of 6 % large size WSRPs.
- The addition of WSRPs in mortar was able to partially lower the permeability, which was decreased even further after the samples were immersed in water for 7 days.
- The degree of permeability reduction increases with higher concentration of WSRPs. Larger particles show higher effect of the self-sealing function. The data collected from the permeability test suggest that medium (M) and large (L) particles showed more or less similar impact on permeability decrease. A maximum permeability reduction of 58 % and 64 % can be found for the medium size (M) and large size (L) rubber systems with WSRPs concentration of 6 %.

• In addition, a reinforcement function of WSRPs that can bridge the cracked mortar and prevent the two halves from completely separating was discovered.

This work contributes to the search for an effective material to completely or partially decrease the permeability of cementitious materials with less influence on mechanical properties. Comparing with previous study, the novel preparation and application of WSRPs give the cement mortar, a traditional construction material, a self-sealing ability with less sacrificing the mechanical properties. However, as a new self-sealing agent, some improvements to the proposed study are still needed. Firstly, water swelling rubber particles with less initial swelling at the hydration stage and with higher swelling pressure at the self-sealing period should be developed. Meanwhile it was found that the swelling capacity of WSRPs is highly influenced by the crack size and particle sizes. Therefore optimization procedures of size and concentration of WSRPs to increase the distribution probabilities and improve self-sealing performance should be developed. In addition, in preparing for practical application, further focus needed to be given to an accurate measurement of the potential of the crack bridging function of the WSRPs in cementitious materials.

References

[1] L. Lv, E. Schlangen, and F. Xing, *Self-sealing cementitious materials by using water-swelling rubber particles,* Materials **10**, 979 (2017).

[2] H. X. D. Lee, H. S. Wong, and N. R. Buenfeld, *Self-sealing of cracks in concrete using superabsorbent polymers,* Cement and Concrete Research **79**, 194 (2016).

[3] C. Song, Y. C. Choi, and S. Choi, *Effect of internal curing by superabsorbent polymers - internal relative humidity and autogenous shrinkage of alkali-activated slag mortars,* Construction and Building Materials **123**, 198 (2016).

[4] E. Gruyaert, B. Debbaut, D. Snoeck, P. Diaz, A. Arizo, E. Tziviloglou, E. Schlangen, and N. De Belie, *Self-healing mortar with ph-sensitive superabsorbent polymers: testing of the sealing efficiency by water flow tests,* Smart Materials and Structures **25** (2016).

[5] D. Snoeck, K. Van Tittelboom, S. Steuperaert, P. Dubruel, and N. De Belie, *Self-healing cementitious materials by the combination of microfibres and superabsorbent polymers,* Journal of Intelligent Material Systems and Structures **25**, 13 (2014).

[6] M. C. Bignozzi and F. Sandrolini, *Tyre rubber waste recycling in self-compacting concrete,* Cement and Concrete Research **36**, 735 (2006).

[7] S. Hesami, I. S. Hikouei, and S. A. A. Emadi, *Mechanical behavior of self-compacting concrete pavements incorporating recycled tire rubber crumb and*

reinforced with polypropylene fiber, Journal of Cleaner Production **133**, 228 (2016).

[8] J. H. Xie, Y. C. Guo, L. S. Liu, and Z. H. Xie, *Compressive and flexural behaviours of a new steel-fibre-reinforced recycled aggregate concrete with crumb rubber,* Construction and Building Materials **79**, 263 (2015).

[9] O. Youssf, M. A. ElGawady, J. E. Mills, and X. Ma, *An experimental investigation of crumb rubber concrete confined by fibre reinforced polymer tubes,* Construction and Building Materials **53**, 522 (2014).

[10] T. EN, *196-1. methods of testing cement–part 1: Determination of strength,* European Committee for standardization **26** (2005).

[11] D. Palin, H. Jonkers, and V. Wiktor, *Autogenous healing of sea-water exposed mortar: Quantification through a simple and rapid permeability test,* Cement and Concrete Research **84**, 1 (2016).

[12] E. Gallucci, K. Scrivener, A. Groso, M. Stampanoni, and G. Margaritondo, *3d experimental investigation of the microstructure of cement pastes using synchrotron x-ray microtomography (μct),* Cement and Concrete Research **37**, 360 (2007).

[13] T. EN, *1015-11, 2000,* Methods of test for mortar for masonry-Part **11**.

[14] A. J. Klemm and K. S. Sikora, *The effect of superabsorbent polymers (sap) on microstructure and mechanical properties of fly ash cementitious mortars,* Construction and Building Materials **49**, 134 (2013).

[15] K. S. Son, I. Hajirasouliha, and K. Pilakoutas, *Strength and deformability of waste tyre rubber-filled reinforced concrete columns,* Construction and Building Materials **25**, 218 (2011).

[16] Z. K. Khatib and F. M. Bayomy, *Rubberized portland cement concrete,* Journal of Materials in Civil Engineering **11**, 206 (1999).

7

Conclusions and prospects

If you come up with something new, give it a go and look what happens.

Michael Dell

In this chapter, the main results of this research project are summarized. Contributions of this work to science and engineering application are concluded. Suggestions and recommendations for future research in improving the self-healing of cementitious materials are outlined.

7.1. Conclusions

In this study, novel routes towards realizing self-healing in cementitious materials are explored. Two types of polymer-based healing agent were prepared and characterized. The capsule-based system is designed for micro-scale self-healing while the WSRPs system is prepared for meso-scale self-healing. A numerical lattice model was established to simulate crack formation and estimate the healing efficiency of the capsule-based self-healing system. The self-healing potential of the capsule-based system in terms of permeability and mechanical regain was evaluated. The water blocking and crack bridging function of WSRPs was demonstrated clearly using several advanced tools. Based on the research presented and the results, the following general conclusions can be drawn:

1. **Capsule-based self-healing system for micro-scale crack self-healing in cementitious materials**

   - A new type of phenol-formaldehyde resin (PF resin) shell / dicyclopentadiene (DCPD) core microcapsules for self-healing microcracks in cementitious materials was synthesized via in situ polymerization. The synthesized microcapsules possess a regular globe shape and smooth surface with a distinctively shell thickness/diameter ratio. The mean diameter and distribution of microcapsules could be controlled through adjusting the agitation rate during the synthesis. The microcapsules exhibited an excellent thermal stability and chemical resistance in the cementitious environment. XCT results showed that the microcapsules had a good dispersibility in the cement matrix and could be partially triggered by the crack. The OM investigation of the crack surface confirms the result of XCT that the self-healing function of the incorporated microcapsules could be partially triggered by cracking and the healing agent could be released simultaneously to heal the cracks.
   - A feasible numerical model was developed for simulating and evaluating fracture and trigger behaviour of capsule-based self-healing cementitious material. A 2D lattice fracture model was built to simulate the fracture performance and to obtain the tensile strength of the SIC zone. The tensile strength of the SIC zone which was obtained from the 2D simulation, 0.125 ± 0.009 MPa, is consistent with the tensile strength value which was obtained by the experiment, 0.091 ± 0.006 MPa. After that, a 3D lattice network which was used for numerical simulation of the crack behaviour of microcapsule-based self-healing system is constructed based on XCT microstructure. The parametric study on the constructed 3D model shows that both interlayer strength and shell strength can influence the trigger efficiency of microcapsules embedded self-healing systems. When the interlayer strength increased from 0.05 to 1.2 MPa, the trigger efficiency rose from 30 % to 61 %. The healable volume and crack width increased accordingly from 0.023 to 0.046 mm and from 3.3 to 6.5 µm, respectively. Compared to the interlayer strength, the trigger efficiency seems to be more sensitive than the shell strength.

- The self-healing potential in cementitious materials by applying the proposed two-component polymeric capsule-based self-healing system is explored and quantified through a simplified test. It was found that the successfully prepared granular wax-protected catalyst can be used to catalyze the microencapsulated healing agent, DCPD. The results of the permeability test demonstrate that, more than 96 % water blocking can be achieved when the volume of available healing agent is equal to the volume of crack space. While only a maximum of 6 % of mechanical regain can be observed under an ideal condition. The result suggests that the capsule-based self-healing system holds a great application potential in crack sealing, although there is little chance in realizing a completely mechanical regain of cracked cementitious materials in a real practice.

2. **WSRPs-based self-healing system for meso-scale crack self-healing in cementitious materials**

   - Granulated WSRPs were prepared and applied for reducing permeability of meso-scale cracks (width: 0.4 to 1 mm). The XCT result shows that the WSRPs have an obvious self-sealing effect in the cracked mortar. The incorporation of WSRPs into the system lowered the compressive strength by a maximum of 19 % with addition of 6 % of large size WSRPs, and the flexural strength by a maximum of 20 % with incorporation of 6 % large size WSRPs.
   - The addition of WSRPs in mortar was able to reduce the permeability of cementitious materials, which decreased even further after the samples were immersed in water for another 7 days. The degree of permeability reduction increases with higher concentration of WSRPs. Larger particles show higher effect of the self-sealing function. The data collected from the permeability test suggests that medium (M) and large (L) particles showed more or less similar impact in permeability decrease. A maximum permeability reduction of 58 % and 64 % can be found for the medium size (M) and large size (L) rubber systems with WSRPs concentration of 6 %.
   - Although the incorporation of WSRPs into the system lowered the compressive strength by a maximum of 19 % with addition of 6 % of large size WSRPs, and the flexural strength by a maximum of 20 % with incorporation of 6 % large size WSRPs, a reinforcement function of WSRPs that can bridge the cracked mortar and prevent the two halves from completely separating was observed.

7.2. Contribution to science and engineering

- Owing to its good dispersibility and stability, the novel PF/DCPD microcapsules developed in this work provide a promising carrier for healing agent to be applied in, but not limited to, self-healing cementitious materials.

- The established numerical model offers a approach for researchers in the field of microcapsule-based self-healing materials to predict and evaluate the crack behaviour and healing efficiency of microcapsule-based systems. Meanwhile, the application of XCT technology makes the simulated condition more close to the reality and, therefore, makes the simulation result more reliable.

- It is the first time that granulated WSRPs are used as healing agent to realize a crack sealing and bridging function in cementitious materials. It is a novel application of this type of water swelling rubber. The experimental results showed that the WSRPs can be directly used in cementitious materials as an additive to reduce the permeability and lower the harmful risk coming from crack propagation in concrete structures. The outstanding crack sealing and bridging function induced by WSRPs broadens the field of self-healing cementitious materials.

7.3. Prospects

This thesis mainly focuses on exploring new healing additives for autonomous healing of cementitious materials. Although many efforts have been made to achieve the objectives of this research project, further research is required to realize the self-healing function of cementitious materials. The following paragraphs propose some prospections and suggestions for the future.

- The trigger sensitivity of the synthesized PF/DCPD microcapsules is not yet stable enough and satisfying in order to realize a complete release of healing agent from the microcapsules to the crack. In the future, it is necessary to strengthen the bond between the shell material of microcapsules and cement matrix. Physically increasing the roughness or chemically modifying the functional group of the surface of microcapsules can be good solutions.

- In this thesis, the reaction of healing agent can only be ignited by heating the sample as the wax that was used to protect the catalyst has to melt to allow the catalyst to encounter with the healing agent. It is interesting to make a 2-in-1 microcapsules by attaching the catalyst on or embedding the catalyst in the shell of microcapsules.

- Some improvements of the experimental procedure to the proposed crack behaviour simulation method of capsule-based self-healing system are still needed. Firstly, a better procedure for accurate measurement of bond strength should be developed. The boundary conditions of the tensile test should be well controlled. In addition, since the ratio between the measured hardness and the tensile strength of cement paste is only an assumed value in this study, further work will be needed to establish an appropriate relationship between local hardness and the fracture strength of the cement paste.

- The quantification results of self-healing effect suggested that, for the system developed in this thesis, it is still difficult for microcapsules to realize a

profound mechanical healing of the crack without human intervention. In the future, microcapsules with particularly designed healing agent that could mechanically repair cracks at micro-level and stop cracks from growing bigger has to be invented.

- Despite the less efficient mechanical healing effect, the crack blocking effect, as the main application of the capsule-based system developed in this thesis, is still very promising. It contributes towards building a multi-scale self-healing cementitious system. Further study involves exploring more economic catalyst alternatives to replace present relatively expensive one and gradually decreasing the degree of human intervention during the healing process.
- For meso-scale self-healing cementitious materials that uses WSRPs as additives, WSRPs which are particularly applicable to our application have to be developed. It means that the WSRPs should have less initial swelling at the hydration stage and higher swelling pressure at the self-sealing period.
- In addition, although the crack bridging function has been visually observed in the lab by using WSRPs, further focus will be given to accurate measuring the bridging effect provided by the WSRPs. Combined numerical and experimental methods will be applied to evaluate the potential of the crack bridging function of the WSRPs in a large scale.
- The influence of the addition of WSRPs on ductility and fatigue resistance of cementitious materials is interesting as it has the possibility to make the WSRPs to be a suitable additive for concrete applied in seismic environment.

Summary

Cementitious materials are the most widely used construction materials on this planet. However, due to its heterogeneous and quasi-brittle nature, they are susceptible to many sources of damage during their entire service life. Although man-made repair can prolong the service life of reinforced concrete structures, it gives rise to large amounts of rehabilitation work, associated costs and waste of resources.

To decrease the frequency of maintenance and prolong the life-span of concrete structure, the self-healing concept was introduced to cementitious materials and has already shown its great application potential in the past decade. In this concept, self-healing additives are first blended with fresh mortar. When the cracks encounter the additives, the self-healing additives will be triggered and then react to the environmental change accordingly.

However, up to date, the available self-healing additives for cementitious materials are not able to deal sufficiently enough with all the diverse situations. The self-healing potential that the self-healing agent brings is not very clear. The size of cracks can vary from the micrometer to millimeter level in real situations. Nevertheless, strategies for multi-scale crack healing are still lacking. Based on these problems, in this thesis, two different types of self-healing additives, microencapsulated adhesive and water swelling rubber particles (WSRPs) were designed and prepared particularly for micro-scale (<500μm) and meso-scale (>500μm) cracks in cementitious materials. The healing effect and potential of using microcapsule-based self-healing system was evaluated and predicted through both experimental and numerical methods. The water sealing function to meso-scale cracks by applying WSRPs was characterized and monitored using X-ray Computed Tomography (XCT) technology and a water flow rate recording device. It is believed that this work can give insight into the future implementation of self-healing strategies in practical cementitious materials application.

Capsule-based self-healing system for micro-scale crack self-healing in cementitious materials

In Chapter 3, novel PF/DCPD microcapsules were synthesized via in situ polymerization. The synthesized microcapsules possess a regular globe shape and smooth surface with a distinctively shell thickness/diameter ratio. The synthezied microcapsules have an ideal thermal stability against the hydration heat and excellent chemical resistance in both simulated pore solution and real cement environment. Micro-mechanical test shows that with the increase of the mean size and decrease of shell thickness of microcapsules, the mechanical force which is required to trigger the microcapsules increased correspondingly. The optical microscope (OM)

observation and XCT results suggested that the microcapsules could be triggered by the crack and had a good dispersibility in cementitious materials.

In Chapter 4, a feasible approach was developed for simulating and evaluating of the fracture and trigger behaviour of capsule-based self-healing cementitious material. A 2D lattice fracture model was built to simulate the fracture performance and to obtain the tensile strength of the shell-interlayer-cement (SIC) zone. Subsequently, a 3D lattice network for numerical simulation of the crack behaviour of microcapsule-based self-healing cementitious system is constructed based on XCT images. The parametric study of the constructed 3D model shows that both interlayer strength and shell strength can influence the trigger efficiency of microcapsule embedded self-healing systems. When the interlayer strength increased from 0.05 to 1.2 MPa, the trigger efficiency rose from 30 % to 61 %. The healable volume and crack width increased accordingly from 0.023 to 0.046 mm and from 3.3 to 6.5 µm respectively. Comparing to the interlayer strength, the trigger efficiency seems to be more sensitive than the shell strength.

In Chapter 5, the self-healing potential in the cementitious matrix of the above proposed two-component polymeric capsule-based self-healing system is explored and quantified. Granular wax-protected Grubbs' catalyst was prepared and successfully catalyzed the polymerization of DCPD. The permeability test demonstrates that, more than 96 % water blocking can be achieved when the volume of available healing agent is equal to the volume of crack space. However, the potential of the self-healing system in mechanical regain is not very promising. Only a maximum 6 % of mechanical healing can be observed under an ideal condition. The results suggest that the capsule-based self-healing system holds a great application potential in sealing cracks while there is little chance that it can help in realizing mechanical regain in a real application.

WSRPs-based self-healing system for meso-scale crack self-healing in cementitious materials

In Chapter 6, the application of WSRPs for providing the cracked concrete with a self-sealing function was developed. The feasibility of applying WSRPs and the influence of incorporating WSRPs on the mechanical properties of concrete was investigated. The self-sealing efficiency of WSRPs incorporated in concrete with different content and particle size was quantified through a permeability test. The sealing effect of WSRPs was monitored by XCT. The XCT result shows that the WSRPs has an obvious self-sealing effect in the cracked mortar. The incorporation of MSRPs lowered the compressive strength by a maximum of 19 % with addition of 6 % of large size WSRPs, and the flexural strength by a maximum of 20 % with incorporation of 6 % large size WSRPs. The water sealing test demonstrates that the addition of WSRPs in mortar was able to partially lower the permeability. Larger particles shows higher effect of the self-sealing function. The degree of permeability reductions increases with higher concentration of WSRPs. The data collected from permeability test suggests that medium (M) and large (L) particles showed more or less similar impact in permeability decrease. A maximum permeability reduction of 58 % and 64 % can be found for the medium size (M) and large size (L) rubber

systems with WSRPs concentration of 6 %. In addition, a reinforcement function of WSRPs that can bridge the cracked mortar and prevent the two halves from completely separating was observed.

This work contributes to searching for an effective additive to decreases the permeability of cracked cementitious materials. Comparing with previous studies, the novel preparation and application of WSRPs give the cementitious material, which is a traditional construction material, self-sealing ability with limited sacrificing the mechanical properties.

Samenvatting

Cementgebonden materialen zijn de meest gebruikte bouwmaterialen op deze planeet. Vanwege de heterogene en quasi-brosse aard ervan zijn ze echter gedurende hun gehele levensduur gevoelig voor vele bronnen van schade. Hoewel door de mens gemaakte reparaties de levensduur van gewapende betonconstructies kunnen verlengen, leidt dit tot grote hoeveelheden renovatiewerkzaamheden, bijkomende kosten en verspilling van middelen.

Om de onderhoudsfrequentie te verlagen en de levensduur van de betonconstructie te verlengen, werd het zelfherstellende concept geïntroduceerd in cementgebonden materialen. Dit concept heeft in de afgelopen tien jaar al een groot toepassingspotentieel getoond. In dit concept worden zelfherstellende additieven eerst gemengd met verse mortel. Wanneer de scheuren op de additieven bereiken, worden de zelfherstellende additieven geactiveerd en reageren deze vervolgens op de omgevingsverandering.

De beschikbare zelfherstellende additieven voor cementgebonden materialen zijn echter niet in staat om voldoende om te gaan met alle uiteenlopende situaties. Het zelfherstellend vermogen dat het zelfgenezende middel met zich meebrengt, is niet erg duidelijk. De grootte van scheuren kan variëren van het micrometer- tot millimeterniveau in praktijksituaties. Desalniettemin ontbreken er nog steeds strategieën voor multi-schaal scheurherstel. Op basis van deze problemen werden in dit proefschrift twee verschillende soorten zelfherstellende additieven, microingekapselde kleefmiddelen en water-zwellende rubberdeeltjes (water swelling rubber particles, WSRP's) ontworpen en vervaardigd, met name voor microschaal (< 500 µm) en meso-schaal (> 500 µm) scheuren in cementgebonden materialen. Het genezende effect en het potentieel van het gebruik van een op microcapsules gebaseerd zelfherstellend systeem werd geëvalueerd en voorspeld door middel van zowel experimentele als numerieke methoden. De waterafdichtende functie voor scheurtjes op mesoschaal door toepassing van WSRP's werd gekarakteriseerd en gevolgd met behulp van X-ray Computed Tomography (XCT) technologie en een waterpermeabiliteitopstelling. Er wordt aangenomen dat dit werk inzicht kan geven in de toekomstige implementatie van zelfhelende strategieën in praktische toepassingen van cementgebonden materialen.

Op capsules gebaseerd zelfherstellend systeem voor zelfheling op microschaal in cementgebonden material

In Hoofdstuk 3 werden nieuwe PF/DCPD-microcapsules gesynthetiseerd via in situ polymerisatie. De gesynthetiseerde microcapsules bezitten een gelijkmatige bolvorm en een glad oppervlak met een kenmerkende schaaldikte / diameterverhouding. De microcapsules hebben een ideale thermische stabiliteit tegen de hydratatiewarmte en uitstekende chemische weerstand in zowel gesimuleerde poriënop-

lossing als echte cementomgeving. Micro-mechanische testen onen aan dat met de toename van de gemiddelde afmeting en afname van de dikte van de schaal van microcapsules, de mechanische kracht die vereist is om de microcapsules te activeren dienovereenkomstig toeneemt. De optische microscoop (OM) waarnemingen en XCT-resultaten suggereerden dat de microcapsules door de scheur konden worden getriggerd en een goede dispergeerbaarheid in cementgebonden materialen hadden.

In Hoofdstuk 4 is een haalbare aanpak ontwikkeld voor het simuleren en evalueren van het breuk- en trigger-gedrag van op capsules gebaseerd zelfherstellend cementachtig materiaal. Een 2D-roosternetwerk werd gebouwd om de breukprestaties te simuleren en om de treksterkte van de shell-interlayer-cement (SIC) zone te bepalen. Vervolgens wordt op basis van XCT-afbeeldingen een 3D-roosternetwerk opgebouwd voor numerieke simulatie van het scheurgedrag van het op microcapsules gebaseerd zelfherstellend cementachtig systeem. De parametrische studie van het geconstrueerde 3D-model toont aan dat zowel de sterkte tussen de lagen als de sterkte van de schaal de trigger-efficiëntie van microcapsule ingebedde zelfherstellende systemen kan beïnvloeden. Toen de sterkte van de tussenlaag steeg van 0,05 naar 1,2 MPa, steeg het triggerrendement van 30 % tot 61 %. Het te herstellen volume en de scheurwijdte namen dienovereenkomstig toe van respectievelijk 0,023 tot 0,046 mm en van 3,3 tot 6,5 µm. In vergelijking met de sterkte tussen de lagen lijkt de trigger-efficiëntie gevoeliger dan de schaalsterkte.

In hoofdstuk 5 wordt het zelfherstellend vermogen in de cementgebonden matrix van het hierboven voorgestelde, uit twee polymeercomponenten bestaande, op een capsule gebaseerde zelfgenezingssysteem onderzocht en gekwantificeerd. Een granulaire met was beschermde Grubbs-katalysator werd bereid en heeft met succes de polymerisatie van DCPD gekatalyseerd. De permeabiliteitstest toont aan dat meer dan 96 % waterblokkering kan worden bereikt wanneer het volume van beschikbaar zelfgenezend middel gelijk is aan het volume van de scheurruimte. Het potentieel van het zelfherstellende systeem voor mechanische erstel is echter niet erg veelbelovend. Hooguit kan 6 % mechanische herstel worden waargenomen onder een ideale conditie. De resultaten suggereren dat het op capsules gebaseerde zelfherstellend systeem een groot toepassingspotentieel biedt bij het afdichten van scheuren, terwijl er weinig kans is dat het kan helpen bij het verkrijgen van mechanisch herstel in een echte toepassing.

Op WSRP's gebaseerd zelfherstellend systeem voor zelfherstel van scheuren op mesoschaal in cementgebonden materialmen

In hoofdstuk 6 is een toepassing van WSRP's ontwikkeld als zelfafdichtende functie voor escheurd beton. De haalbaarheid van het toepassen van WSRP's en de invloed van het opnemen van WSRP's op de mechanische eigenschappen van beton werd onderzocht. De zelfdichtende efficiëntie van WSRP's ingebouwd in beton met verschillende hoeveelheid en deeltjesgrootte werd gekwantificeerd door middel van een permeabiliteitstest. Het afdichtende effect van WSRP's werd gevolgd door XCT. Het XCT-resultaat laat zien dat de WSRP's een duidelijk zelfdichtend effect hebben in de gescheurde mortel. De integratie van MSRP's verlaagde de druksterkte met

maximaal 19 % met toevoeging van 6 % WSRP's van grote afmetingen en de buigsterkte met maximaal 20 % met de toevoeging van 6 % WSRP's van groot formaat. De waterdichtheidstest toont aan dat de toevoeging van WSRP's in mortel in staat was om de permeabiliteit gedeeltelijk te verlagen. Grotere deeltjes vertonen een hoger effect van de zelfafdichtende functie. De mate van doorlaatbaarheidsvermindering neemt toe met een hogere concentratie van WSRP's. De gegevens verzameld uit de permeabiliteitstest suggereren dat medium (M) en grote (L) deeltjes een min of meer vergelijkbare invloed vertoonden in de permeabiliteitsafname. Een maximale permeabiliteitsvermindering van 58 % en 64 % kan worden gevonden voor de middelgrote (M) en grote maat (L) rubbersystemen met een WSRP-concentratie van 6 %. Daarnaast werd een versterkende functie van WSRP's waargenomen waar deze de gescheurde mortel kunnen overbruggen en zo voorkomen dat de twee helften volledig worden gescheiden.

Dit werk draagt bij aan het zoeken naar een effectief additief om de doorlaatbaarheid van gescheurde cementgebonden materialen te verminderen. In vergelijking met eerdere studies, levert de nieuwe bereiding en toepassing van WSRP's het cementgebonden materiaal, dat een traditioneel constructiemateriaal is, zelfdichtend vermogen met beperkte opoffering van de mechanische eigenschappen…

Acknowledgements

I first would like to express my acknowledgement to Prof. Erik Schlangen. Thank you for accepting me as a PhD candidate to work here in such an outstanding Lab and beautiful country. I will never forget the interview we had in Shenzhen 5 years ago when you announced me to be a part of Microlab. The discussions with you were always informative to me. Without your continuously encourage, guidance and support, it is impossible for me to finish my PhD journey and upgrade my life.

Same acknowledgement to my host department, Guangdong Province Key Laboratory of Durability for Marine Civil Engineering at Shenzhen University, for providing this valuable opportunity and financial support to me. Particularly, I want to thank Prof. Xing Feng, Tang Jiaoning, Han Ningxu and all the related personnel at Shenzhen University, who raised the funding and recommended me to be a candidate of PhD here in Delft University of Technology.

I also want to say thanks to my dear colleagues. Thank you, Dr. Henk Jonker, your vision and innovation expand my horizon and triggered my curiosity to self-healing materials. Thank you, Ger. Your dedicated attitude to work is the first lesson I learned here. Thank you, Maiko. When you said the concrete is like a baby, your passion to concrete really amazed me. Thank you, Arjan, for your rigorous and hard work. Thank you, our team player, Hongzhi, Branko, Oguzhan, Ma Xu, Claudia, Stefan and Xu Shi, I enjoyed so much to talk and even debate with you on our group meeting. Hongzhi, for sure we will have more opportunity to cooperate in the future. That you all Microlabers, John, Renée, Lupita, Yibing, Zhiwei, Tianshi, Zhipei, Eirini, Balquis, Dong Hua, Huang Hao, Tim, Amir, Shizhe, Bahman, Xuliang, Nynke, Wenjuan, Mladena and Branko, Farad, Natalie, Jiayi, Stefan, Marija, Hitham, Martin and Dr. Ye, it is my lucky and honor to meet you in my life.

I feel grateful to my parents. Great thanks to them for bringing me up and providing me a good life. They always stand behind me and 24 hours prepared to give me a hand whenever I need. In fact, it is beyond my ability to compensate them even a portion of the love they gave to me.

At the end, I want to express my deepest gratitude to my wife Tang Xueer, my daughter Lyu Fanxi and my son Lyu Yankun. Xueer, I cannot image how my life will be without your thoughtful care, unconditional love and sacrifice. Your courage and wisdom always guide me to be better and better. Fanxi and Yankun, you are simply the best. I thank you for all the happiness and joy you bring to me and our big family. The present of you make me complete.

Curriculum Vitæ

Leyang LU

03-10-1987 Born in Shandong, China.

Education

2006–2010 BSc Student
Material Science and Engineering
Shenzhen Univerisity

2010–2013 MSc Student
Material Science
Shenzhen Univerisity

2013–2018 Ph.D. Candidate
Delft Univerisity of Technology
Promotor: Prof. Erik Schlangen

Awards

2016 1^{st} Prize
Competition of Creative Idea on Sustainable/Durable Construction Materials

List of Publications

Journal Publications

1. **L. Lv**, H. Zhang, E. Schlangen, F. Xing, *Experimental and numerical study of crack behaviour for capsule-based self-healing cementitious materials*, Construction and Building Materials **156**,219 (2017).

2. **L. Lv**, E. Schlangen, F. Xing, *Self-sealing cementitious materials by usingwater-swelling rubber particles*, Materials **10**, 979 (2017).

3. **L. Lv**, E. Schlangen, Z. Yang, and F. Xing, *Micromechanical properties of a new polymeric microcapsule for self-healing cementitious materials*, Materials **9**, 1025 (2016).

4. **L. Lv**, Z. Yang, G. Chen, G. Zhu, N. Han, E. Schlangen, F. Xing, *Synthesis and characterization of a new polymeric microcapsule and feasibility investigation in self-healing cementitious materials*, Construction and Building Materials **105**, 487 (2016).

Conference Proceedings

1. **L. Lv**, J. Tang, G. Zhu, G. Chen, N. Han, E. Schlangen, F. Xing. Synthesis and characterization of novel mechanical triggered phenol-formaldehyde microcapsules containing a rejuvenator for self-healing cement-based materials. Durham, ICSHM2015

2. **L. Lv**, J. Tang, F. xiao, E. Schlangen, G. Zhu, N. Han, F. Xing. Applying nanoindentation to measure micromechanical properties of phenol–formaldehyde microcapsules for self-healing cement-based materials. Durham, ICSHM2015

3. G. Zhu, **L. Lv**, J. Tang, B. Dong, N. Han, F. Xing. Preparation of mono-sized epoxy/MF microcapsules in the appearance of polyvinyl alcohol as co-emulsifier. Ghent, ICSHM2013